Universidade do Minho
Escola de Medicina

Rita de Melo Miranda

Mechanisms underlying *Mycobacterium avium* infection-induced thymic atrophy

Setembro de 2019

Rita de Melo Miranda **Mechanisms underlying *Mycobacterium avium* infection-induced thymic atrophy** UMinho | 2019

Universidade do Minho
Escola de Medicina

Rita de Melo Miranda

Mechanisms underlying *Mycobacterium avium* infection-induced thymic atrophy

Dissertação de Mestrado
Mestrado em Ciências da Saúde

Trabalho Efetuado sob a orientação da
Doutora Palmira Barreira-Silva
e da
Professora Doutora Margarida Correia-Neves

Setembro de 2019

Agradecimentos

À Palmira, por me ter recebido e orientado dedicadamente desde o primeiro dia. Por tudo o que me ensinou, dentro do laboratório e para lá dele. Por me ter ajudado a crescer e sempre me ter dado espaço e ferramentas para isso. Um enorme, enorme obrigada.

À Professora Margarida, por me ter aceitado e recebido prontamente no laboratório. Por ser uma enorme inspiração como cientista e ser humano. Obrigada pelo privilégio de receber a sua orientação e poder discutir ciência e a vida consigo.

À Escola de Medicina, ao Instituto de Investigação em Ciências da Vida e Saúde (ICVS) e seus domínios de investigação (PopHealth, NERD, MIRD, SSRD) pelo ambiente de entreajuda.

À Diretora do Mestrado em Ciências da Saúde, Professora Doutora Patrícia Maciel, e à Coordenadora do Domínio da Saúde das Populações, Professora Doutora Margarida Correia-Neves.

A todos os colegas de laboratório, pelo ótimo ambiente científico e companheirismo que se estende para além das paredes do Instituto. Um obrigada especial às minhas meninas (Ângela, Carolina, Gi), verdadeiras companheiras ao longo deste ano.

Aos meus colegas e amigos do mestrado, por todas as conversas, partilhas, risos e momentos para descarregar a tensão. Não imaginam a diferença que fizeram em certas alturas.

À minha outra família no ICVS (#Pessoas), que perto ou já há muito tempo longe de lá, são pessoas lindas e sempre presentes.

Aos BBiologiaUA, por nos carregarmos uns aos outros desde os tempos da licenciatura. Por me fazerem esquecer o resto da minha vida durante aquelas preciosas horas dos nossos jantares.

Aos meus melhores e mais antigos amigos (Rafaela, Nuno), a prova de que amizades de duas décadas são possíveis. Não há palavras suficientes para vos agradecer.

Ao Daniel, pela paciência, compreensão, otimismo e amor ao longo deste e de todos os outros anos. Nunca saberei como te agradecer por tudo aquilo que trouxeste e trazes à minha vida.

À minha mãe, a melhor. Sem todo o teu apoio incondicional, sacrifício e energia inesgotável, nunca teria chegado a este ponto. Que eu possa um dia retribuir um décimo do que me deste.

O trabalho apresentado nesta tese foi realizado no ICVS, Universidade do Minho. O financiamento provém do projeto NORTE-01-0145-FEDER-000013, do Programa Operacional Regional do Norte (NORTE 2020/FEDER), e do projeto POCI-01-0145-FEDER-007038, sob o Programa Operacional Fatores de Competitividade (COMPETE) e de fundos nacionais da Fundação para a Ciência e Tecnologia (FCT).

STATEMENT OF INTEGRITY

I hereby declare having conducted this academic work with integrity. I confirm that I have not used plagiarism or any form of undue use of information or falsification of results along the process leading to its elaboration.

I further declare that I have fully acknowledged the Code of Ethical Conduct of the University of Minho.

Mecanismos associados à atrofia tímica causada por infeção por *Mycobacterium avium*

Resumo

A atrofia tímica ocorre naturalmente a partir da puberdade. No entanto, a atrofia tímica prematura pode ter um impacto negativo no sistema imunitário. A infeção por vários agentes patogénicos causa atrofia tímica prematura através de mecanismos frequentemente associados ao aumento da produção de glucocorticoides e/ou citocinas pró-inflamatórias.

A infeção de murganhos C57BL/6 com uma estirpe de alta virulência (25291) de *Mycobacterium avium*, mas não com uma de virulência intermédia (2447), induz atrofia tímica progressiva. Esta atrofia resulta da sinergia entre glucocorticoides e óxido nítrico (NO) produzido por macrófagos ativados por interferão gama (IFNγ). Resultados recentes sugerem ainda que o IFNγ afeta o timo, ao aumentar a morte de timócitos, e a medula óssea (MO), ao alterar os precursores de linfócitos T. Todavia, o papel do NO no timo é ainda desconhecido. O principal objetivo deste trabalho foi esclarecer se o aumento da morte de timócitos contribui para a atrofia induzida pela infeção por *M. avium* 25291 e qual o papel de moléculas pró-inflamatórias específicas neste processo.

Neste trabalho, revelamos que a atrofia tímica induzida pela infeção por *M. avium* 25291 está associada a um aumento dos timócitos em morte celular por apoptose. A apoptose de populações específicas de timócitos parece ser dependente da produção local de IFNγ e de sintase de NO induzível (iNOS). Esta hipótese é suportada por duas observações: por um lado, a apoptose não ocorre em murganhos que não expressam cada uma destas moléculas; por outro, ocorre sobre-expressão de *Ifng* e *Inos* no timo em períodos avançados da infeção. Adicionalmente, também em momentos mais tardios da infeção por *M. avium* 25291, observamos sobre-expressão de interleucina 6 (*Il6*) e fator de necrose tumoral (*Tnf*), os quais foram previamente associados à atrofia tímica prematura noutros modelos de infeção. Este resultado sugere um possível papel para estas citocinas na atrofia prematura do timo.

Propomos, assim, que a produção de IFNγ e NO no timo contribui para a sua atrofia precoce através da apoptose de timócitos, o que complementa o conhecimento sobre os mecanismos moleculares subjacentes à atrofia tímica causada pela infeção por *M. avium* 25291. Sugerimos ainda a IL-6 e o TNF como potenciais intervenientes neste processo, incentivando assim a investigação mais detalhada dos mecanismos desencadeados por estas moléculas.

Palavras-chave: Infeção por *Mycobacterium avium* | Óxido nítrico | Citocinas pró-inflamatórias | Atrofia tímica | Apoptose de timócitos

Mechanisms underlying *Mycobacterium avium* infection-induced thymic atrophy

Abstract

Thymic atrophy naturally occurs after puberty. However, premature thymic atrophy might weaken the immune system. Infection by several pathogenic microorganisms induces premature thymic atrophy through mechanisms often associated with increased production of glucocorticoids and/or proinflammatory cytokines.

Infection of C57BL/6 mice with a highly virulent strain (25291) of *Mycobacterium avium*, but not with a strain of intermediate virulence (2447) induces progressive thymic atrophy, in a process mediated by glucocorticoids and nitric oxide (NO) produced by interferon gamma (IFNγ)-activated macrophages. Recent data indicate that IFNγ affects the thymus, by increasing the percentage of dead thymocytes, and the bone marrow (BM), by altering BM T cell precursors. Yet, the role of NO in the thymus remains unknown. The main goal of this work was to further investigate thymocyte death as a potential mechanism underlying *M. avium* 25291 infection-induced thymic atrophy and the role of specific pro-inflammatory molecules in this process.

Here we demonstrate that *M. avium* 25291 infection-induced thymic atrophy is accompanied by an increase in apoptotic thymocytes. Apoptosis of specific thymocyte populations seems dependent on the local production of IFNγ and inducible NO synthase (iNOS), as apoptosis does not occur in mice deficient for each of these molecules and upregulation of *Ifng* and *Inos* genes occurs in the thymus at late timepoints of infection. Additionally, the expression of interleukin 6 (*Il6*) and tumor necrosis factor (*Tnf*), molecules that have been associated with premature thymic atrophy in other models of infection, is upregulated at late timepoints of infection with *M. avium* 25291. This hints at possible participation of these cytokines in premature thymic atrophy.

With this work, we propose that IFNγ and NO production in the thymus contribute to premature thymic atrophy through thymocyte apoptosis, complementing the knowledge on the molecular mechanisms underlying *M. avium* 25291 infection-induced thymic atrophy. Furthermore, we added IL-6 and TNF as possible players and opened the door for the study of the mechanisms triggered by these molecules.

Keywords: *Mycobacterium avium* infection | Nitric oxide | Pro-inflammatory cytokines | Thymic atrophy | Thymocyte apoptosis

Table of Contents

Abbreviations

7-AAD	7-Aminoactinomycin D
AM	Alveolar macrophages
APC	Antigen-presenting cell
Bak	Bcl-2 associated death promoter
Bax	Bcl-2 associated X protein
BCG	Bacillus Calmette-Guérin
Bcl-2	B-cell lymphoma 2
Bcl-X_L	B-cell lymphoma-extra large
BH3	Bcl-2 homology domain 3
BIM	Bcl-2-like protein 11
BM	Bone marrow
CARD11	Caspase recruitment domain-containing protein 11
CD	Cluster of differentiation
CFU	Colony forming unit
DC	Dendritic cell
DIABLO	Direct inhibitor of apoptosis protein binding protein with low pI
DN	Double negative
DP	Double positive
Dpi	Days post-infection
FOXP3	Forkhead box p3
GR	Glucocorticoid receptor
HIV	Human immunodeficiency virus
IFNγ	Interferon gamma
IL	Interleukin
iNOS	Inducible nitric oxide synthase
KO	Knock-out
MAC	*Mycobacterium avium* complex
Mcl-1	Myeloid cell leukemia 1
MHC	Major histocompatibility complex
Mtb	*Mycobacterium tuberculosis*

NK-kB	Nuclear factor kappa-light-chain-enhancer of activated B cells
NO	Nitric oxide
Noxa	Phorbol-12-myristate-13-acetate-induced protein 1
NTM	Non-tuberculous mycobacteria
PCR	Polymerase chain reaction
PI	Propidium iodide
PUMA	p53 upregulated modulator of apoptosis
RAG	Recombination-activating gene
Rpm	Revolutions per minute
SD	Standard deviation
SP	Single positive
TB	Tuberculosis
TCR	T cell receptor
TEC	Thymic epithelial cell
TNF	Tumor necrosis factor
TUNEL	Terminal deoxynucleotidyl transferase dUTP nick end labeling
WT	Wild-type

Figures Index

Tables Index

1. INTRODUCTION

1.1. The *Mycobacterium* genus

The *Mycobacterium* genus comprises 188 rod-shaped, acid-fast bacterial species (1). Recently, a division into five different genera based on genomic studies has been proposed, although its acceptance is still under discussion (2). Mycobacteria have a particular cell wall constitution, with three different layers composed mainly by peptidoglycan, arabinogalactan and mycolic acids, that contribute to its virulence and resistance to antibiotics and disinfectants (3). This genus includes strict human pathogens such as *Mycobacterium tuberculosis (Mtb)* and *Mycobacterium leprae* (the etiological agents for tuberculosis (TB) and leprosy, respectively); non-tuberculous mycobacteria (NTM), that include opportunistic human pathogens such as the *Mycobacterium avium* Complex (MAC) and numerous non-pathogenic and less-known species (2).

1.1.1. Infections caused by mycobacteria

In 2017*, Mtb* was estimated to infect 1.7 billion people worldwide, from which 5-10% presented active disease, most frequently in the pulmonary form (4). Although these numbers have been globally decreasing, TB remains one of the top 10 causes of death, and the leading cause from a single infectious agent, with an estimated 1.6 million deaths in 2017 (4).

NTM are a group of mycobacteria including fast- and slow-growing species capable of causing chronic disease in several forms (e.g. pulmonary, cutaneous, disseminated) in humans (8). Contrary to *Mtb*, NTM are found predominantly in the soil and water systems like domestic and hospital premise plumbing (5). The main infection route is through the environment (e.g. soil, water systems) and not person-to-person contact (6). Epidemiological data show a global increase in NTM infections even in immunocompetent individuals during the last years (6–8). Although there is regional variability regarding the isolated NTM species and associated risk factors, old-age is consistently associated with NTM pulmonary infection (6), as is often also the case for immunosuppression and previous respiratory infections (e.g. chronic obstructive pulmonary disease) (9). Treatment for NTM infections differs according to the infectious agent: therapy for MAC infection consists in a macrolide (azithromycin or clarithromycin), rifampicin and ethambutol, while *Mycobacterium kansasii*, *Mycobacterium malmonense* and *Mycobacterium xenopi* require a different drug cocktail (10). Treatment usually lasts for at least 12

months after bacteria cultures become negative (9,10). In case of pulmonary infection, diagnosis requires that one of the following criteria is met: 1) at least two positive separate sputum cultures, 2) a positive result from at least one bronchial wash or lavage, 3) a positive result in transbronchial or other lung biopsy (10). In case of extra-pulmonary infection, bacteria culture is done from clinical samples of other fluids or tissues (e.g. blood, BM, lymph nodes). Species identification should resort to molecular techniques such as polymerase chain reaction (PCR)-based assays, whole genome sequencing or biochemical tests (11).

The NTM most commonly associated with pulmonary mycobacterial infections belongs to the MAC (9). This complex includes *M. avium* (subsp. *avium*, *silvaticum*, *hominissuis*, and *paratuberculosis*), *Mycobacterium intracellulare*, *Mycobacterium chimaera*, *Mycobacterium colombiense*, *Mycobacterium marseillense*, *Mycobacterium arosiense*, *Mycobacterium timonense*, *Mycobacterium bouchedurhonense*, *Mycobacterium ituriense* and *Mycobacterium vulneris* (12). Slow growth of these mycobacteria has been associated with the need for high energy to synthesize mycolic acids. These are long-chain fatty acids contributing to the impermeability of the outer membrane of the mycobacterial cell wall. The lipid richness of the bacterial cell wall limits nutrient uptake but also favors resistance against adverse environments (e.g. high temperatures, extreme pH fluctuations), antibiotics and disinfectants, and supports persistent biofilm formation in plumbing, showerheads and similar surfaces (5).

M. avium is frequently the most prevalent species from the MAC in the clinical setting (12,13) and includes several different subspecies and strains. In this work, we used two strains of *M. avium* that present differences in virulence: strains 2447 and 25291. After systemic inoculation, *M. avium* 2447, a strain of intermediate virulence, causes chronic infection in C57BL/6 mice with subsequent stabilization of bacterial burden. On the other hand, infection with the highly virulent strain 25291 leads to uncontrolled bacterial growth, culminating in death around 80-90 days post-infection (dpi). In addition, infection with *M. avium* 25291 is accompanied by premature thymic atrophy (14).

1.1.2. Immune response to mycobacteria

Most of what is described regarding the immune response to mycobacteria were defined for *Mtb* infection, however, there are also several studies on the immune response elicited by NTM. Yet, we still do not understand the full picture of a protective immune response against mycobacteria. Mycobacterial disease progression is difficult to follow in humans as it may take a few months to years to develop after contact, so animal models were and still are a valuable tool to dissect the immune response to these pathogens.

The most commonly used animal model to study mycobacterial infections is the mouse model, and the C57BL/6 strain is frequently used. Mice are relatively easy and affordable to house and maintain, and many different strains and genetically modified models are available. This allows, for instance, studying the role of a specific molecule of interest during the immune response to mycobacterial infections. Besides, the diversity of available laboratory reagents for mice facilitates the use of this model. Importantly, the murine and human immune responses to mycobacteria share similarities (15), making it a suitable model to study the associated immune response. Data from animal models together with studies on human genetic syndromes associated with increased NTM infection susceptibility (16,17) were fundamental to elucidate the mechanisms of immune response during mycobacterial infections.

Mycobacteria are engulfed by phagocytes (neutrophils, monocytes, macrophages and dendritic cells (DCs)) (11), which express pattern recognition receptors (e.g. Toll-like receptors, C-type lectin receptors, among others) that allow pathogen recognition and subsequent phagocytosis (18). However, within these phagocytes, mycobacteria may manage to avoid elimination, for instance by taking advantage of their cell wall components: as an example, glycolipids present in both *Mtb* and *M. avium* such as lipoarabinomannans (LAM) and lipomannan (LM) can, respectively, inhibit phagocyte apoptosis and inhibit phago-lysosome fusion, allowing mycobacteria to proliferate inside phagocytes (19,20). When the innate response is unable to clear the bacteria, antigen presenting-cells (APCs) carrying mycobacterial antigens and/or bacteria migrate to the draining lymph nodes and prime naïve mycobacteria-specific T cells (21). Primed T cells then proliferate and migrate to the site of infection, where APC-T cell interactions drive T cell activation. Secretion of IL-12 by infected macrophages leads to interferon gamma (IFNγ) production by T cells. IFNγ activates macrophages and induces the production of nitric oxide (NO) via inducible NO synthase (iNOS) and other antimicrobial molecules (22). The role of IFNγ production by T cells in fighting *Mtb* and NTM has been demonstrated by several studies. IFNγ knock-out (KO) mice are unable to control *Mtb* infection (23) and produce undetectable levels of reactive nitrogen intermediates (derived from NO) in the serum (24). In humans, patients with genetic alterations that lead to reduced

IFNγ production are highly susceptible to mycobacterial infections (17,25). As for NO, in mice, *Mtb* infection of iNOS KO mice progresses faster than in WT counterparts (26). In humans, however, most data come from *in vitro* or *ex vivo* experiments with monocytes/macrophages and there is still controversy regarding NO role in mycobacterial infections (27). Some evidence point to an important role, as NO-derived compounds were detected in the urine and breath of *Mtb*-infected patients (28), abnormal production of exhaled NO was found in NTM pulmonary disease patients (29) and inhibiting iNOS reduces human alveolar macrophages (AM)-induced killing of *M. bovis* Bacillus Calmette-Guérin (BCG) (30). Yet, curiously, the outcomes from IFNγ and NO action depend on the bacterial strain. Infection of IFNγ KO mice with *M. avium* 2447 causes a slight increase in bacterial load compared to WT mice, while iNOS KO mice present no alterations on bacterial burden or infection outcome. On the other hand, after infection with the highly virulent strain 25291, IFNγ KO and iNOS KO mice present, respectively, similar and lower bacterial burden when compared to WT counterparts (31). Thus, IFNγ and NO might contribute to mycobacteria pathogenicity in *M. avium*, favoring disease progression instead of leading to pathogen clearance and infection resolution, in a strain-dependent manner.

Tumor necrosis factor (TNF) also plays an important role in the immune response to mycobacteria, as it drives the development of granulomas (organized lesion of infected cells surrounded by non-infected phagocytes and lymphocytes) (32), activates macrophages upon *Mtb* infection and participates in NO production. Evidence for this lies in the fact that TNF KO mice produce lower amounts of NO during *Mtb* infection and fail to control disease (33) and that patients receiving anti-TNF therapy display a significantly higher incidence of TB (34).

1.2. The thymus – Anatomy and function

The thymus is a primary lymphoid organ essential for the differentiation of T cells. T cells differentiate from hematopoietic precursors that migrate from the bone marrow (BM) and seed the thymus (35).

The thymus can be divided into two distinct anatomical regions: the cortex (the outer layer) and the medulla (the inner layer). Both areas participate in different moments of T cell differentiation. T cell precursors from the BM continuously seed the thymus through the corticomedullary junction (35). Thymocytes then migrate through the cortex, which supports the early stages of differentiation and T cell receptor (TCR) rearrangement (37) and is populated by cortical thymic epithelial cells (cTECs) and DCs. Finally, thymocytes enter the medulla, that sustains the final stages of differentiation and is composed by medullary TECs (mTECs), DCs, macrophages and B cells (38).

1.2.1. T cell differentiation in the thymus

There are four main thymocyte populations in the thymus, defined according to the expression of the TCR co-receptors CD4 and CD8. The most immature thymocytes are the double negative (DN) thymocytes ($CD4^-CD8^-$). These cells acquire later both CD4 and CD8 expression becoming double positive (DP; $CD4^+CD8^+$). The transition from DN to DP thymocytes occurs essentially in the cortex. Then, DP thymocytes migrate to the medulla, mature into CD4 or CD8 single positive (SP; $CD4^+CD8^-$ and $CD4^-CD8^+$) thymocytes and egress to the blood and secondary lymphoid organs after 4-5 days in the medulla (39). A summary of the main events occurring during T cell differentiation in mice is illustrated in Fig. 1.

The TCR is a transmembrane protein specific of T cells. It is composed by a two-chain heterodimer (α and β, or δ and γ) each with constant and variable regions, forming a complex with CD3 subunits. The TCR allows T cells to recognize antigens (most frequently peptides) embedded in a self-major histocompatibility complex (MHC) – from now on designated MHC-peptide complex (40). During T cell differentiation, a panoply of different TCRs is generated by random rearrangement of the gene segments encoding the variable portions of the TCR chains, through recombination-activating genes (RAG) enzymes (41). A useful TCR is tolerant to self-molecules and restricted to self-MHCs. However, during TCR rearrangement, some TRCs are not functional, others do not recognize MHC-peptide complexes or recognize them too strongly (42). Thus, to prevent the migration of useless or autoreactive T cells to the periphery, thymocytes undergo a highly regulated process of selection.

DN thymocytes can be subdivided according to CD44 and CD25 expression: $CD44^+CD25^-$ (DN1) become $CD44^+CD25^+$ (DN2), which give rise to $CD44^-CD25^+$ (DN3) and then $CD44^-CD25^-$ (DN4), the most mature DN thymocytes (37). At the DN stage, TCR rearrangement begins (35,43). At this point, the *Tcrb* gene undergoes random rearrangements, encoding the TCRβ chain. In parallel, *Tcrd* and *Tcrg* genes also recombine to generate the TCRδ and TCRγ chains, giving rise to a much smaller subset of T cells. This subset corresponds to γδ T cells and diverges at the DN2 stage from αβ T cells. At the DN3 stage, in the case of αβ T cells, TCRαβ formation initiates with the assembly between the newly formed TCRβ chain and an invariant pre-Tα and CD3 subunits to form the pre-TCR (43). If the *Tcrb* rearrangement results in a functional TCRβ chain, signaling through the pre-TCR leads to high proliferation and progression to DN4. If the process fails due to the formation of a non-coding TCRβ chain, thymocytes are not able to receive proliferation signals and die. This set of events occurring at the DN3 stage constitutes the first checkpoint during thymocyte differentiation and is known as beta selection (44).

At the DP stage, in the cortex, rearrangement of *Tcra* genes for the TCRα chain occurs and the TCRαβ is completely formed (45). Here, thymocytes contact with cTECs presenting MHC-peptide complexes, where the peptide is usually composed by self-peptides derived from cellular metabolism (35). If the TCR is capable of recognizing those MHC-peptide complexes, thymocytes proceed to differentiate into SP thymocytes, in an event named positive selection. The ones that do not recognize MHC-peptide complexes undergo death by neglect. Also, if the affinity/avidity of the interaction with MHC-peptide complexes is excessive to the point of TCR autoreactivity, thymocytes may be deleted at this stage (negative selection) (46).

DP thymocytes that continue the differentiation process migrate to the medulla to reach the SP stage. The medulla is a specialized site for negative selection, eliminating thymocytes reactive to tissue-specific molecules (47). Also, T cell fate is determined: thymocytes interacting with MHC class II molecules become CD4SP, while thymocytes that bind MHC class I become CD8SP (39). In parallel, a minority of cells with strong TCRαβ binding to MHC-peptide complexes manages to escape pro-death molecules such as B cell lymphoma 2 (Bcl-2)-like protein 11 (BIM) and p53 upregulated modulator of apoptosis (PUMA). This occurs due to activation of the signaling pathway Caspase recruitment domain-containing protein 11/NF-kB (CARD11/NF-kB), that acts as a pro-survival stimulus in this context (48). These cells downregulate the expression of CD8 and upregulate forkhead box P3 (FOXP3), becoming regulatory T cells (49).

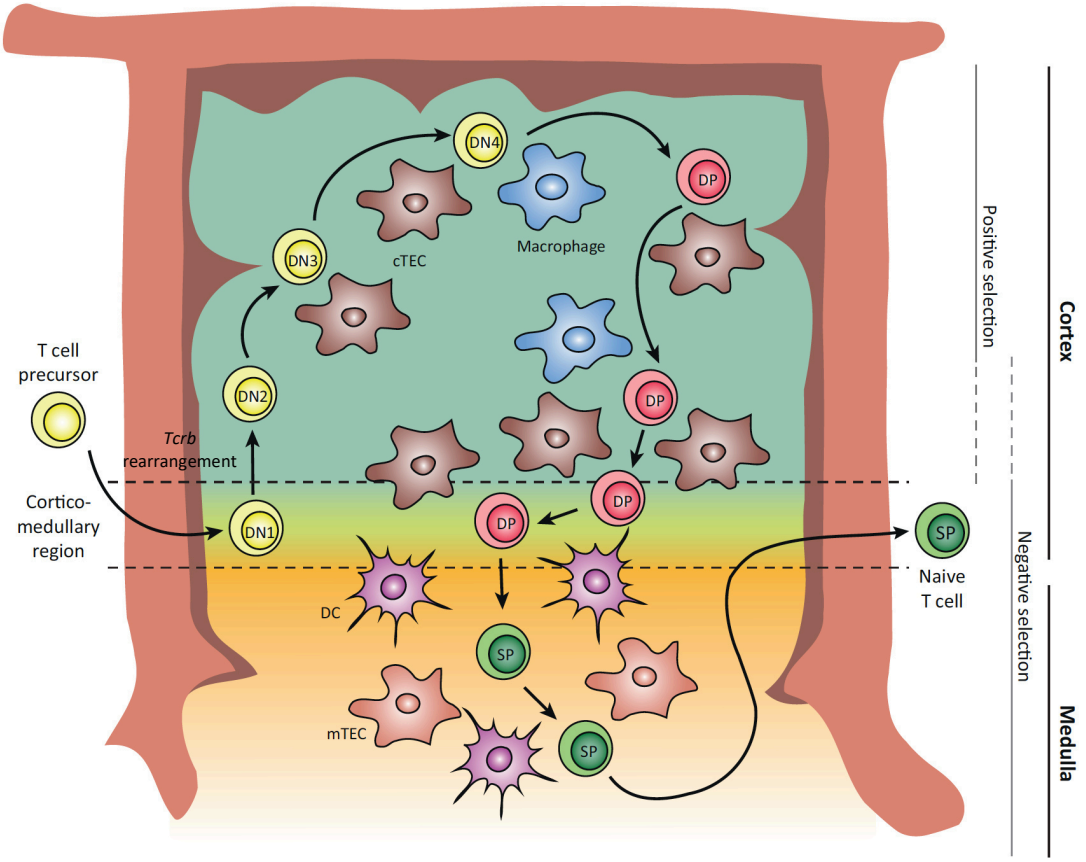

FIGURE 1. T cell differentiation in the mouse. Representation of the main T cell differentiation events, from the BM to the periphery. Adapted from (36).

Cell death by apoptosis plays a central role in T cell differentiation. Two different apoptosis pathways are involved in this process: the intrinsic/mitochondrial and the death receptor/extrinsic pathways (Fig. 2).

The intrinsic apoptosis pathway is controlled by elements of the Bcl-2 protein family, which comprises proteins that are apoptosis initiators (Bcl-2 homology domain 3 (BH3)-only proteins like BIM, PUMA and Phorbol-12-myristate-13-acetate-induced protein 1 (Noxa)), apoptosis effectors (such as Bcl-2 associated X protein (Bax) and Bcl-2 associated death promoter (Bak)) and anti-apoptotic (for instance, Bcl-2, B-cell lymphoma extra-large (Bcl-X_L), Myeloid cell leukemia 1 (Mcl-1)). When activated by BH3-only proteins such as Noxa, pro-apoptotic effector proteins (Bax, Bak) lead to the disruption of the mitochondrial outer membrane, causing the release of factors like cytochrome c and Direct inhibitor of apoptosis binding protein with low pI (DIABLO). This leads to the activation of pro-caspase 9 (50), followed by caspases 3, 6 and 7, culminating in cell death (51).

The extrinsic apoptosis pathway is activated by the binding of external ligands and subsequent signaling through TNF-family receptors (52). As an illustrative example, the TNF-family receptor Fas, when bound to its ligand FasL, leads to the attachment of FADD, which associates with pro-caspase 8. Activation of caspase 8 activates caspase 3 and leads to cell death (53).

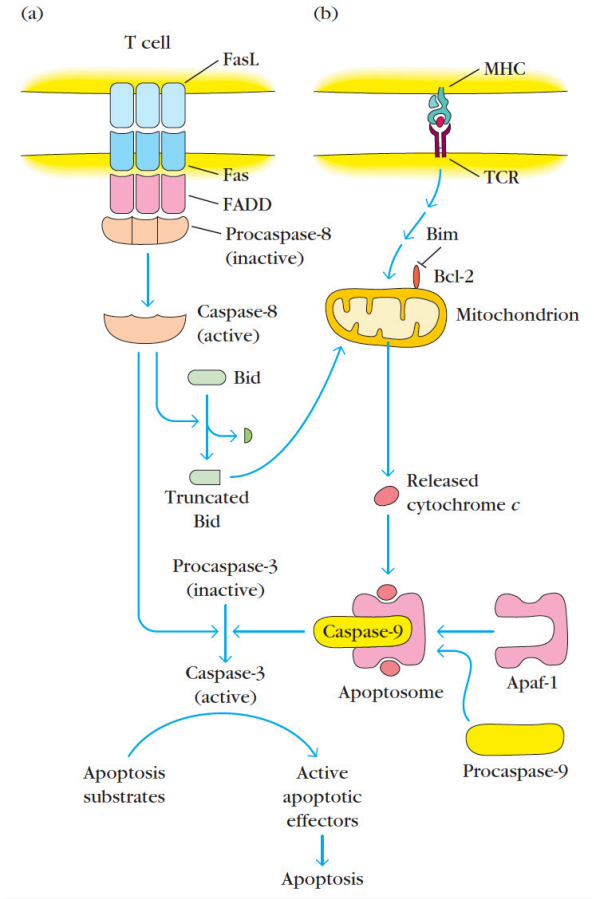

FIGURE 2. Summary of the events occurring in thymocyte apoptosis. a) extrinsic/death receptor pathway; b) intrinsic/mitochondrial pathway. From (35).

In the context of thymocyte differentiation, during beta selection (DN3 stage), both the intrinsic and the extrinsic apoptosis pathways are involved. Bcl-2 upregulation upon functional pre-TCR signaling leads to the inhibition of apoptosis initiators (BIM) and effectors (Bax, Bak), allowing progression to DN4. Also, mice deficient in Bax and Bak present disrupted T cell differentiation at this stage, supporting the involvement of the intrinsic apoptosis pathway in beta selection (54). Yet, a study using mice with severe combined immunodeficiency (SCID) (incapable of productive TCR rearrangement, thus presenting apoptosis of immature thymocytes before beta selection) showed that overexpressing Bcl-2 allowed the progression of B cell but not T cell differentiation (55). Thus, further investigation is needed to fully understand the role of the intrinsic apoptosis pathway in beta selection. On the other hand, inhibiting the

extrinsic pathway in mice lacking RAG expression (thus not being able to perform TCR rearrangement) recovered thymocyte differentiation (56), suggesting a role for this pathway in beta selection.

Death by neglect at the DP stage occurs through the intrinsic apoptosis pathway, as it was shown that overexpression of Bcl-2 allows the survival of thymocytes with a TCRαβ unable to recognize MHC-peptide complexes (55,57). Also, the anti-apoptotic Bcl-X_L is upregulated in cells transitioning from DP to SP and its absence leads to excessive DP apoptosis (58). During positive selection, upon TCRαβ signaling, thymocytes rely on Bcl-2 and Mcl-1 instead of Bcl-X_L to survive (59,60), as a way to compensate for BIM overexpression, which also occurs due to TCRαβ signaling. Still, those are not sufficient to support positive selection, so, DP thymocyte differentiation may also require other signals (55,57).

Negative selection (DP and SP stage) involves the intrinsic apoptosis pathway (61). In general terms, negative selection involves downregulation of Bcl-2 and overexpression of Bax and Bak, and the opposite inhibits thymocyte negative selection via TCR signaling (54,57,62). BIM and PUMA are also necessary as apoptosis initiators (63). Similarly, the steroid receptor Nur77 seems to play a role in promoting negative selection, although the mechanism remains somewhat unclear (64).

The vast majority of thymocytes differentiating within the thymus fail to complete the highly regulated process of thymocyte selection (65), being eliminated. The ones completing the differentiation process exit the thymus and migrate to the periphery as recent thymic emigrants.

1.2.2. Thymic involution

The thymus naturally involutes with age, progressively decreasing in size and T cell export mainly after puberty in humans (66). Age-related thymic involution is also observed in mice (67). Yet, several pathological conditions such as stress (68), radiation (69), estrogens (70,71), chemicals (72,73) and infection may induce premature thymic atrophy. In healthy adults, thymic atrophy does not tend to severely impact the immune system, as T cells stored in secondary lymphoid organs (e.g. spleen and lymph nodes) already express a highly diverse TCR repertoire. However, in young children, whose immune system is still developing, or in immunocompromised individuals experiencing peripheral lymphopenia, thymic atrophy may lead to premature aging of the immune system and render the immune system unable to recover T cell numbers and TCR diversity (74–76).

1.2.3. Infection and premature thymic atrophy

Infection by different microorganisms (bacteria, fungi, viruses, protozoans) can lead to premature thymic atrophy. This pathological involution of the thymus may be caused by immature thymocyte egress (77), thymic stroma disturbances (78), BM T cell precursors alterations that affect the seeding of the thymus (79) and increased thymocyte death (80). This thesis focuses mainly on thymocyte death on the context of *M. avium* 25291 infection-induced thymic atrophy, so microorganisms causing thymocyte death are explored below and summarized in Table 1.

There are several approaches to evaluate thymocyte death, each targeting different events occurring during the process. The techniques used to study infection-induced thymocyte death target loss of membrane asymmetry (by Annexin V stain), DNA fragmentation (by TUNEL assay), cell viability (PI, 7-AAD) and caspase 3 activation (detection of active caspase 3 through colorimetric or fluorescence-based assays).

Often the most affected cells upon thymic infection are DP thymocytes. That is reported for infection with protozoans (*Trypanosoma cruzi* (81)), viruses (HIV-1 (82), strain Chicago-1 of measles (83), murine leukemia virus (84), influenza (A(H1N1)pdm09) strain (85)), fungi (*Paracoccidioides brasiliensis* (86)), bacteria (type A *Francisella tularensis* (87), *Salmonella enterica* serovar *Typhimurium* (80)) and parasites (murine malaria parasite *Plasmodium yoelii* (88)). As DP thymocytes are particularly sensitive to glucocorticoids, several of these and other studies investigated its role in the context of infection by evaluating serum levels, performing adrenalectomies and/or blocking glucocorticoid receptors. Elevated serum levels of glucocorticoids were observed in a model of *Histoplasma capsulatum* infection (89), polymicrobial sepsis (90), type A *F. tularensis* (87), *T. cruzi* (91) and *M. avium* infections (14). Adrenalectomy partially prevented thymocyte depletion in *H. capsulatum* infection (89), *Listeria monocytogenes* (92) and in type A *F. tularensis* infection (87); blocking glucocorticoid receptors also produced the same effect in *M. avium* infection (14), while both approaches combined resulted in prevention of thymic atrophy during *T. cruzi* infection (93). Taken together, these results strongly suggest a pivotal role for glucocorticoids in thymocyte death during infection by different pathogens.

Yet, other molecules are also involved in thymocyte death upon infection, as it is the case of specific pro-inflammatory cytokines. IFNγ contributes to thymocyte death during influenza A(H1N1)pdm09 (85) and *S. typhimurium* infection (80). In type A *F. tularensis* infection, TNF levels (protein in the serum and mRNA in the lung) were shown to be elevated and infected TNF-receptor 1 and 2 KO mice did not present thymic alterations (87). TNF serum levels were also increased after *T. cruzi* infection (81) and polymicrobial sepsis (90), although TNF does not seem to be involved in thymocyte

death in the two latter studies. Conversely, in a model of administration of Mycobacterial Cord Factor from *Mtb*, serum TNF levels were not increased but administration of anti-TNF inhibited thymocyte apoptosis (94).

Alterations in the expression of other molecules in models of premature thymic atrophy, such as downregulation of IL-2 in a rat model of sepsis (95), increase in the levels of IL-10 and IL-1β throughout *T. cruzi* infection (81) and upregulation of interleukin 6 (IL-6) and IFNγ, accompanied by downregulation of IL-2 genes in HIV-1 (96), were also observed and at least partially accounted for thymocyte death in these reports. NO produced via iNOS by IFNγ-activated macrophages together with increased glucocorticoid levels was also shown to be fundamental to induce premature thymic atrophy after infection with a highly virulent strain of *M. avium* (14), although the role of NO in thymocyte death remains undisclosed.

Despite often presenting common players, the mechanisms leading to increased thymocyte death upon infection differ according to the infectious agent, and several players on this process remain unknown, as it is the case for infection with cytomegalovirus (97), Mouse Thymic Virus (98), parainfluenza (99), measles virus (83) and *Paracoccidioides brasiliensis* (86).

Collectively, data highlight the role for systemically produced glucocorticoids and pro-inflammatory cytokines like TNF and IFNγ in thymocyte death induced by infection but also hint at the participation of other molecules that remain to be further explored.

TABLE 1. Summary of the main microorganisms and triggered mechanisms leading to thymocyte death.

Microorganism	Consequence in the thymus	Technique to evaluate cell death	Potentially involved molecules	References
Cytomegalovirus	Necrosis	Histological observation of pyknosis, karyolysis, and karyorrhexis	N/A	(97)
Francisella tularensis (type A)	DP apoptosis	TUNEL assay; DNA fragmentation	Glucocorticoids, TNF 1 and 2	(87)
Histoplasma capsulatum	Thymocyte depletion	N/A	Glucocorticoids	(89)
HIV-1	DP apoptosis	TUNEL assay	IFNγ, IL-6 (increased) IL-2 (decreased)	(96)
Influenza A(H1N1)pdm09 virus	DP apoptosis	Annexin V/PI stain	IFNγ	(85)
Listeria monocytogenes	Thymus weight and cell numbers decreased	N/A	Glucocorticoids	(92)
Measles virus (strain Chicago-1)	DP apoptosis	TUNEL assay	N/A	(83)
Mouse Thymic Virus	Necrosis	Histological observations	N/A	(98)
Murine leukemia virus	DP apoptosis	7-AAD stain; DNA fragmentation; caspase 3 activation	N/A	(84)
Mycobacterium avium 25291	Depletion of the four thymocyte populations	N/A	Glucocorticoids, IFNγ, NO	(14)
Paracoccidioides brasiliensis	DP apoptosis	TUNEL assay	N/A	(86)
Plasmodium yoelii	DP apoptosis	Annexin V stain	N/A	(88)
Salmonella enterica serovar *Typhimurium*	DP apoptosis	Annexin V/PI stain; caspase 3 activation	Glucocorticoids, IFNγ	(80)
Trypanosoma cruzi	DP apoptosis	TUNEL assay	Glucocorticoids, IL-10, IL-1β	(81,91,93)

1.2.4. Thymic infection with mycobacteria

Thymic infection with mycobacteria produces different consequences depending on the mycobacteria species and strain. *Mtb*, *M. avium* and *M. bovis* BCG were shown to colonize the thymus after infection of different mouse strains (100).

After aerosol infection of mice with *Mtb*, bacterial colonization of the thymus is observed three weeks after infection. No granulomas are observed in the thymus, while present in the lung; instead, small macrophage aggregates containing bacteria are found in the medulla and occasionally in the cortex. Additionally, bacterial load stabilizes in the thymus at later infection timepoints in comparison with other organs (100).

Following *M. bovis* BCG intravenous (i.v.) infection, bacterial colonization is only detectable in the thymus when bacterial burden in the lung, liver and spleen is already decreasing (2-3 weeks post-infection) and continue to rise until the ninth week post-infection (100).

In the case of *M. avium*, the most frequently used model relies on i.v. bacterial inoculation to mimic the advanced stage of disseminated infection that may occur in severely immunocompromised individuals (e.g. AIDS patients) (101). *M. avium* infects mainly the thymic medulla and corticomedullary junction, also not forming granulomas but presenting the bacteria engulfed by macrophages (characterized by the expression of CD11c and F4/80) (102). In C57BL/6 mice, the *M. avium* strain of intermediate virulence (2447) infects the thymus, not resulting in thymic atrophy. Yet, this infection affects thymocyte differentiation as it leads to the differentiation of T cells that are specifically tolerant to *M. avium* antigens and unable to control the infection in the periphery when transferred to nude mice (that do not have a thymus – therefore lacking T cell differentiation) (102). In comparison, the highly virulent strain 25291 also colonizes the thymus but progressively induces severe premature thymic atrophy, and leads to a higher bacterial burden. *M. avium* 25291 infection-induced premature thymic atrophy occurs through the synergy between glucocorticoids and NO produced by IFNγ–activated macrophages, as mice: 1) IFNγ KO, 2) iNOS KO, 3) whose macrophages are insensitive to IFNγ or 4) with blocked glucocorticoid receptors do not present thymic atrophy (14). Although these players are known, the mechanisms culminating in *M. avium* 25291 infection-induced premature thymic atrophy are still under investigation. Specifically, NO effects on the BM T cell precursors are now under study while its role on the thymus remains undetermined.

2. AIMS

Although IFNγ and NO are key players underlying *M. avium* infection-induced thymic atrophy, its specific effects and the mechanisms triggered by them are still unknown in this context.

We hypothesized that NO produced by IFNγ-activated macrophages increases thymocyte apoptosis upon infection with *M. avium* 25291. In addition, we questioned if, after infection, NO, IFNγ and other pro-inflammatory molecules are locally produced in the thymus and may be triggering thymocyte apoptosis.

Thus, our main goal was to investigate thymocyte apoptosis as a potential mechanism underlying *M. avium* 25291 infection-induced thymic atrophy and the role of pro-inflammatory molecules in this process.

Specifically, we aim to:

1. Uncover the role of NO and IFNγ in thymocyte death upon *M. avium* 25291 infection, using multicolor flow cytometry and Real-Time PCR (qPCR).
2. Evaluate thymic gene expression of pro-inflammatory molecules involved in other models of premature thymic atrophy, in the context of *M. avium* 25291 infection, using qPCR.

3. MATERIALS AND METHODS

3.1. Mice, housing and welfare

C57BL/6 wild-type (WT) (purchased from Charles River Laboratories (Barcelona, Spain) and bred in our facilities), IFNγ knock-out (IFNγ KO) (bred in our facilities from a breeding pair purchased from The Jackson Laboratory (Bar Harbor, ME)) and iNOS KO (provided by Drs. J. Mudgett, J.D. MacMicking, and C. Nathan, Cornell University, New York; bred in our facilities) 8-12 weeks-old female mice were used in the experiments described below (Topics 3.2 and 3.3). In the case of the dexamethasone control group, male mice were used as we observed no differences in the impact of dexamethasone in the thymus between males and females.

All mice were maintained in standardized conditions (55% humidity, 22-24°C, 12h/12h day/night cycle) under the laws concerning animal welfare (*Decreto-Lei* n. ° 113/2013 *de 7 de agosto*) and approved by the local ethics committee (SECVS 017/2018; Annex 2). Food and water were available *ad libitum* and mice used in infection experiments were weighed weekly, at the same time of the day, to ensure welfare. Humane endpoints were applied for mice presenting signs of decreased activity or any suffering, or that lost more than 20% of body weight in one week. At the end of each experiment, euthanasia was performed through an overdose of Ketamine (150 mg/kg) + Medetomidine (2 mg/kg) injected intraperitoneal (i.p.), followed by lethal blood collection (performed after confirmation of anesthesia) and thoracotomy.

3.2. Dexamethasone administration

C57BL/6 mice were injected i.p. with 1 mg/kg or 3 mg/kg of dexamethasone (Sigma-Aldrich) at 18 h, 18 h and 3 h, or 3 h before euthanasia. A stock of dexamethasone was prepared by dissolving the compound powder in absolute ethanol at 10 mg/mL, followed by dilution in apyrogenic PBS to a concentration of 1 mg/mL. The stock was frozen at -20 °C in 1 mL sterile aliquots and only thawed and diluted in sterile and apyrogenic saline solution at the time of infection.

3.3. Infection with *Mycobacterium avium*

Mice were infected via i.v. injection in the lateral tail vein with 10^6 CFUs of *M. avium* 2447 (provided by Dr. F. Portaels, Institute of Tropical Medicine, Antwerp, Belgium) or *M. avium* ATCC 25291 SmT (obtained from the American Type Culture Collection, Manassas, VA) diluted in saline 0.05% Tween-80. The inoculum was plated on Middlebrook 7H10 agar (BD Biosciences) supplemented with OADC (2.50 g of Bovine albumin fraction V, 1 g of dextrose, 0.002 g catalase 0.025 g of oleic acid and 0.425 g of sodium chloride per 50 mL of dH_2O) and incubated at 37°C for 1 or 2 weeks (strain 2447 and strain 25291, respectively) to confirm inoculum concentration.

To eliminate the interference of the naturally occurring age-related alterations in the thymus, mice were infected at different timepoints (30, 50, 60, 70 days before euthanasia) and euthanized all with the same age, at the same time. Besides confirming inoculum concentration, the infection was also controlled by euthanizing 3 additional mice and evaluating splenic bacterial burden at day 1 of infection. For this, the spleen was removed in sterile conditions, homogenized in H_2O 0.05% Tween-80 and plated at several dilutions in 7H10 agar supplemented with OADC. Colonies of *M. avium* were counted after 1 or 2 weeks (for strain 2447 and strain 25291, respectively). The same method was performed at the end of each experiment, to evaluate splenic bacterial burden in all mice.

3.4. Flow cytometry

Thymocyte death was evaluated by multicolor flow cytometry using two antibody panels: Annexin V/Propidium Iodide (PI) and Caspase 3/Live Dead fixable dye. Both panels included other antibodies to characterize the main thymocyte populations (detailed in Tables 2 and 3).

Annexin V binds to phosphatidylserine, an internal membrane phospholipid that is externalized in the early moments of apoptosis. In turn, PI is a cell-impermeant viability dye that binds nucleic acids and only enters the cell if the membrane is compromised. These markers allowed us to study five populations: viable (Annexin V^-/PI^-), early apoptotic (Annexin V^+/PI^-), apoptotic (Annexin V^+/PI^{int}), late apoptotic/necrotic (Annexin V^+/PI^{high}) and necrotic cells (Annexin V^-/PI^+).

Caspase 3 is a protease often activated in early stages of apoptosis (103) and Live/Dead is a fixable dye that covalently binds to intracellular and extracellular amines present in a cell. This way, Caspase 3/Live Dead staining allowed the distinction between four populations: viable ($Casp3^-$/Live $Dead^{low}$), early apoptotic via caspase 3 ($Casp3^+$/Live $Dead^{low}$), late apoptotic via caspase 3 (Casp3+/Live $Dead^{high}$) and dying/dead cells not via caspase 3 (Casp3/$LiveDead^{high}$).

The whole thymus was mechanically dissociated in cold RPMI 1640 with stable L-Glutamine (Merck) supplemented with a final concentration of 1 mM Sodium Pyruvate (Merck), Penicillin-Streptomycin (final concentrations of 100 units/mL and 100 µg/mL, respectively); Gibco) and 10% heat-inactivated FBS (Merck), to obtain a single-cell suspension. The total number of thymocytes was quantified using an automated cell counter (Countess™, Thermo Fisher Scientific) by Trypan Blue (Gibco) stain cell death exclusion.

For Annexin V/PI staining, 10^6 thymocytes were washed (centrifuged at 1300 rpm, 2 min, 4°C) in FACS Buffer (PBS, 0.3% BSA, 0.01% sodium azide) and stained with 50 µL of the surface antibody mix (Table 1; except PI and Annexin V) diluted in FACS Buffer. After a 20 minute-incubation at 4°C in the dark, thymocytes were washed twice with FACS buffer to remove not-bound antibody excess. Thymocytes were then resuspended in 50 µL of Annexin V Binding Buffer and transferred to FACS tubes. 50 µL of Annexin V/PI mix diluted in Binding Buffer was then added to the cells and incubated for 15 min in the dark at room temperature (RT). Lastly, 200 µL of Annexin V Binding Buffer were added and the samples acquired in the flow cytometer within the next 15 min.

Caspase 3/Live Dead staining was performed in three main steps. First, 10^6 thymocytes were washed in PBS 1x and incubated for 30 min at RT in the dark with fixable Live/Dead dye diluted in 100 µL of PBS 1x. Next, thymocytes were washed with FACS Buffer and stained for surface molecules (similar protocol as in Annexin V/PI staining), using the antibody mix on Table 3 (except Live Dead and Caspase 3). From this point, an intracellular staining was performed to detect active caspase 3. First, thymocytes were fixed with 100 µL of PFA 2% for 30 min in the dark at RT. Then, thymocytes were washed with Perm Buffer (BioLegend, CA, USA), resuspended in 100 µL of Perm Buffer and incubated for 15 min in the dark at RT. Thymocytes were finally incubated for 30 min at RT in the dark with anti-active caspase 3 diluted in 50 µL of Perm Buffer. Finally, thymocytes were washed twice with Perm Buffer and resuspended in 150 µL of FACS Buffer. Samples were transferred to FACS tubes and acquired in the flow cytometer within the next 24 hours.

Unstained, single-color stained and Fluorescence Minus One (FMO) controls (for CD25, CD44, Annexin V, PI, Caspase 3 and Live Dead) were performed for compensation of fluorochrome spillover at the flow cytometer and gating design during the analysis.

All samples were acquired in a BD LSR II flow cytometer (BD Biosciences, CA, USA) equipped with 3 lasers (488 nm, 640 nm, 405 nm) and with the BD FACSDiva software. The analysis was performed in FlowJo® 10 (BD Biosciences, CA, USA). A schematic example of the gating strategies used is presented in Annex 1.

TABLE 2. Antibody panel for Annexin V/PI assay in total thymocytes.

Specificity	Clone	Fluorochrome	Brand	Dilution
CD3	145-2C11	FitC	BioLegend	1:100
CD4	RM4-5	BV421	BioLegend	1:100
CD8	53-6.7	BV510	BioLegend	1:200
CD25	PC61	APC-Cy7	BioLegend	1:100
CD44	IM7	BV605	BioLegend	1:200
PI	—	—	Sigma	1:50
Annexin V	—	Alexa 647	BioLegend	1:25

TABLE 3. Antibody panel for Caspase 3/Live Dead assay in total thymocytes.

Specificity	Clone	Fluorochrome	Brand	Dilution
CD3	145-2C11	Pe	BioLegend	1:100
CD4	RM4-5	FitC	BioLegend	1:100
CD8	53-6.7	BV510	BioLegend	1:200
CD25	PC61	APC-Cy7	BioLegend	1:100
CD44	IM7	PeCy7	BioLegend	1:400
Fixable Live/Dead dye	—	eFluor 450	Thermo Fisher Scientific	1:1000
Active caspase 3	C92-605	Alexa 647	BD Biosciences	1:20

3.5. RNA extraction

Total RNA was extracted from half of the thymus (except for 70 dpi, where the whole thymus was used due to severe atrophy) using TRIzol™ Reagent (Invitrogen). Previously frozen thymi (-80 °C) were homogenized in cold TRIzol (1 mL per 50-100 mg of tissue) using a 23G needle and 1 mL syringe, after which thymi homogenates were frozen at -80 °C for 1 or 2 days. When thawed, homogenates were incubated at room temperature for 5 min. Next, chloroform (0.2 mL per 1 mL of TRIzol™ Reagent) was added, the samples thoroughly mixed and incubated for 2-3 min. A centrifugation step (12000 *g*, 15 min, 4 °C) followed, separating the mixture into a lower red phenol-chloroform (protein fraction), an interphase (DNA) and a colorless upper aqueous phase (RNA). The RNA phase was carefully transferred to a new tube and 1 µL of glycogen was added to aid in RNA precipitation. Then, isopropanol (0.5 mL per 1 mL of TRIzol™ Reagent) was added, gently mixed and incubated for 10 min at room temperature. A

centrifugation step (12000 *g*, 10 min, 4 °C) was then performed to precipitate the RNA, forming a pellet in the bottom. The supernatant was discarded and the pellet washed with 75% ethanol (brief vortexing followed by centrifugation at 7500 *g*, 5 min, 4 °C). Next, the supernatant was discarded and the pellet air-dried for 5 min. RNA was resuspended in 15-30 µL of UltraPure™ distilled water (Invitrogen). Finally, RNA was incubated at 57 °C on a heat block for 10 min to fully dissolve the pellet and stored at -80 °C.

RNA was quantified using NanoDrop 2000 (Thermo Scientific) and 1 µg was run on a 1% agarose gel to check for degradation (120 V, 25 min). RNA was considered intact when two sharp bands corresponding to 18S and 28S rRNA subunits were present.

All materials and reagents used while handling RNA were RNase-free to prevent its degradation.

3.6. cDNA synthesis

Complementary DNA (cDNA) was synthesized using iScript™ Advanced cDNA Synthesis Kit for RT-PCR (Bio-Rad Laboratories). Briefly, 4 µL of 5x iScript Advanced Reaction Mix and 1 µL of iScript Advanced Reverse Transcriptase were added to 3 µg of RNA and toped up with nuclease-free water to a final volume of 20 µL. Samples were submitted to an incubation of 46 °C for 20 min, followed by enzyme inactivation (95 °C for 1 min), and stored at -20 °C.

3.7. Real-Time PCR

Real-Time Quantitative PCR (qPCR) was performed to measure expression levels of several genes associated with cell death (*Bax*, *Bcl-2*), premature thymic atrophy (*Gr*, *Ifng*, *Il6*, *Inos*, *Tnf*) and housekeeping genes (*18S*, *Gapdh*, *Hprt*) (Table 4). One reaction included 1 µL of cDNA, 10 µL of SsoFast EvaGreen Supermix (Bio-Rad Laboratories), 0.2 µL of each primer (at 50 µM; STAB VIDA) and nuclease-free water up to a final volume of 19 µL. A cDNA serial dilution curve was performed in every analysis to control for reaction yield. All qPCRs were done using Hard-Shell® 96-Well PCR Plates (white bottom) (Bio-Rad Laboratories).

Amplification conditions involved a step of initial denaturation at 95 °C for 1 min, 40 cycles of denaturation at 95 °C for 15 s, annealing for 20 s and elongation at 72 °C for 20 s; and a final step to generate the melting curve (65 – 95 °C, increments of 0.5 °C per 5 s).

Gene expression data were analyzed on CFX™ Manager (Bio-Rad Laboratories) using the "Gene Study" function and exported to Microsoft Excel™ for further calculations.

TABLE 4. Genes analyzed by qPCR: corresponding primer sequences and annealing temperature.

Target gene	Annealing temperature (°C)	Primer sequence (5' -> 3')
18S rRNA	58	F: GTA ACC CGT TGA ACC CCA TT
		R: CCA TCC AAT CGG TAG TAG CG
Bax	58	F: GTC CAC CAA CAA GCT GAG CG
		R: TGG GAA AAA GAC CTC TCG GG
Bcl-2	58	F: CCT GGT GCA CAA CAT CGC C
		R: AAT CAA ACA GAG GCC GCA TGC
GAPDH	58	F: GGG CCC ACT TGA AGG GTG GA
		R: TGG ACT GTG GTC ATG AGC CCT T
GR	58	F: AGA GCA GTG GAA GGA CAG CAC A
		R: GCA GCG CGG CAG GAA CTA TT
HPRT	58	F : GCT GGT GAA AAG GAC CTC T
		R: CAC AGG ACT AGA ACA CCT GC
IFNγ	58	F: CAA CAG CAA GGC GAA AAA GG
		R: GGA CCA CTC GGA TGA GCT CA
IL-6	59	F: CCG GAG AGG AGA CTT CAC AG
		R: TCC ACG ATT TCC CAG AGA AC
iNOS	59	F: CTC GGA GGT TCA CCT CAC TGT
		R: GCT GGA AGC CAC TGA CAC TT
TNF	58	F: ACT TCG GGG TGA TCG GTC CCC
		R: GTG GTT TGC TAC GAC GTG GGC TA

F=forward; R=reverse.

3.8. Statistical analysis

Four to eight mice were used *per* group. Late-stage infected mice comprised the larger groups as they are more likely to reach humane endpoints during infection, thus requiring premature euthanasia.

Statistical analyses were performed using Prism GraphPad 7 (GraphPad Software, La Jolla, California, USA). Data are reported as the mean + standard deviation (SD). For gene expression data, individual fold change was calculated in Excel™, using the formula: (Mean value – Baseline)/Baseline. Outliers (only in gene expression analysis) were calculated and removed using Grubbs' test (https://www.graphpad.com/quickcalcs/grubbs1/). Significance level was set at 0.05: p values lower than 0.05 were considered statistically significant differences.

The normal distribution of the data was tested using Shapiro-Wilk test and variances equality was tested with Levene's test. Differences between groups were evaluated using one-way or two-way ANOVA followed by Sidak's post-hoc test.

4. RESULTS

4.1. Development of a positive control for thymocyte apoptosis using dexamethasone administration

One of the goals of this work was to evaluate thymocyte death, so it was essential to develop a positive control for apoptosis. The premises for a good positive control of thymocyte apoptosis in the context of thymic atrophy are: 1) thymic atrophy induction (reduction in thymus weight and thymocyte numbers) and 2) clear positive staining for apoptosis markers (Annexin V and/or active caspase 3) in thymocytes.

Dexamethasone is a widely used drug known to cause thymocyte depletion by apoptosis, affecting mainly the DP population (104,105). Taking advantage of this we optimized dexamethasone i.p. administration in C57BL/6 mice to achieve the premises needed. The different concentrations and timepoints of administration that were tested are summarized in Table 5.

TABLE 5. Conditions tested for optimization of dexamethasone administration in C57BL/6 mice.

Dexamethasone dosage	Time of injection before euthanasia
No dexamethasone (vehicle only)	18h / 18+3h / 3h
1 mg/kg	18 h
3 mg/kg	
1 mg/kg	18+3 h
3 mg/kg	
1 mg/kg	3 h
3 mg/kg	

Both concentrations tested (1 mg/kg and 3 mg/kg), administered either 18 h (one injection) or 18 and 3 h (two injections) before euthanasia were similarly efficient at significantly reducing thymus weight and thymocyte numbers (Fig. 3).

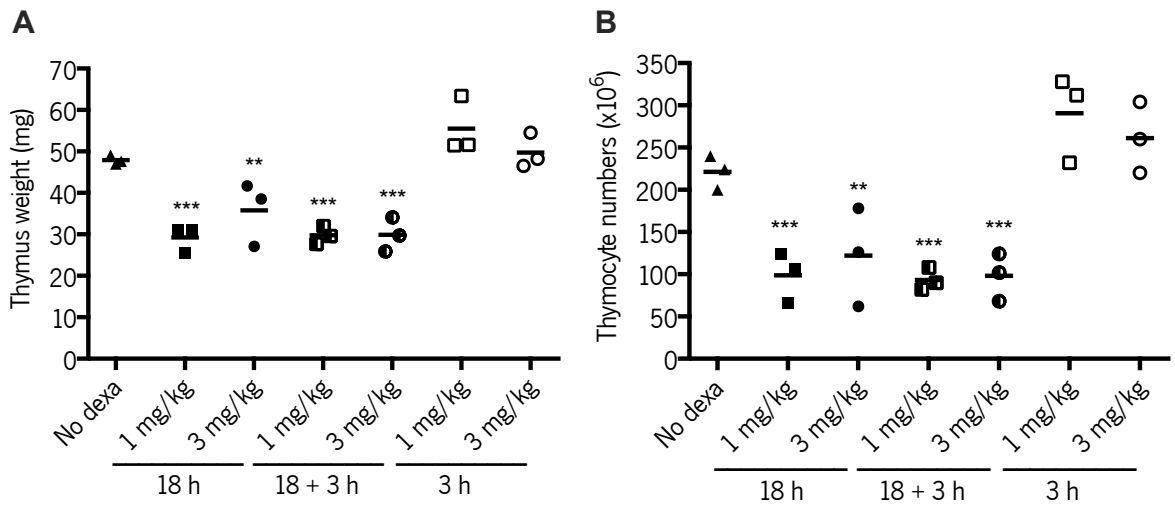

FIGURE 3. Administration of 1 mg/kg of dexamethasone 18 h before euthanasia is sufficient to induce thymic atrophy. (A) Thymus weight and **(B)** total thymocyte numbers after dexamethasone administration. Each dot represents one mouse (*n*=3 mice/group from one experiment). *p<0.05, **p<0.01, ***p<0.001, ****p<0.0001 compared to mice that received vehicle solution (no dexa), using two-way ANOVA and Sidak's post-hoc test.

Yet, we observed that the only condition that leads to a decrease in the percentage of DP thymocytes is 3 mg/kg administered twice, at 18 and 3 h (Fig. 4A). This condition was also the one causing the biggest reduction on the percentage of viable (Annexin V^-, Pi^-) and the highest increase in the percentage of early apoptotic thymocytes (Annexin V^+, Pi^-) (Fig. 4B).

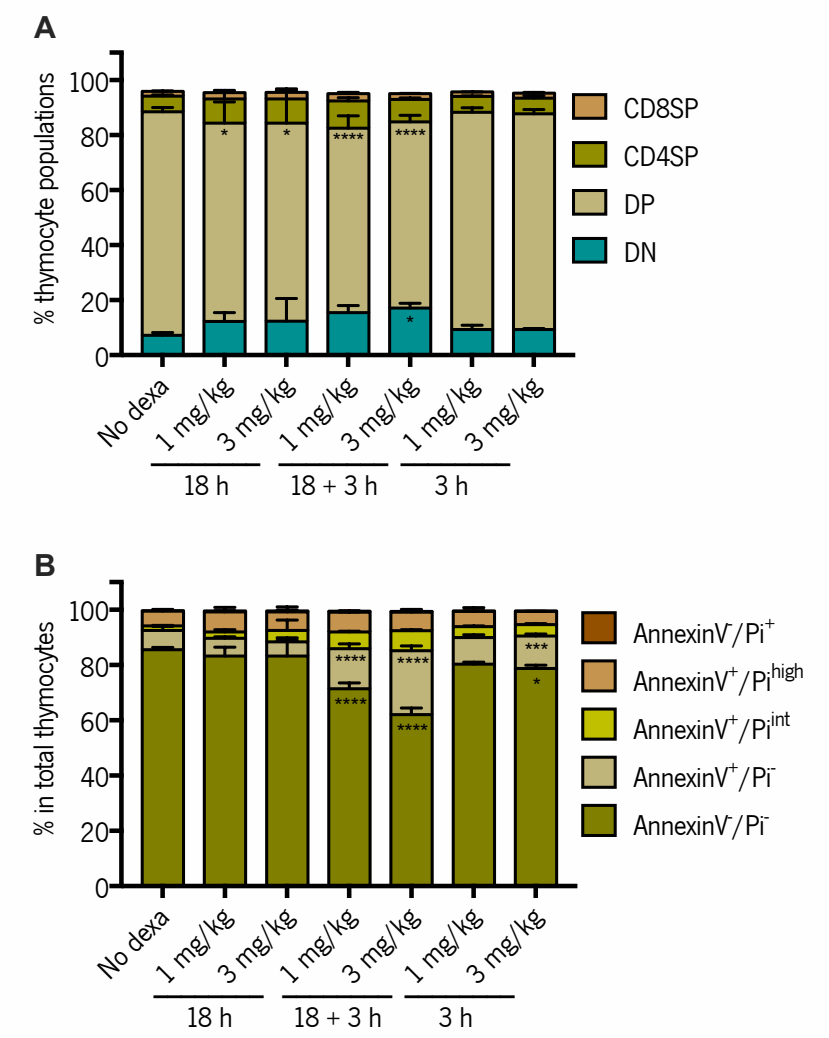

FIGURE 4. Administration of 3 mg/kg of dexamethasone 18 h and 3 h before euthanasia causes the highest increase in DP thymocyte apoptosis. (A) Percentage of main thymocyte populations after different conditions of dexamethasone administration, assessed by flow cytometry. **(B)** Percentage of viable (Annexin V^-/PI^-), early apoptotic (Annexin V^+/PI^-), apoptotic (Annexin V^+/PI^{int}), late apoptotic/necrotic (Annexin V^+/PI^{high}) and necrotic (Annexin V^-/PI^+) total thymocytes. Columns represent mean+SD. (*n*=3 mice/group from one experiment). *p<0.05, **p<0.01, ***p<0.001, ****p<0.0001 compared to mice that received vehicle solution (no dexa), using two-way ANOVA and Sidak's post-hoc test.

Additionally, we evaluated apoptosis within the four main thymocyte populations. It is clear that upon two dexamethasone injections (18 + 3 h) the most affected population is DP thymocytes, and the strongest effect occurs with 3 mg/kg, as observed by the biggest decrease in the percentage of viable thymocytes and increase in the early apoptotic ones (Fig. 5B). Thus, we selected the administration of 3 mg/kg of dexamethasone 18 and 3 h before euthanasia as a positive control to study thymocyte apoptosis.

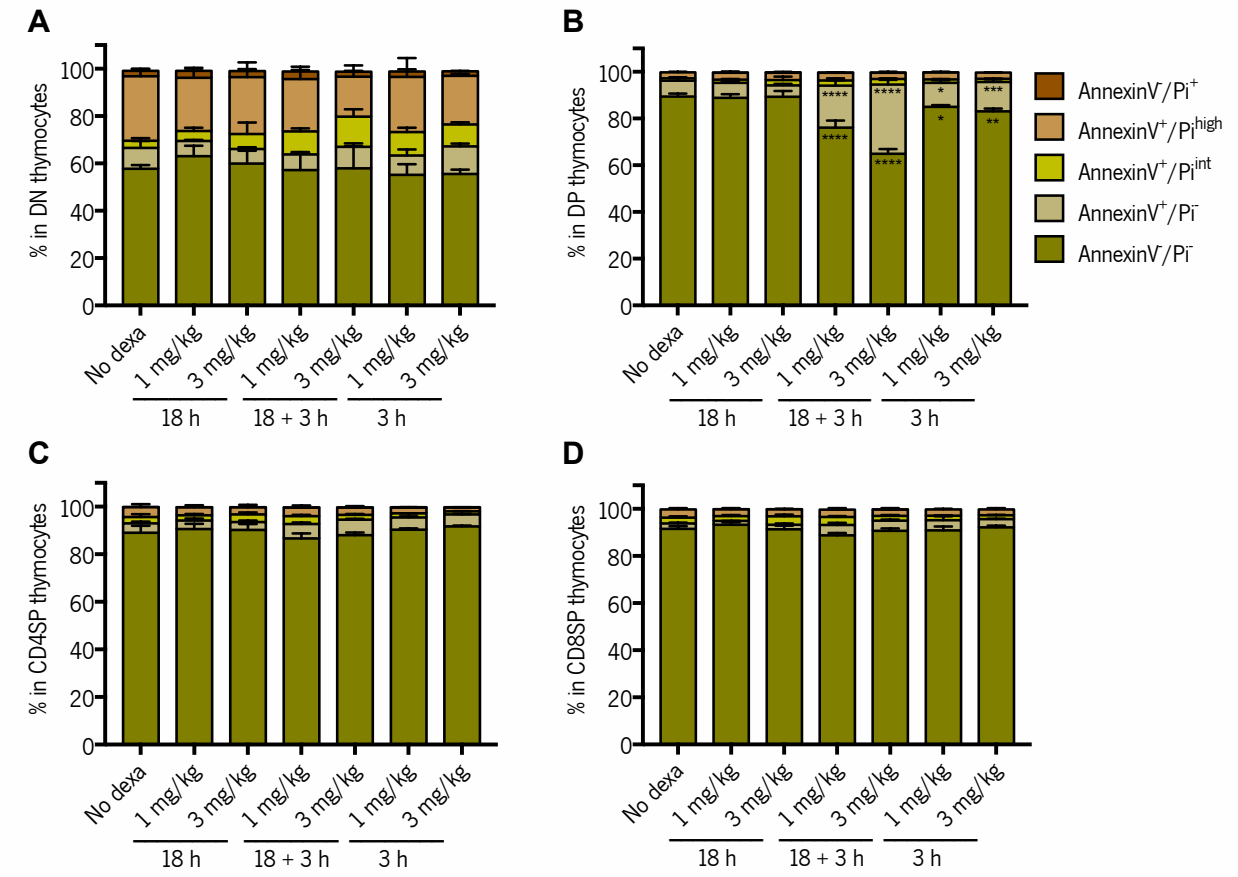

FIGURE 5. The administration of 3 mg/kg of dexamethasone 18 h and 3 h before euthanasia induces apoptosis specifically on DP thymocytes. Percentage of viable (Annexin V$^-$/PI$^-$), early apoptotic (Annexin V$^+$/PI$^-$), apoptotic (Annexin V$^+$/PI^{int}), late apoptotic/necrotic (Annexin V$^+$/PI^{high}) and necrotic (Annexin V$^-$/PI$^+$) on **(A)** DN; **(B)** DP; **(C)** CD4SP and **(D)** CD8SP thymocytes. Columns represent mean+SD. (n=3 mice/group from one experiment). *p<0.05, **p<0.01, ***p<0.001, ****p<0.0001 compared to mice that received vehicle solution (no dexa), using two-way ANOVA and Sidak's post-hoc test.

As dexamethasone is known to activate the intrinsic apoptosis pathway, we also evaluated the gene expression of *Bax* and *Bcl-2* in thymocytes. *Bax/ Bcl-2* ratios higher than 1 are indicative of apoptosis, as *Bax* is a pro-apoptotic molecule and *Bcl-2* is anti-apoptotic. Curiously, the condition that causes more thymocyte apoptosis presents ratios around 1, lower than in controls. This is also true for all the groups injected 3 h before euthanasia (Fig. 6).

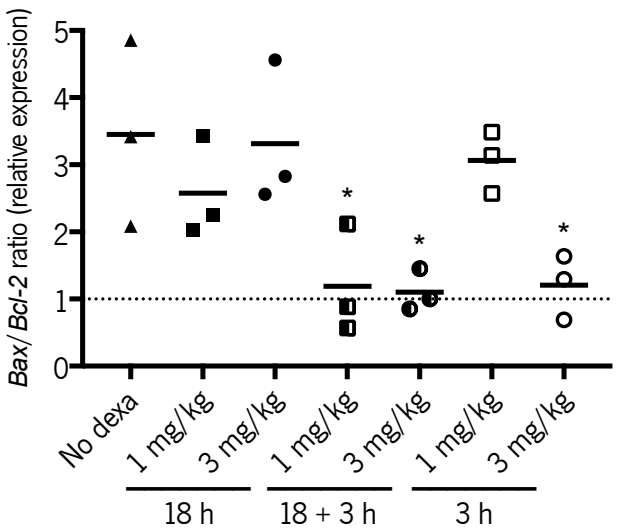

FIGURE 6. *Bax/ Bcl-2* ratio is decreased upon administration of 3 mg/kg of dexamethasone 18 and 3 h before euthanasia. *Bax/ Bcl-2* (pro-apoptotic/anti-apoptotic genes) ratio (from relative expression values) in the thymus measured by qPCR. Relative expression was normalized to *18S*, *Hprt* and *Gapdh* housekeeping genes. Each dot represents one mouse (n=3 mice/group from one experiment). *p<0.05 compared to mice that received vehicle solution (no dexa), using two-way ANOVA and Sidak's post-hoc test. Dashed line on ratio=1.

4.2. Thymocyte death by apoptosis is involved in *M. avium* infection-induced thymic atrophy

In the context of *M. avium* 25291 infection, we studied thymocyte death as a potential mechanism of premature thymic atrophy and the involvement of key players in the process.

4.2.1. Infection by *M. avium* 25291 induces thymocyte apoptosis

As *M. avium* infection with the highly virulent strain 25291, but not with the strain of intermediate virulence 2447, progressively leads to severe premature thymic atrophy, we investigated if this was associated with alterations in thymocyte death upon infection. For this, we infected C57BL/6 mice with *M. avium* 2447 or 25291. Mice were sacrificed 30, 60 and 70 days after infection. The variation on mice body weight was monitored throughout the time of infection as a measure of distress. Only mice infected for 60 and 70 days with *M. avium* 25291 lost weight as a result of the infection (Fig. 7A).

We also monitored splenic bacterial load (in colony forming units, CFU) throughout infection and found that, as previously described, in mice infected with strain 25291, bacterial burden continues to rise throughout all infection, while in mice infected with strain 2447, bacterial burden stabilization is already observed at 30 dpi (14) (Fig. 7B).

Moreover, as expected, infection with *M. avium* 25291, but not with *M. avium* 2447, lead to severe thymic atrophy, as shown by a significant and sharp decrease in thymus weight and thymocyte numbers at 60 and 70 dpi (Figs. 7C, 7D).

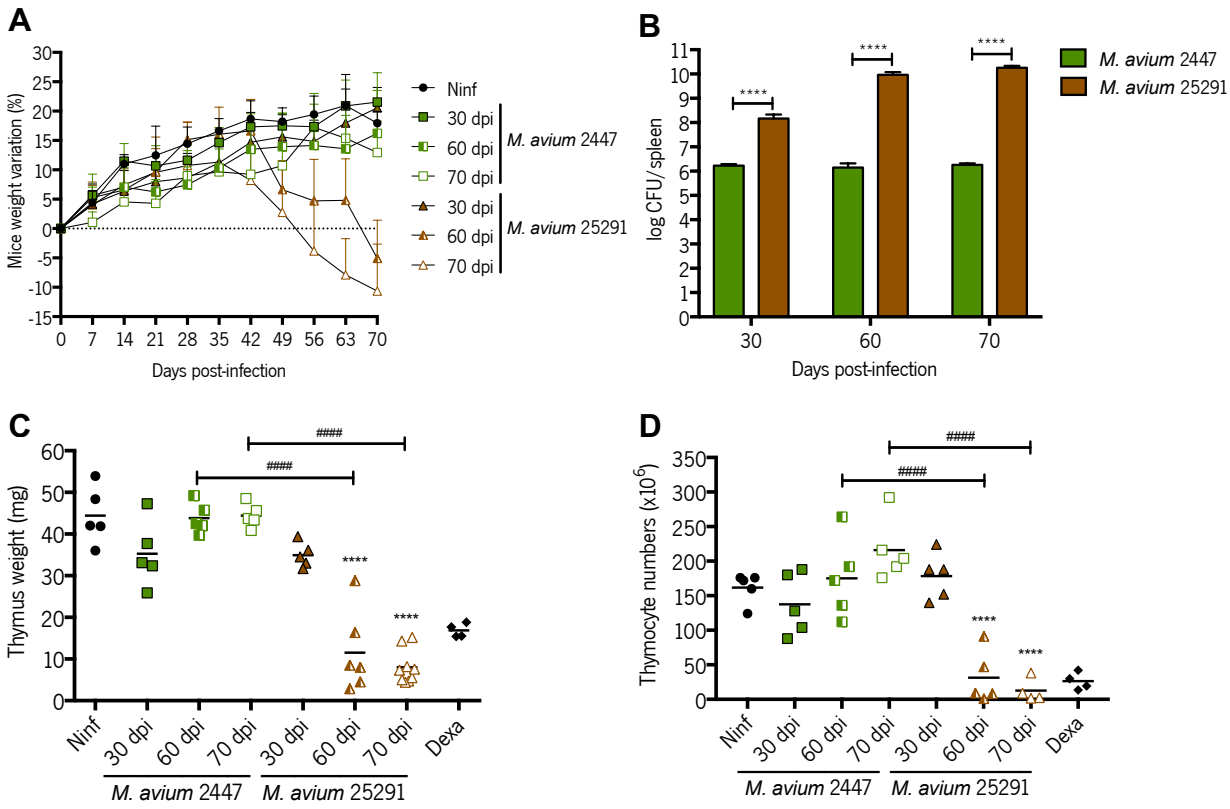

FIGURE 7. *M. avium* 25291, but not 2447, causes body weight loss, continuous increase in bacterial burden and thymic atrophy. (A) Variation on mice weight (%) throughout *M. avium* infection. Data is presented as mean+SD. *n*=5–10 mice/group. **(B)** Splenic bacterial load after 30, 60 and 70 days of infection. Data is presented as log(CFU) of each mouse. *n*=5-10 mice/group. ****p<0.0001 compared between strain 25291 and 2447 at each timepoint, using one-way ANOVA and Sidak's post-hoc test. **(C)** Thymus weight and **(D)** total thymocyte numbers after 30, 60 and 70 days of infection. Each dot represents one mouse (*n*=4-10 mice/group from one experiment). *p<0.05, **p<0.01, ***p<0.001, ****p<0.0001 compared to non-infected mice (ninf), and ####p<0.0001 compared between 2447 and 25291. In all datasets except B, two-way ANOVA and Sidak's post-hoc test were used to determine statistically significant differences. Dexa=positive control for thymocyte apoptosis.

Our results by Annexin V/PI staining show a reduction in the percentage of viable thymocytes (Annexin V^-, PI^-) and a significant increase in early apoptotic (Annexin V^+, PI^-) and apoptotic (Annexin V^+, PI^{int}) thymocytes, in mice infected with *M. avium* 25291 (Fig. 8A). This is true in all infection timepoints becoming more evident as the infection progresses. By contrast, mice infected with strain 2447 exhibited a slight decrease in viable thymocytes and an increase in apoptosis, only at later infection timepoints (60 and 70 dpi).

Given that increased thymocyte apoptosis upon *M. avium* 25291 infection seems to contribute to severe thymic atrophy, we investigated the possible involvement of the intrinsic or extrinsic apoptosis pathway. For that, we evaluated caspase 3 activation by flow cytometry. We observed that 15-20% of the total thymocytes are apoptotic via caspase 3 activation ($Casp^+$/$LiveDead^{low}$ population) in homeostatic conditions (non-infected controls), and that this percentage significantly decreases upon infection with both strains of *M. avium* (Fig. 8B). This result could indicate that infection-induced apoptosis is not occurring via caspase 3 and/or that phagocytes in the thymus rapidly clear active caspase 3-positive thymocytes.

To further investigate the associated mechanism of cell death, we evaluated the gene expression of *Bax* and *Bcl-2* in the total thymus from mice infected for 30, 60, 70 days and found higher expression of *Bax* relatively to *Bcl-2*, as evidenced by *Bax*/*Bcl-2* ratios higher than 1 (Fig. 8C). Moreover, no differences among experimental groups were found, suggesting that the intrinsic apoptosis pathway is not involved in *M. avium* infection-induced thymocyte apoptosis.

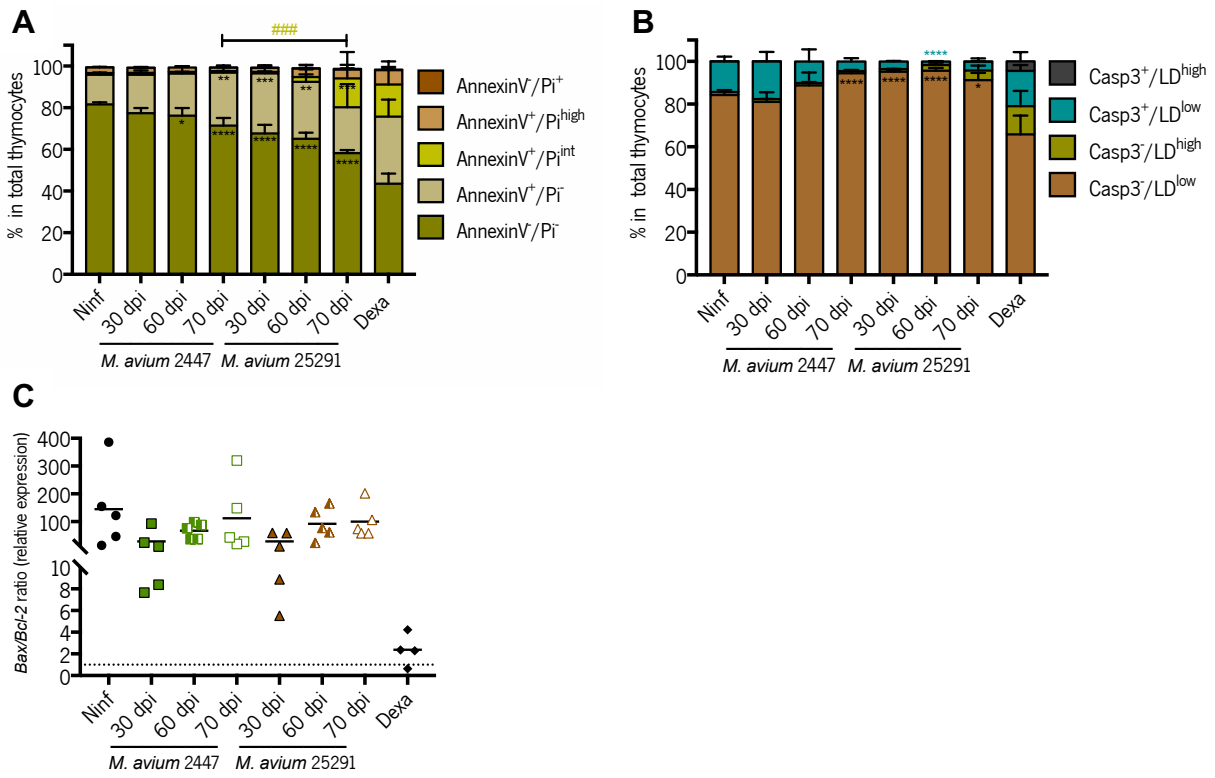

FIGURE 8. ***M. avium*** **infection progressively reduces thymocyte viability and induces thymocyte apoptosis by a mechanism independent of caspase 3 activation and** ***Bax/Bcl-2*****. (A)** Percentage of viable (Annexin V^-/PI^-), early apoptotic (Annexin V^+/PI^-), apoptotic (Annexin V^+/PI^{int}), late apoptotic/necrotic (Annexin V^+/PI^{high}) and necrotic (Annexin V^-/PI^+) total thymocytes. Columns represent mean+SD (*n*=4-5 mice/group from one experiment). *p<0.05, **p<0.01, ***p<0.001, ****p<0.0001 compared to non-infected mice (ninf) and ###p<0.001 compared between bacterial strains within the same infection timepoint. **(B)** Percentage of viable ($Casp3^-$/$LiveDead^{low}$), apoptotic via caspase 3 ($Casp3^+$/$LiveDead^{low}$; $Casp3^+$/$LiveDead^{high}$) and dead/dying not via caspase 3 ($Casp3^-$/$LiveDead^{high}$) total thymocytes. Columns represent mean+SD (*n*=4-5 mice/group from one experiment). *p<0.05, ****p<0.0001 compared to non-infected mice. LD=Live/Dead dye. **(C)** *Bax/Bcl-2* (pro-apoptotic/anti-apoptotic genes) ratio (from relative expression values) in the thymus measured by qPCR. Relative expression was normalized to *18S* and *Hprt* housekeeping genes. Each dot represents one mouse (*n*=4-8 mice/group from two independent experiments). Dashed line on ratio=1. In the three datasets, two-way ANOVA and Sidak's post-hoc test were used to determine statistically significant differences. Dexa=positive control for thymocyte apoptosis.

We further investigated if the alteration in apoptosis was affecting all the main thymocyte populations. Our data show that, similarly to what is observed in total thymocytes, DP, CD4SP and CD8SP thymocyte subsets present a significantly lower percentage of viable cells and a significant increase in the percentage of the early apoptotic ones, which increases throughout infection, mainly with *M. avium* 25291 (Fig. 9). The most affected population is DP thymocytes: viable cells decrease from ≈80% (non-infected control) to ≈60% (70 dpi) (Fig. 9B). A decrease in the percentage of viable thymocytes and increase in apoptosis was also observed in the DN population when comparing non-infected and infected thymi, although no significant differences were found in the percentage of viable thymocytes between bacteria strains or timepoints of infection (Fig. 9A). These results show that *M. avium* 25291 infection leads to increased thymocyte apoptosis in all thymocyte populations. Particularly, apoptosis of SP thymocytes is exclusively occurring after infection by strain 25291 and in DN and DP thymocytes apoptosis is increased at a higher proportion by this bacterial strain when compared to strain 2447.

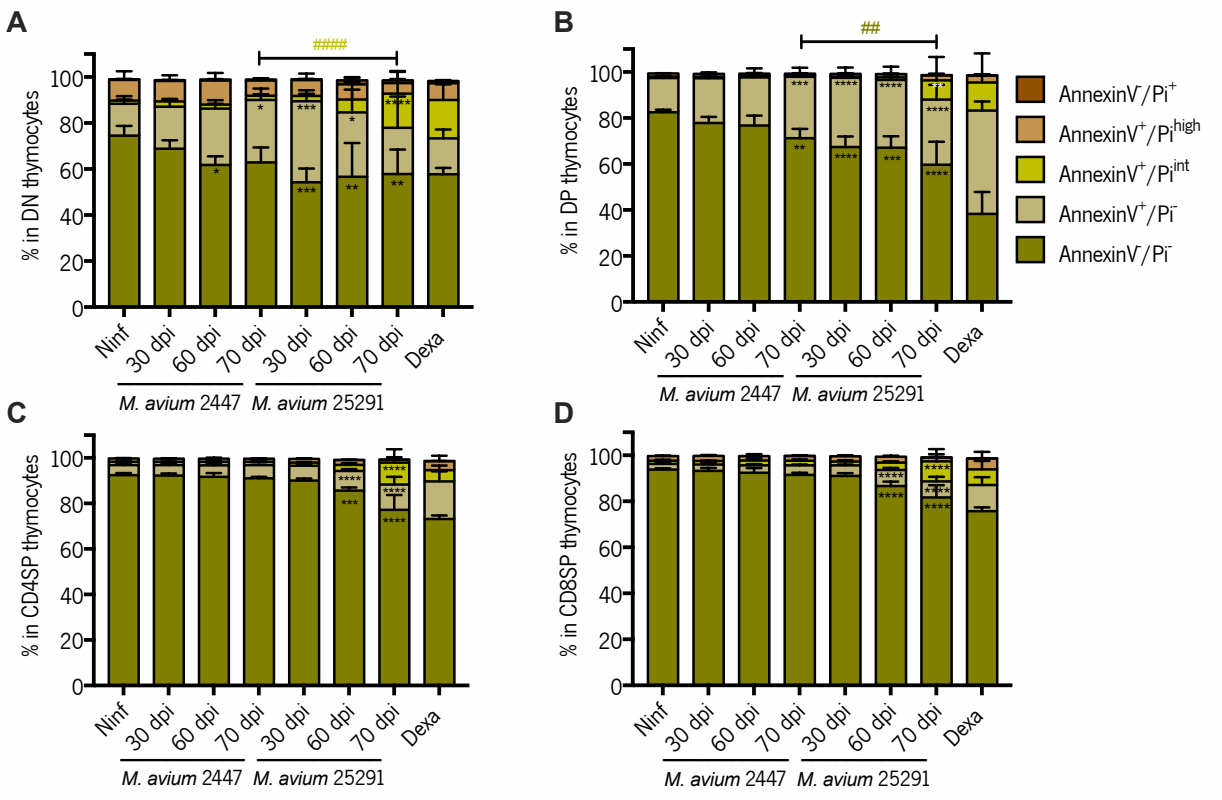

FIGURE 9. *M. avium* 25291 infection progressively reduces viability and increases apoptosis of the four main thymocyte populations. Percentage of viable (Annexin V⁻/PI⁻), early apoptotic (Annexin V⁺/PI⁻), apoptotic (Annexin V⁺/PI^int), late apoptotic/necrotic (Annexin V⁺/PI^high) and necrotic (Annexin V⁻/PI⁺) within **(A)** DN (CD3⁻CD4⁻CD8⁻), **(B)** DP (CD4⁺CD8⁺), **(C)** CD4SP (CD3⁺CD4⁺CD8⁻) and **(D)** CD8SP (CD3⁺CD4⁻CD8⁺) thymocyte populations. Columns represent mean+SD (*n*=4-5 mice/group from one experiment).

*p<0.05, **p<0.01, ***p<0.001, ****p<0.0001 compared to non-infected mice (ninf),. ##p<0.002 and ###p<0.0002 compared between *M. avium* strains at a given infection timepoint, using two-way ANOVA and Sidak's post-hoc test. Dexa=positive control for thymocyte apoptosis.

In respect to caspase 3 activation, we found no significant differences in DN, CD4SP or CD8SP (Figs. 10A, 10C, 10D). DP thymocytes presented a similar profile to the one observed in total thymocytes, showing a decrease in the percentage of thymocytes expressing active caspase 3 upon infection with both *M. avium* strains (Fig. 10B).

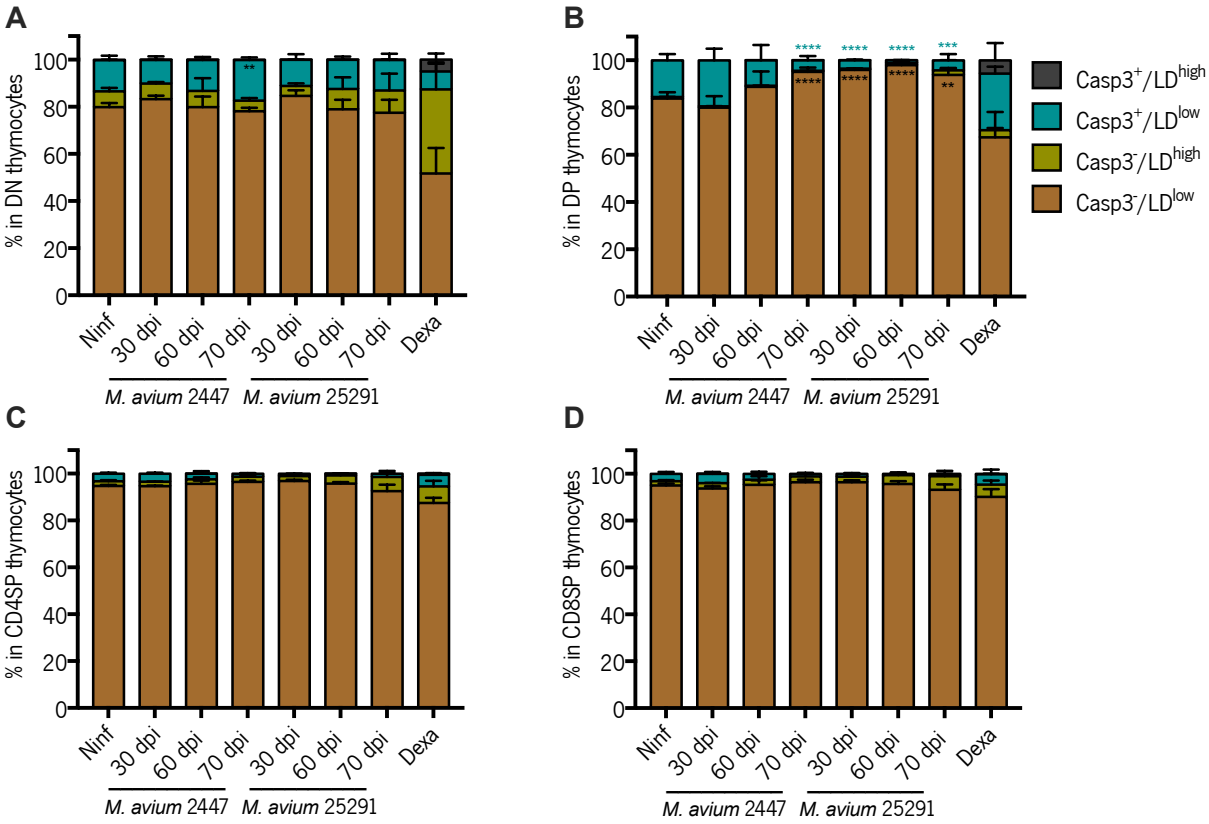

FIGURE 10. The percentage of caspase 3-positive thymocytes within the four main populations decreases or does not alter upon *M. avium* infection. Percentage of viable (Casp3$^-$/LiveDead^{low}), apoptotic via caspase 3 (Casp3$^+$/LiveDead^{low}; Casp3$^+$/LiveDead^{high}) and dead/dying not via caspase 3 (Casp3$^-$/LiveDead^{high}) within **(A)** DN (CD3$^-$CD4$^-$CD8$^-$), **(B)** DP (CD4$^+$CD8$^+$), **(C)** CD4SP (CD3$^+$CD4$^+$CD8$^-$) and **(D)** CD8SP (CD3$^+$CD4$^-$CD8$^+$) thymocyte populations. Columns represent mean+SD (*n*=4-5 mice/group from one experiment). **p<0.01, ****p<0.0001 compared to non-infected mice (ninf), using two-way ANOVA and Sidak's post-hoc test. Dexa=positive control for thymocyte apoptosis. LD=Live/Dead dye.

Concerning the DN thymocytes, we observed that the most immature ones, DN1, present a decrease in the percentage of viable and an increase in apoptotic thymocytes after infection with *M. avium* 25291, but not with 2447 (Fig. 11A). In DN2 and DN3 populations, the same result was observed, although it seems to occur upon infection with both bacterial strains (Figs. 11B, 11C). However, the observed alterations are stronger after infection with strain 25291. The DN4 subset shows no differences in the percentage of viable or apoptotic thymocytes (Fig. 11D).

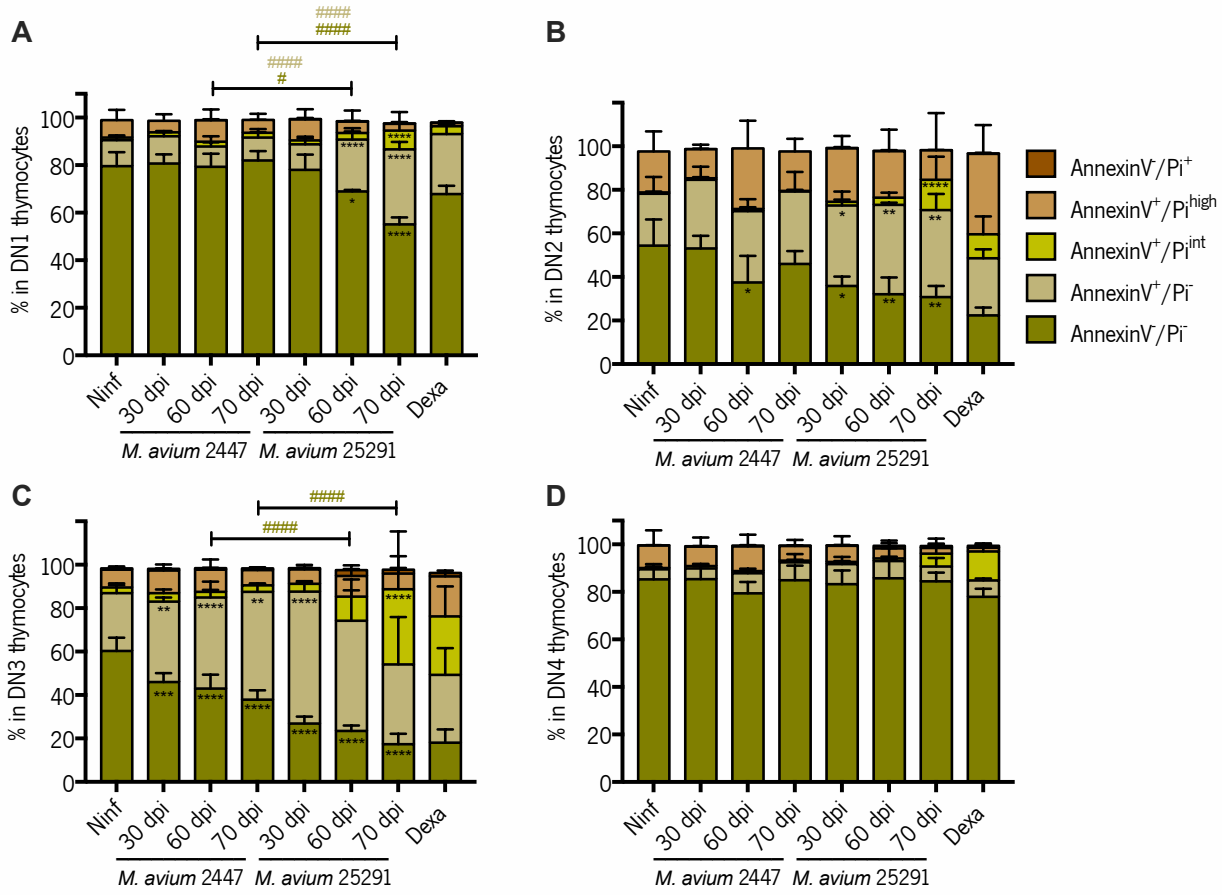

FIGURE 11. Infection with *M. avium* 25291, but not with 2447, increases apoptosis of DN1 thymocytes. Percentage of viable (Annexin V^-/PI^-), early apoptotic (Annexin V^+/PI^-), apoptotic (Annexin V^+/PI^{int}), late apoptotic/necrotic (Annexin V^+/PI^{high}) and necrotic (Annexin V^-/PI^+) within **(A)** DN1 ($CD44^+CD25^-$), **(B)** DN2 ($CD44^+CD25^+$), **(C)** DN3 ($CD44^-CD25^+$) and **(D)** DN4 ($CD44^-CD25^-$) thymocyte populations. Columns represent mean+SD (*n*=4-5 mice/group from one experiment). *p<0.05, ***p<0.001, ****p<0.0001 compared to non-infected mice (ninf). #p<0.05 and ####p<0.0001 corresponds to comparisons between *M. avium* strains, using two-way ANOVA and Sidak's post-hoc test. Dexa=positive control for thymocyte apoptosis.

Alterations in caspase 3 activation also do not seem to occur in any of the DN subpopulations (Fig. 12).

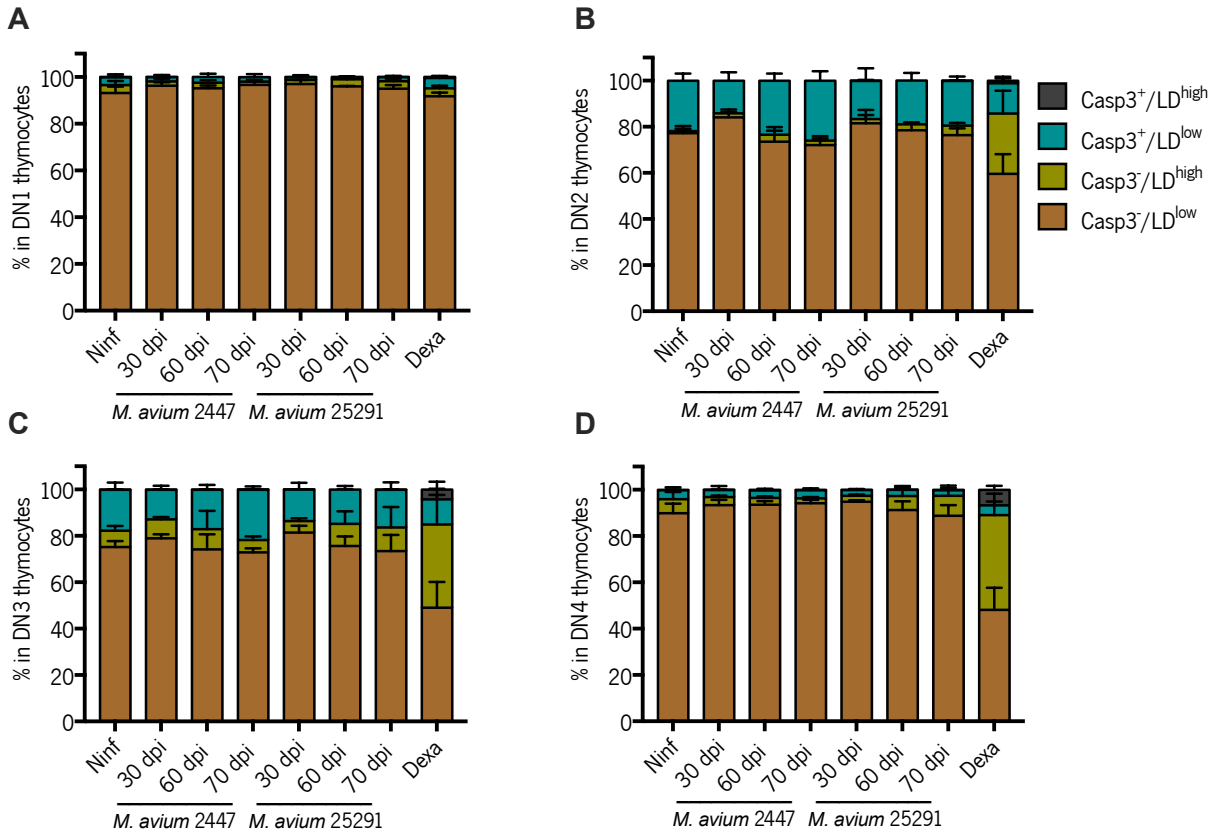

FIGURE 12. The percentage of caspase 3-positive thymocytes within the DN subpopulations does not alter upon *M. avium* infection. Percentage of viable (Casp3$^-$/LiveDead^{low}), apoptotic via caspase 3 (Casp3$^+$/LiveDead^{low}; Casp3$^+$/LiveDead^{high}) and dead/dying not via caspase 3 (Casp3$^-$/LiveDead^{high}) within **(A)** DN1 (CD44$^+$CD25$^-$), **(B)** DN2 (CD44$^+$CD25$^+$), **(C)** DN3 (CD44$^-$CD25$^+$) and **(D)** DN4 (CD44$^-$CD25$^-$) thymocyte populations. Columns represent mean+SD (*n*=4-5 mice/group from one experiment). No statistically significant differences using two-way ANOVA and Sidak's post-hoc test. Dexa=positive control for thymocyte apoptosis. LD=Live/Dead dye.

4.2.2. *M. avium*-induced apoptosis is dependent on IFNγ and NO production at different stages of T cell differentiation

Considering that IFNγ and iNOS are essential for *M. avium* infection-induced thymic atrophy, we investigated their role in the infection-associated thymocyte apoptosis.

Here, we infected C57BL/6 (WT), IFNγ KO and iNOS KO mice with *M. avium* 25291 for 70 days. We evaluated this timepoint because it was the one showing the strongest alterations in thymocyte death.

Mice body weight was monitored during infection to evaluate distress. As previously shown, infected WT, but not IFNγ KO or iNOS KO mice lost weight (Fig. 13A).

Splenic bacterial load was similar between WT and IFNγ KO mice, which is coherent with previous reports (14,106). Also, as expected, iNOS KO mice presented a significantly lower bacterial load (Fig. 13B) (14,106,107).

Results from thymus weight and thymocyte numbers are also coherent with previous studies (14). Infection with *M. avium* 25291 lead to a significant decrease in thymus weight (Fig. 13C) and thymocyte numbers (Fig. 13D), which was not observed in IFNγ or iNOS KO mice.

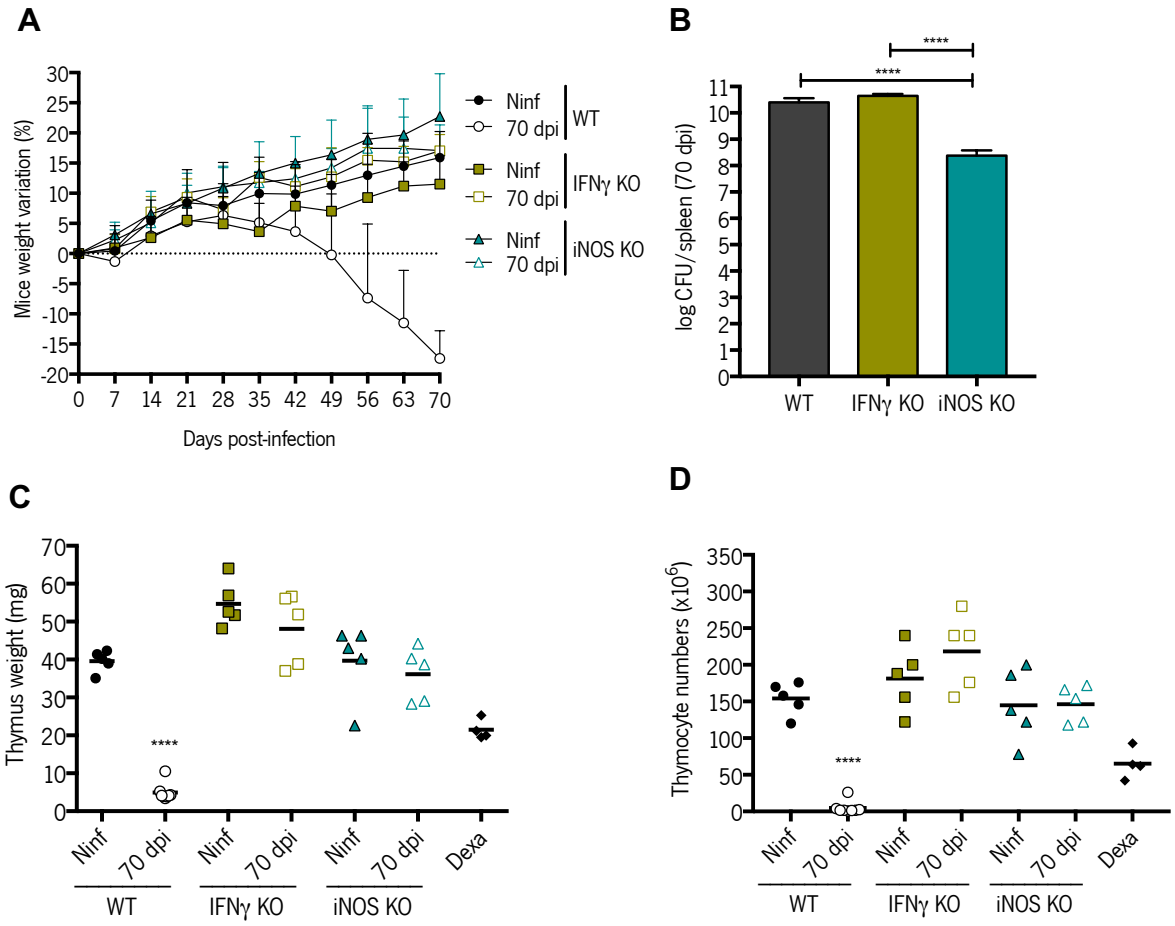

FIGURE 13. *M. avium* 25291 infection causes weight reduction and thymic atrophy on WT but not on IFNγ- or iNOS KO mice. (A) Mice weight variation (%) throughout *M. avium* infection. Data is presented as mean+SD. *n*=5–8 mice/group. **(B)** Splenic bacterial burden at 70 dpi. Columns represent mean+SD. *n*=4–8 mice/group. ****p<0.0001 compared between WT and iNOS KO and ####p<0.0001 compared between IFNγ KO and iNOS KO, using one-way ANOVA and Sidak's post hoc test. **(C)** Thymus weight and **(B)** total thymocyte numbers in WT, IFNγ KO and iNOS KO mice non-infected or infected for 70 days with *M. avium* 25291. Each dot represents one mouse (*n*=5-10 mice/group from one experiment). ****p<0.0001 compared to non-infected counterparts (ninf). In all datasets except B, two-way ANOVA and Sidak's post-hoc test were used to determine statistically significant differences. Dexa=positive control for thymocyte apoptosis.

In respect to total thymocyte death evaluation by Annexin V/PI, we observed a reduction in the percentage of viable thymocytes (Annexin V^-/PI^-) accompanied by an increase in the percentage of early apoptotic (Annexin V^+/PI^-) ones at 70 dpi, regardless of mouse genotype (Fig. 14A).

In accordance with our previous experiment, the percentage of thymocytes positive for active caspase 3 was reduced at 70 dpi with *M. avium* 25291 in WT mice. This also seemed to occur, albeit to a lesser extent, in mice lacking IFNγ or iNOS expression (Fig. 14B).

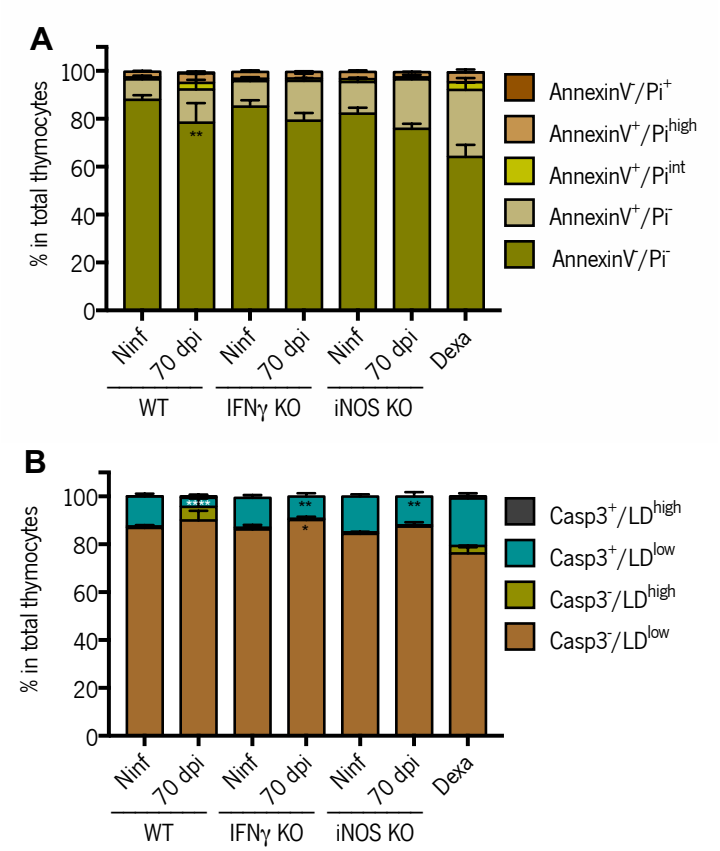

FIGURE 14. IFNγ and iNOS do not play a role in the apoptosis of total thymocytes from *M. avium* 25291-infected mice. (A) Percentage of viable (Annexin V^-/PI^-), early apoptotic (Annexin V^+/PI^-), apoptotic (Annexin V^+/PI^{int}), late apoptotic/necrotic (Annexin V^+/PI^{high}) and necrotic (Annexin V^-/PI^+) total thymocytes. Columns represent mean+SD (*n*=4-10 mice/group from one experiment). *p<0.05, **p<0.01, compared to non-infected counterparts (ninf). **(B)** Percentage of viable ($Casp3^-/LiveDead^{low}$), apoptotic via caspase 3 ($Casp3^+/LiveDead^{low}$; $Casp3^+/LiveDead^{high}$) and dead/dying not via caspase 3 ($Casp3^-/LiveDead^{high}$) total thymocytes. Columns represent mean+SD (*n*=4-8 mice/group from one experiment). *p<0.05, **p<0.01 compared to non-infected counterparts. In both datasets, two-way ANOVA and Sidak's post-hoc test were used to determine statistically significant differences. Dexa=positive control for thymocyte apoptosis. LD=Live/Dead dye.

M. avium 25291 infection does not impact the viability of DN thymocytes in WT, IFNγ KO and iNOS KO, as the percentage of viable thymocytes was similar between infected and non-infected counterparts (Fig. 15A). In DP thymocytes, we found a similar profile to the one observed in total thymocytes, with a reduction on the percentage of viable thymocytes in all host genotypes after infection (Fig. 15B). This suggests no role for IFNγ or iNOS in apoptosis upon *M. avium* 25291 infection, either in DN or DP thymocytes. *M. avium* 25291 infection caused a decrease in the percentage of viable CD4SP and CD8SP thymocytes and an increase in apoptosis in WT mice, but not in the ones lacking IFNγ or iNOS (Fig. 15C, 15D). This suggests that infection-induced SP thymocyte apoptosis is directly or indirectly dependent on both molecules, as the observed effect of IFNγ might be only due to NO, whose production via iNOS depends on IFNγ signaling.

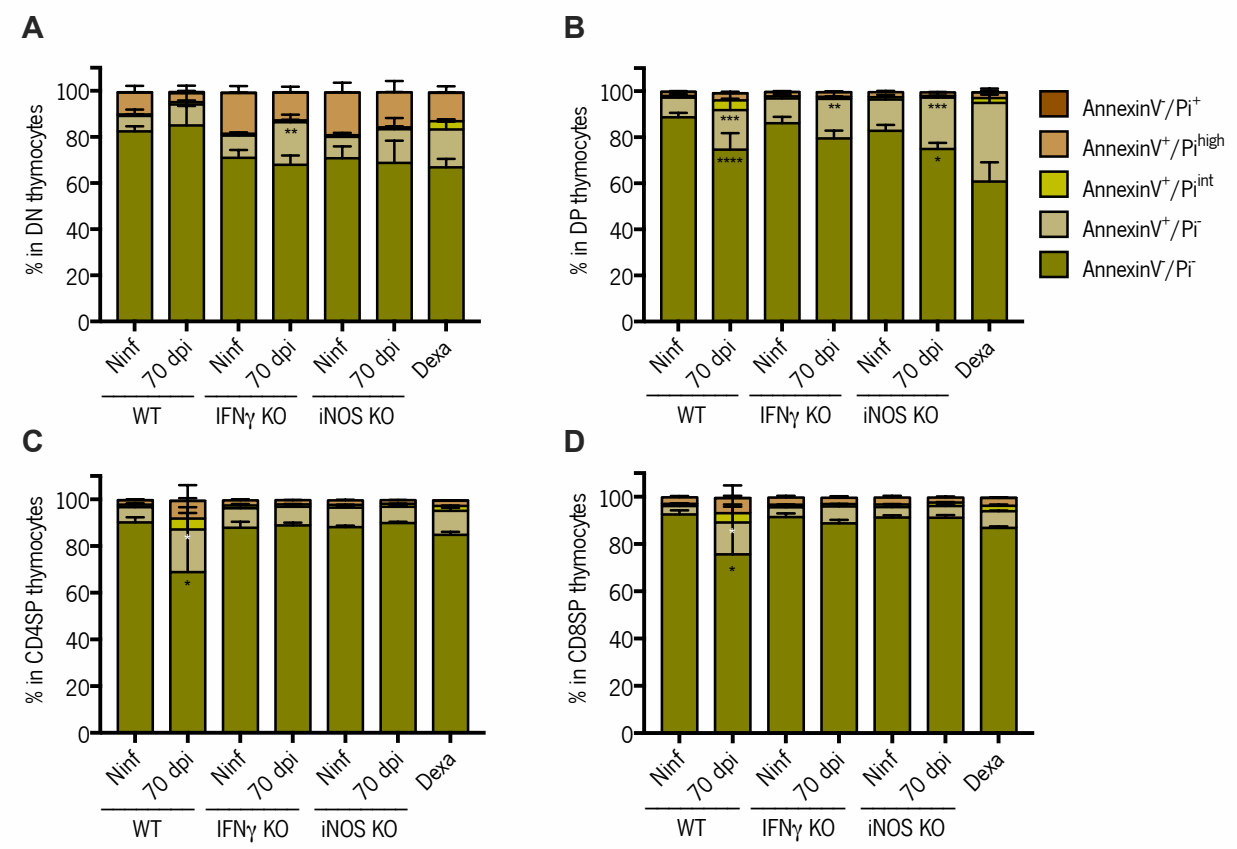

FIGURE 15. *M. avium* 25291 infection-induced apoptosis of SP thymocytes is dependent on IFNγ and iNOS. Percentage of viable (Annexin V$^-$/PI$^-$), early apoptotic (Annexin V$^+$/PI$^-$), apoptotic (Annexin V$^+$/PI^{int}), late apoptotic/necrotic (Annexin V$^+$/PI^{high}) and necrotic (Annexin V$^-$/PI$^+$) within **(A)** DN (CD3$^-$CD4$^-$CD8$^-$), **(B)** DP (CD4$^+$CD8$^+$), **(C)** CD4SP (CD3$^+$CD4$^+$CD8$^-$) and **(D)** CD8SP (CD3$^+$CD4$^-$CD8$^+$) thymocyte populations. Columns represent mean+SD (n=4-9 mice/group from one experiment). *p<0.05, **p<0.01, ***p<0.001, ****p<0.0001 compared to non-infected counterparts (ninf), using two-way ANOVA and Sidak's post-hoc test. Dexa=positive control for thymocyte apoptosis.

In accordance with the previous experiment, the percentage of active caspase 3-positive DN and DP thymocytes from WT mice decreases after 70 days of infection (Figs. 16A, 16B). Furthermore, particularly in the DP subset and similarly to what occurred in total thymocytes, a slight reduction on the percentage of active caspase 3-positive population was also seen in thymocytes from mice lacking the production of IFNγ and iNOS. In CD4SP and CD8SP populations, there were small or no alterations in the percentage of active caspase 3-positive cells.

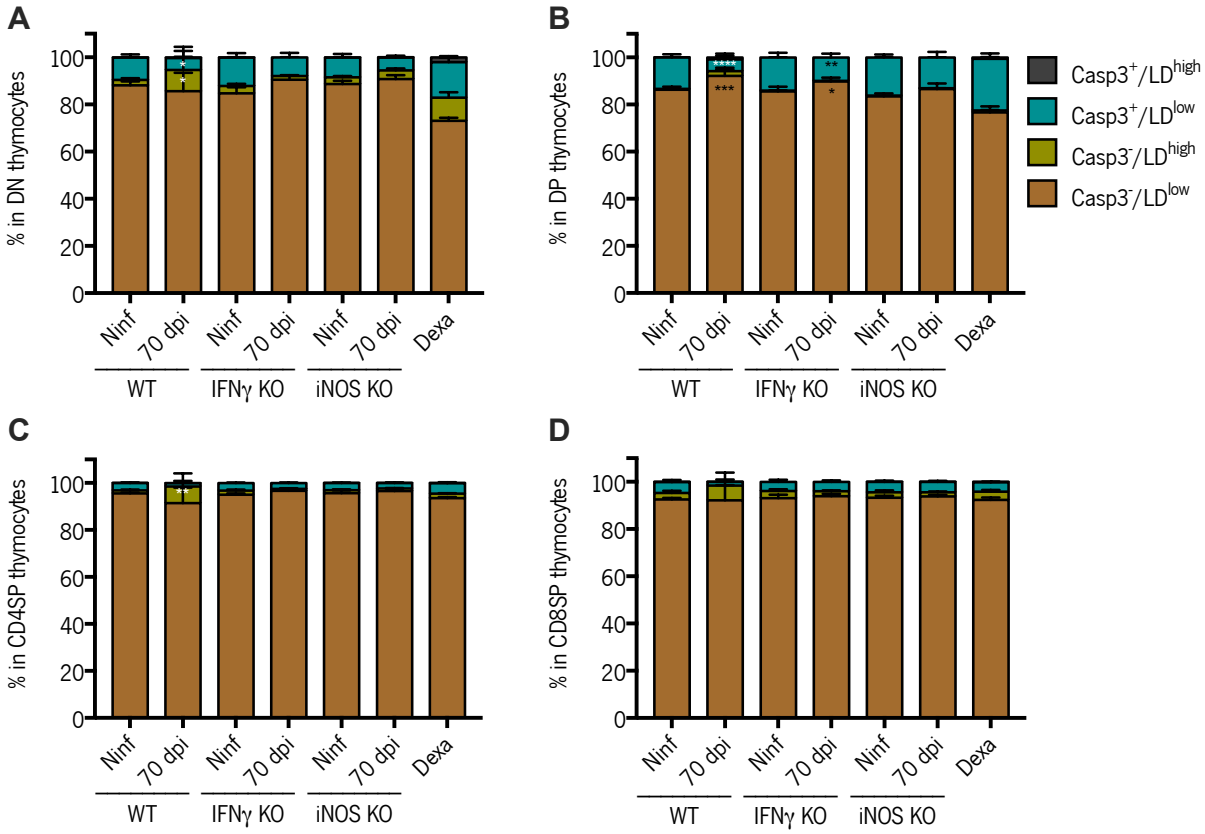

FIGURE 16. The percentage of caspase 3-positive thymocytes within the four main populations decreases or does not alter upon *M. avium* 25291 infection, independently of IFNγ and iNOS expression. Percentage of viable (Casp3$^-$/LiveDead^{low}), apoptotic via caspase 3 (Casp3$^+$/LiveDead^{low}; Casp3$^+$/LiveDead^{high}) and dead/dying not via caspase 3 (Casp3$^-$/LiveDead^{high}) within **(A)** DN (CD3$^-$CD4$^-$CD8$^-$), **(B)** DP (CD4$^+$CD8$^+$), **(C)** CD4SP (CD3$^+$CD4$^+$CD8$^-$) and **(D)** CD8SP (CD3$^+$CD4$^-$CD8$^+$) thymocyte populations. Columns represent mean+SD (*n*=4-9 mice/group from one experiment). *p<0.05, **p<0.01, ****p<0.0001 compared to non-infected counterparts (ninf), using two-way ANOVA and Sidak's post-hoc test. Dexa=positive control for thymocyte apoptosis. LD=Live/Dead dye.

Interestingly, we observed that in the DN1 subset, *M. avium* 25291 infection induced a decrease in the percentage of viable thymocytes, which did not occur in thymocytes from mice lacking IFNγ or iNOS expression (Fig. 17A). On the other hand, apoptosis on DN2 thymocytes from WT or iNOS KO mice was similarly increased after infection, while that did not occur in IFNγ KO mice (Fig. 17B). At the DN3 stage, all infected mice presented an increase in the percentage of early apoptotic thymocytes, regardless of genotype (Fig. 17C). Little or no alterations were observed regarding cell death on DN4 thymocytes on either mouse genotype (Fig. 17D).

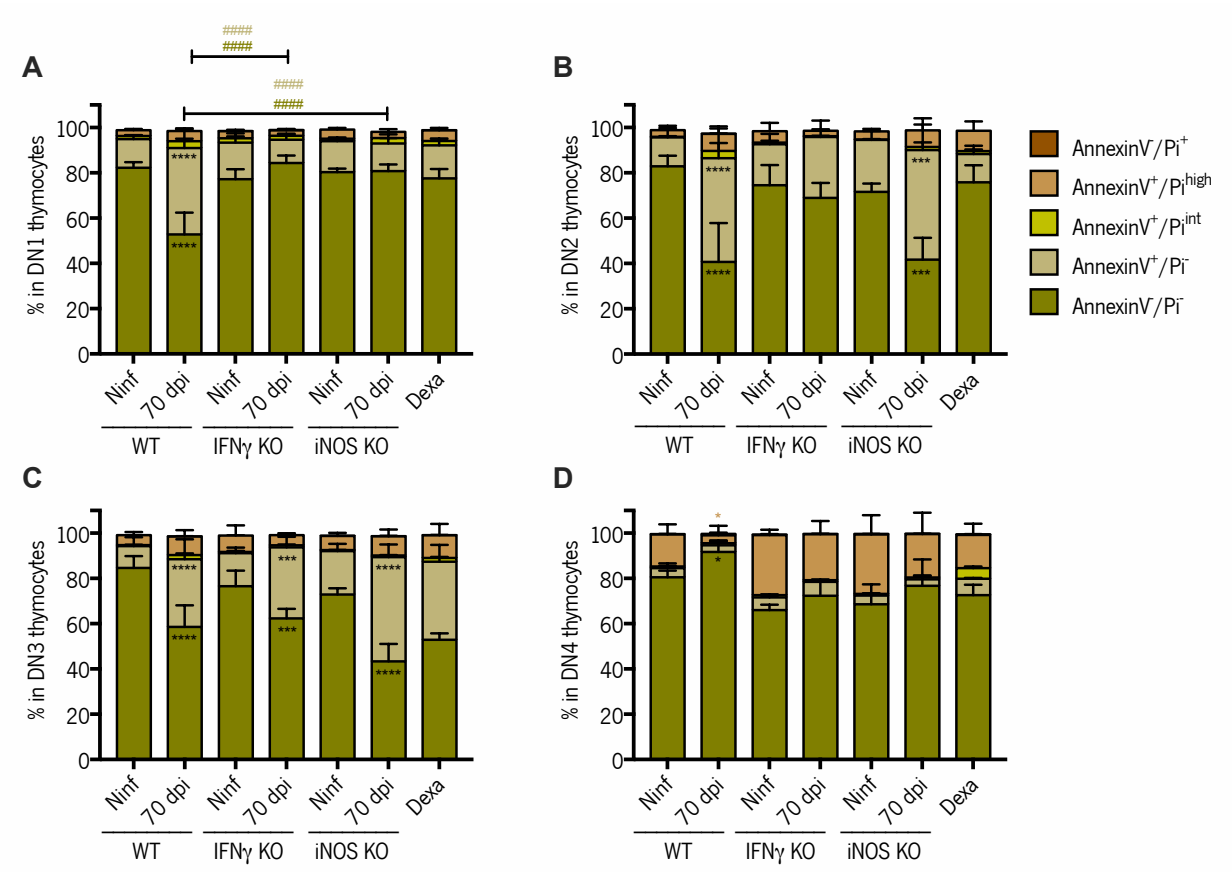

FIGURE 17. *M. avium* 25291 infection-induced apoptosis is dependent on IFNγ and iNOS only in some DN populations. Percentage of viable (Annexin V^-/PI^-), early apoptotic (Annexin V^+/PI^-), apoptotic (Annexin V^+/PI^{int}), late apoptotic/necrotic (Annexin V^+/PI^{high}) and necrotic (Annexin V^-/PI^+) within **(A)** DN1 ($CD44^+CD25^-$), **(B)** DN2 ($CD44^+CD25^+$), **(C)** DN3 ($CD44^-CD25^+$) and **(D)** DN4 ($CD44^-CD25^-$) thymocyte populations. Columns represent mean+SD (*n*=4-9 mice/group from one experiment). *p<0.05, ***p<0.001, ****p<0.0001 compared to non-infected counterparts (ninf). ####p<0.0001 compared between genotypes, using two-way ANOVA and Sidak's post-hoc test. Dexa=positive control for thymocyte apoptosis.

Results regarding active caspase 3 in DN subpopulations showed no alterations on the activation of caspase 3 in DN1 and DN4 thymocytes. We observed a slight decrease in the percentage of active caspase 3-positive DN2 and DN3 thymocytes after infection, irrespectively of the genotype (Figs. 18B, 18C).

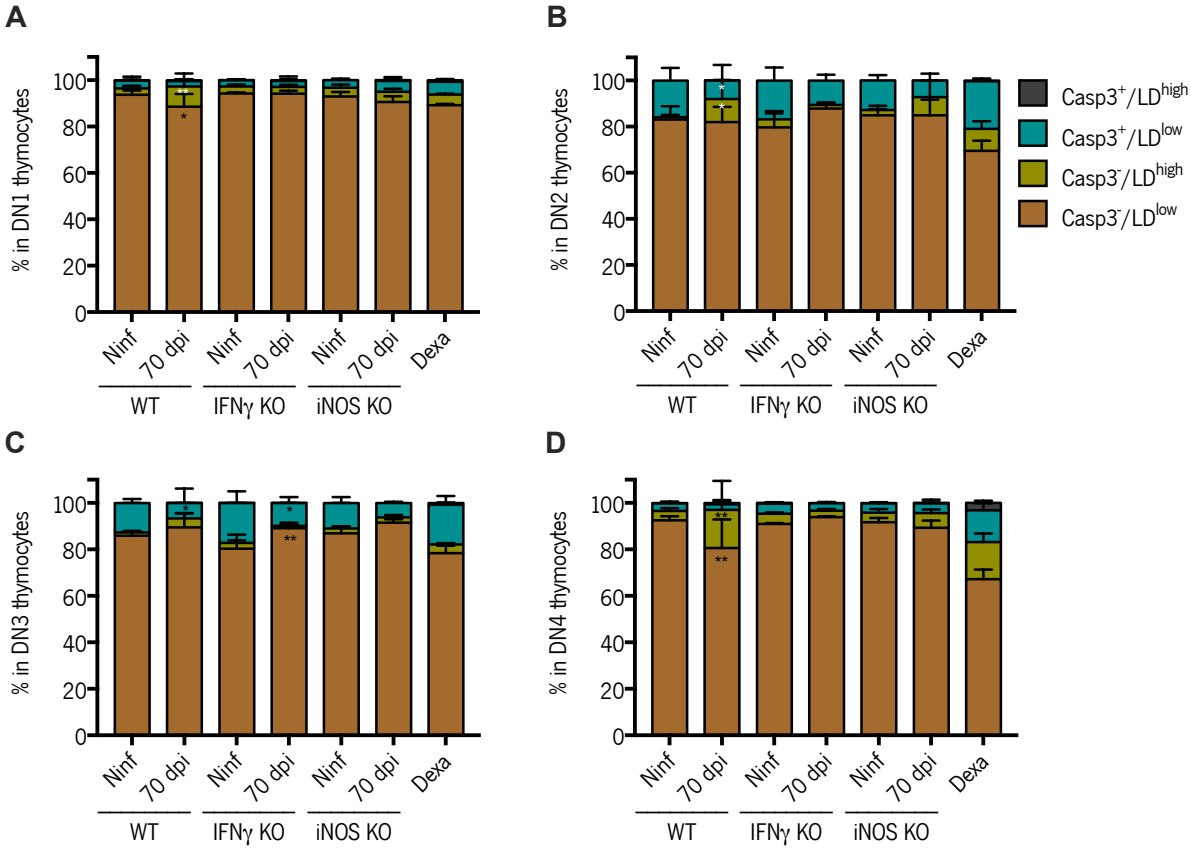

FIGURE 18. Within the DN subpopulations, *M. avium* 25291 infection decreases or does not alter the percentage of caspase 3-positive thymocytes. Percentage of viable (Casp3$^-$/LiveDead^{low}), apoptotic via caspase 3 (Casp3$^+$/LiveDead^{low}; Casp3$^+$/LiveDead^{high}) and dead/dying not via caspase 3 (Casp3$^-$/LiveDead^{high}) within **(A)** DN1 (CD44$^+$CD25$^-$), **(B)** DN2 (CD44$^+$CD25$^+$), **(C)** DN3 (CD44$^-$CD25$^+$) and **(D)** DN4 (CD44$^-$CD25$^-$) thymocyte populations. Columns represent mean+SD (n=4-9 mice/group from one experiment). *p<0.05, **p<0.01, compared to non-infected counterparts (ninf) using two-way ANOVA and Sidak's post-hoc test. Dexa=positive control for thymocyte apoptosis. LD=Live/Dead dye.

4.2.3. NO increases *M. avium*-induced apoptosis mainly at late timepoints of infection

As our results suggest a role for NO via iNOS in *M. avium* 25291 infection-induced thymocyte apoptosis, we followed how infection progression related to increased thymocyte apoptosis in WT and iNOS KO mice.

Mice were weighed throughout the entire period of infection and, as expected, only infected WT mice lost weight, while iNOS KO mice maintained or increased weight (Fig. 19A). Also, as expected, splenic bacterial load was significantly higher in WT than in iNOS KO mice in both timepoints of infection (Fig. 19B). In agreement with previous experiments, infected WT mice suffered from thymic atrophy (Fig. 19C, 19D). Mice lacking iNOS expression did not present thymic atrophy (Fig. 19C, 19D).

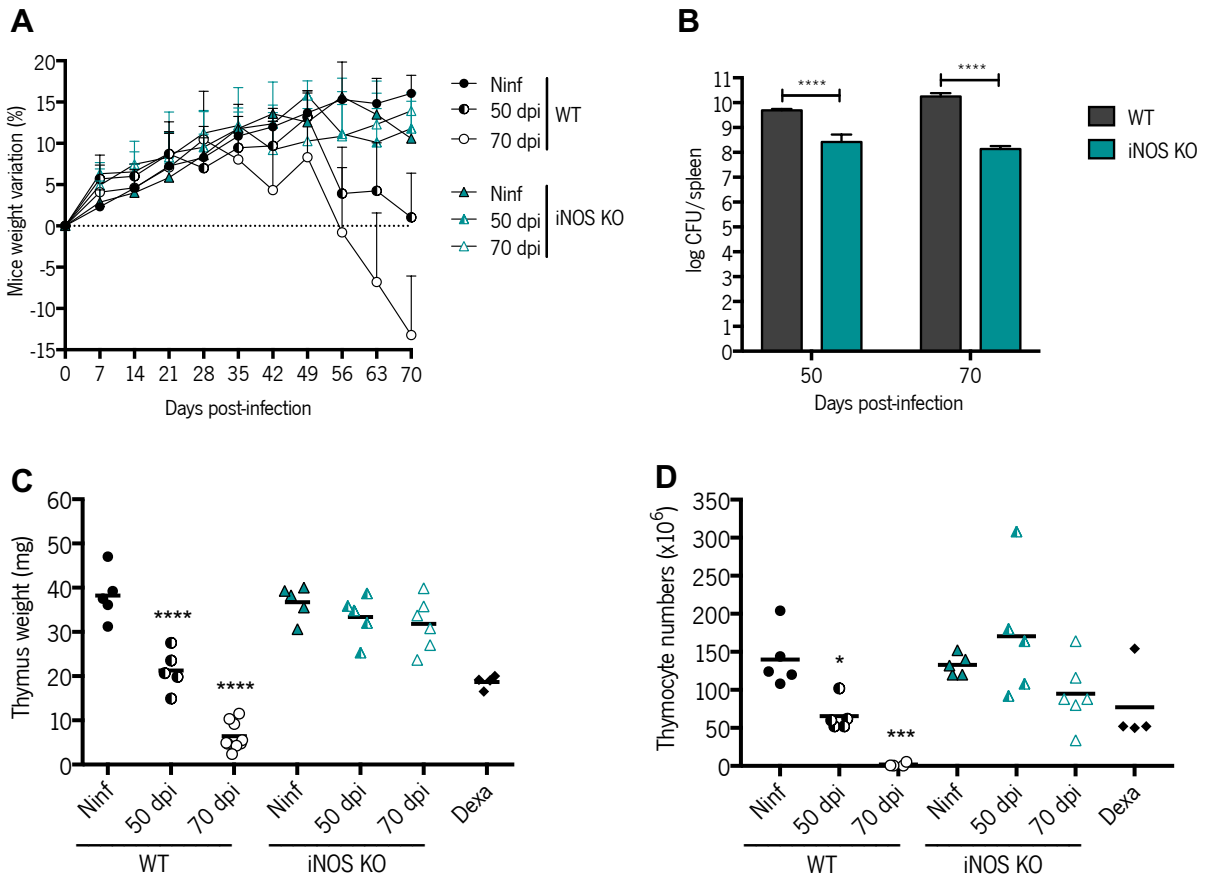

FIGURE 19. *M. avium* 25291 infection causes progressive weight reduction, continuous bacterial growth and thymic atrophy on WT but not on iNOS KO mice. (A) Mice weight variation (%) throughout *M. avium* infection. Data is presented as mean+SD. *n*=5–9 mice/group. **(B)** Splenic bacterial burden at 50 and 70 dpi. Data is presented as log(CFU) of each mouse. *n*=5–9 mice/group. ****p<0.0001 compared between WT and iNOS KO mice at a given infection timepoint, using one-way ANOVA and Sidak's post-hoc test. **(C)** Thymus weight and **(D)** total thymocyte numbers in non-infected (ninf)and infected mice for 50 and 70 days. Each dot represents one mouse (*n*=4-9 mice/group from one experiment). ****p<0.0001 compared to non-infected counterparts. In all datasets except B, two-way ANOVA and Sidak's post-hoc test were used to determine statistically significant differences. Dexa=positive control for thymocyte apoptosis.

Thymocyte death assessment by Annexin V/PI stain in total thymocytes showed a significant increase in the percentage of viable (Annexin V$^-$/PI$^-$) and decrease of apoptotic thymocytes (Annexin V$^+$/PI$^-$ and Annexin V$^+$/PI^{int}) in iNOS KO mice compared to WT at 70 dpi (Fig. 20A), suggesting a partial role for NO in thymocyte apoptosis upon *M. avium* 25291 infection, although requiring further confirmation.

Concerning the involvement of the intrinsic apoptosis pathway in thymocyte death in *M. avium* 25291-infected WT and iNOS KO mice, we found that, while no differences were found in WT, *Bax/ Bcl-2* ratio values were decreased in iNOS KO mice at 70 dpi compared to non-infected counterparts. Yet, variability was high in the non-infected control group.

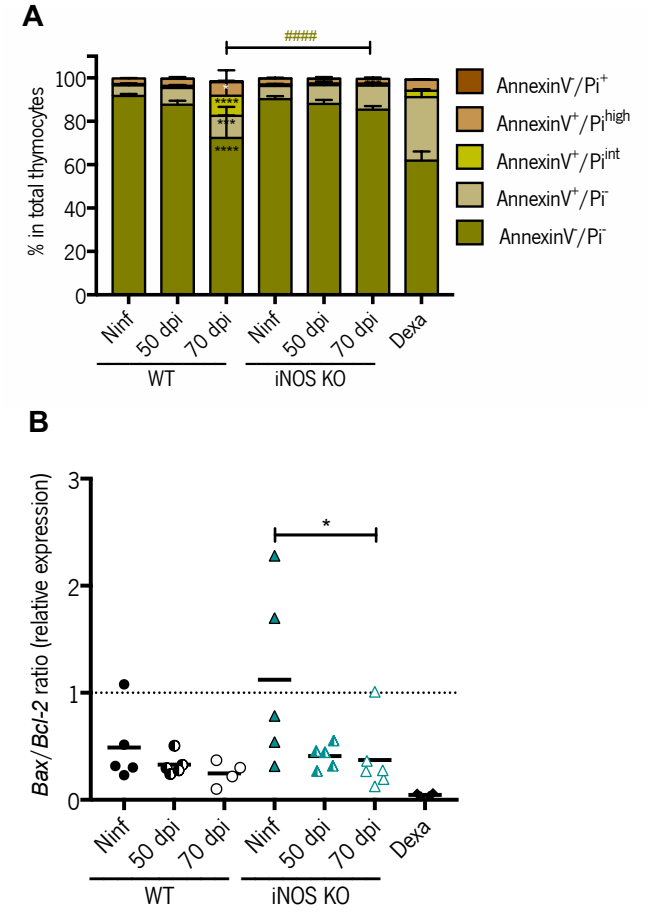

FIGURE 20. *M. avium* infection reduces thymocyte viability and induces thymocyte apoptosis, mediated by iNOS and independent of *Bax/ Bcl-2*. (A) Percentage of viable (Annexin V$^-$/PI$^-$), early apoptotic (Annexin V$^+$/PI$^-$), apoptotic (Annexin V$^+$/PI^{int}), late apoptotic/necrotic (Annexin V$^+$/PI^{high}) and necrotic (Annexin V$^-$/PI$^+$) total thymocytes. Columns represent mean+SD (*n*=4-5 mice/group from one experiment). *p<0.05, **p<0.01, ***p<0.001, ****p<0.0001 compared to non-infected counterparts (ninf), ####p<0.0001 compared between mouse genotypes at a given infection timepoint. **(B)** *Bax/ Bcl-2* (pro-apoptotic/anti-apoptotic genes) ratio (from relative expression values) in the thymus measured by qPCR in WT and

iNOS KO mice. Relative expression was normalized to *18S* and *Hprt* housekeeping genes. Each dot represents one mouse (n=4-6 mice/group from one experiment). *p<0.05 compared to non-infected counterparts. In both datasets, two-way ANOVA and Sidak's post-hoc test were used to determine statistically significant differences. Dexa=positive control for thymocyte apoptosis.

When analyzing the four main thymocyte populations through Annexin V/PI, no alterations were observed at 50 dpi. Similarly to what was observed for total thymocytes, iNOS KO mice showed a significant increase in the percentage of viability and a decrease in the percentage of apoptosis in DP thymocytes, when compared to WT counterparts (Fig. 21B). This result raises the hypothesis that NO might be partially mediating *M. avium* 25291 infection-induced DP thymocyte apoptosis. Consistent with preceding data, SP thymocytes in WT mice presented a decrease in the percentage of viable thymocytes and an increase in the percentage of apoptosis only at 70 dpi, which was not observed in iNOS KO mice (Figs. 21C, 21D). This reinforces that NO is mediating SP thymocyte apoptosis upon infection with *M. avium* 25291.

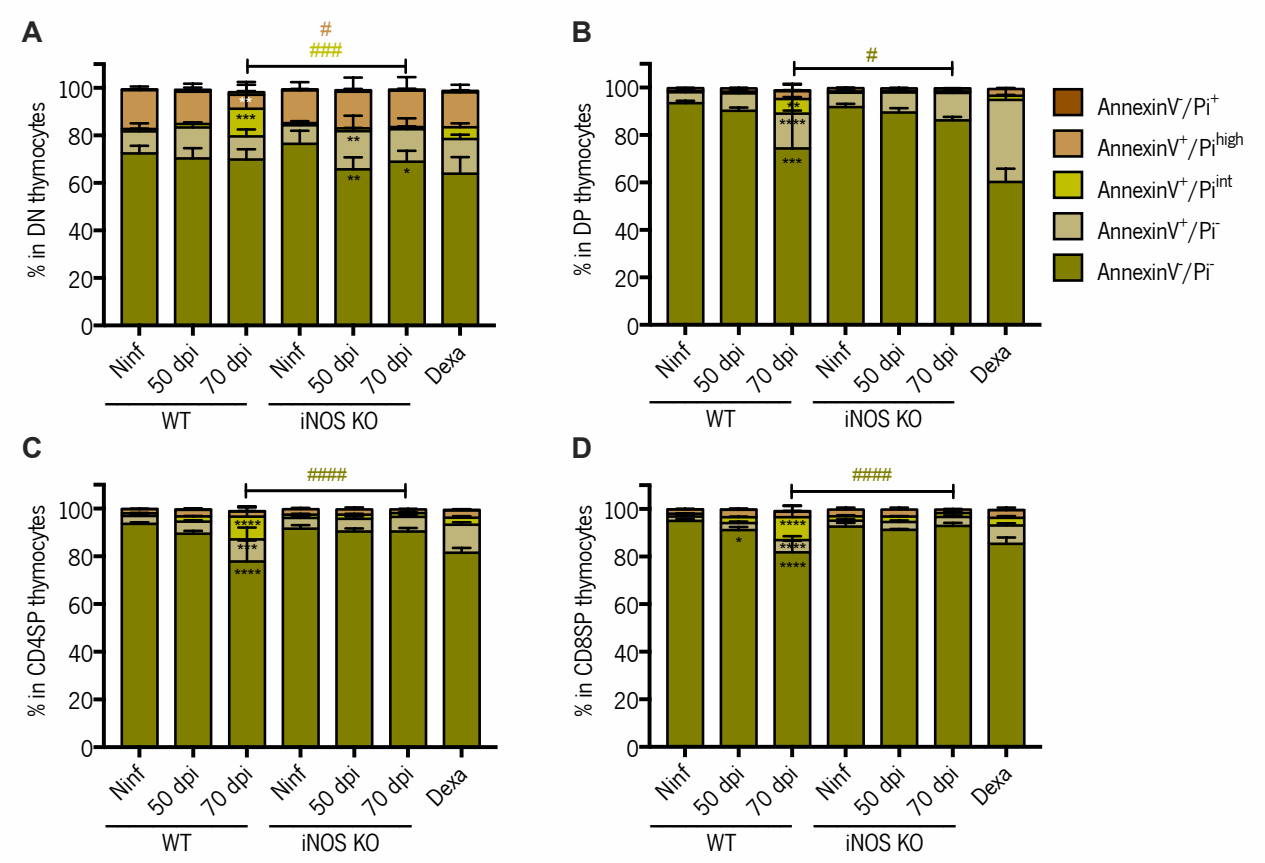

FIGURE 21. *M. avium* 25291 infection-induced apoptosis is dependent on iNOS in some thymocyte populations. Percentage of viable (Annexin V^-/PI^-), early apoptotic (Annexin V^+/PI^-), apoptotic (Annexin V^+/PI^{int}), late apoptotic/necrotic (Annexin V^+/PI^{high}) and necrotic (Annexin V^-/PI^+) within **(A)** DN ($CD3^-CD4^-CD8^-$), **(B)** DP ($CD4^+CD8^+$), **(C)** CD4SP ($CD3^+CD4^+CD8^-$) and **(D)** CD8SP ($CD3^+CD4^-CD8^+$) thymocyte populations. Columns represent mean+SD (*n*=4-5 mice/group from one experiment). *p<0.05, **p<0.01, ***p<0.001, ****p<0.0001 compared to non-infected counterparts (ninf), using two-way ANOVA and Sidak's post-hoc test. #p<0.05, ###p<0.0002, ####p<0.0001 compared between genotypes. Dexa=positive control for thymocyte apoptosis.

In DN1 thymocytes from WT mice, we observed again a progressive decrease in the percentage of viable thymocytes and an increase in the percentage of the apoptotic ones. As in previous findings, this alteration did not occur in iNOS KO mice (Fig. 22A). In DN2 and DN3, *M. avium* 25291 infection caused a progressive increase in the percentage of apoptotic thymocytes, in both WT and iNOS KO mice (Figs. 22B, 22C), being coherent with prior data. As for the DN4 population, and similarly to what was detected before, thymocyte death did not increase with infection, as the percentage of dying thymocytes (Annexin V^+/PI^{high}) was even decreased in WT mice and not altered in iNOS KO mice (Fig. 22D).

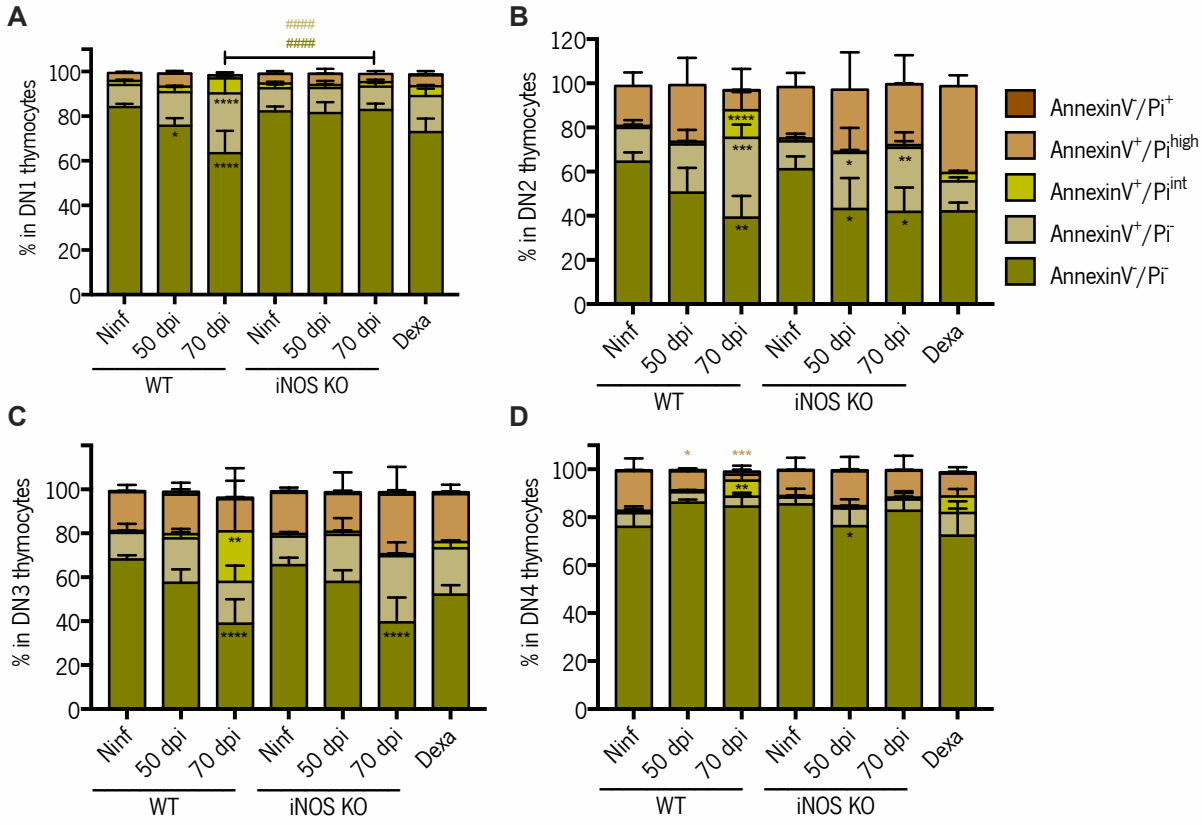

FIGURE 22. *M. avium* 25291 infection-induced apoptosis is dependent on iNOS in the DN1 subpopulation. Percentage of viable (Annexin V^-/PI^-), early apoptotic (Annexin V^+/PI^-), apoptotic (Annexin V^+/PI^{int}), late apoptotic/necrotic (Annexin V^+/PI^{high}) and necrotic (Annexin V^-/PI^+) within **(A)** DN1 ($CD44^+CD25^-$), **(B)** DN2 ($CD44^+CD25^+$), **(C)** DN3 ($CD44^-CD25^+$) and **(D)** DN4 ($CD44^-CD25^-$) thymocyte populations. Columns represent mean+SD (*n*=4-5 mice/group from one experiment). *p<0.05, ***p<0.001, ****p<0.0001 compared to non-infected counterparts (ninf), using two-way ANOVA and Sidak's post-hoc test. ####p<0.0001 compared between genotypes. Dexa=positive control for thymocyte apoptosis.

4.3. Pro-inflammatory molecules associated with infection-induced thymic atrophy are locally expressed in the thymus

IFNγ, NO via iNOS and glucocorticoids are essential players of *M. avium* infection-induced thymic atrophy. Here we evaluated the expression of these molecules in the thymus upon *M. avium* 25291 infection. Since IL-6 and TNF are involved in thymic atrophy in other models of infection, we also investigated the thymic expression of these molecules by qPCR.

4.3.1. Expression of atrophy-related molecules upon *M. avium* infection is dependent on strain virulence and time of infection

In this section, two similar experiments are presented in separate figures due to differences in the last timepoint of infection (70 *vs.* 80 dpi).

Our data showed a progressive upregulation of *Inos* (at 60 and 70/80 dpi) upon infection with *M. avium* 25291 but not with 2447 (Figs. 23B, 24B), and a similar tendency in *Ifng* expression (Figs. 23A, 24A). The glucocorticoid receptor (*Gr*) gene expression, related to glucocorticoid sensitivity, appeared upregulated only at 80 dpi (Fig. 23C, 24C).

We also found that both *Il6* and *Tnf* expression was upregulated after infection with *M. avium* 25291 but not 2447, especially at late stages of infection (70 or 80 dpi) (Fig. 23D, 23E; 24D, 24E). Thus, local alterations in the gene expression levels of these inflammation-related molecules may be associated and possibly playing a role in *M. avium* 25291 infection-induced thymic atrophy.

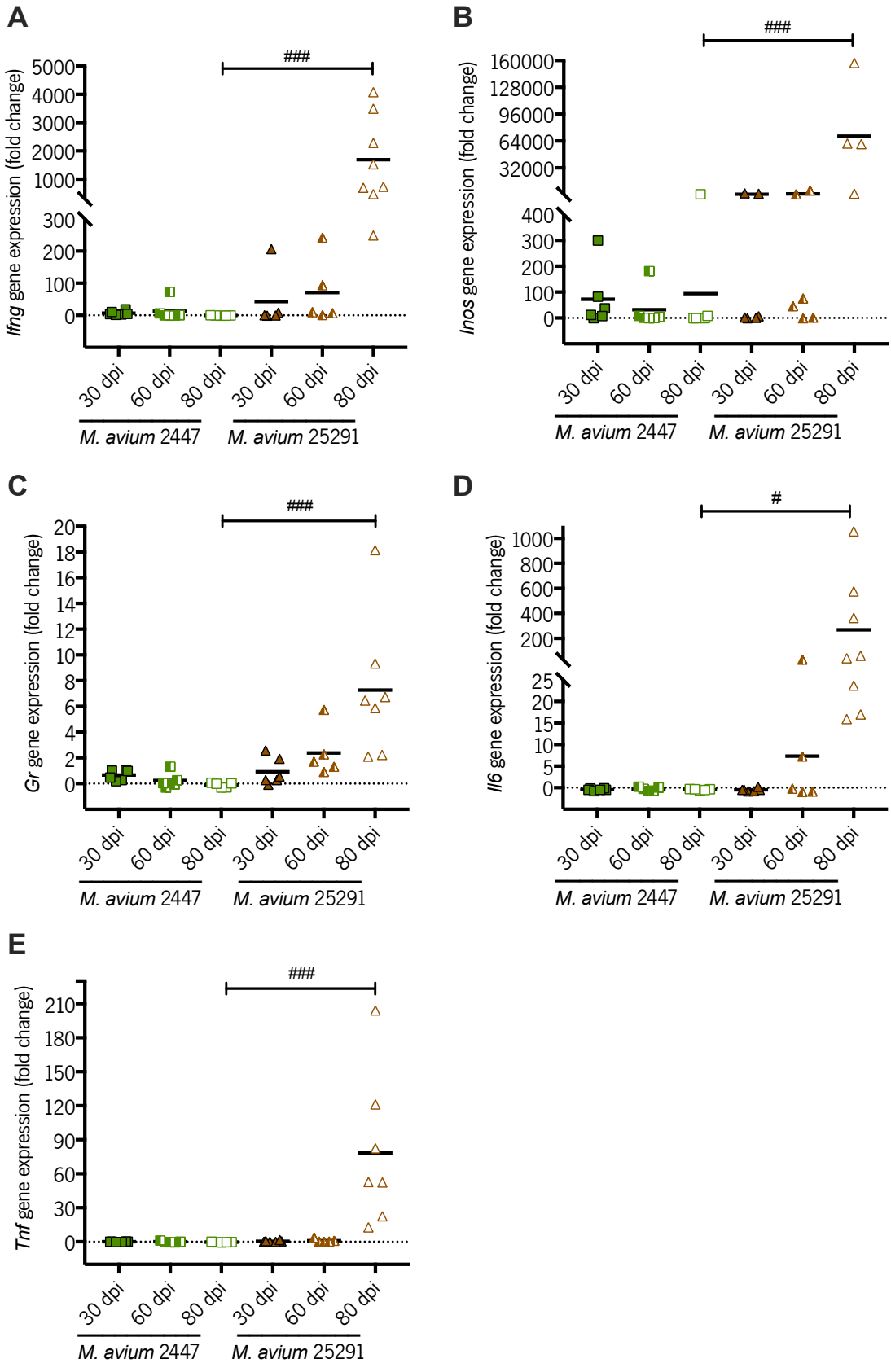
A
Ifng gene expression (fold change)
5000
4000
3000
2000
1000
300
200
100
0
###
30 dpi
60 dpi
80 dpi
30 dpi
60 dpi
80 dpi
M. avium 2447
M. avium 25291
B
Inos gene expression (fold change)
160000
128000
96000
64000
32000
400
300
200
100
0
###
30 dpi
60 dpi
80 dpi
30 dpi
60 dpi
80 dpi
M. avium 2447
M. avium 25291
C
Gr gene expression (fold change)
20
18
16
14
12
10
8
6
4
2
0
###
30 dpi
60 dpi
80 dpi
30 dpi
60 dpi
80 dpi
M. avium 2447
M. avium 25291
D
Il6 gene expression (fold change)
1000
800
600
400
200
25
20
15
10
5
0
#
30 dpi
60 dpi
80 dpi
30 dpi
60 dpi
80 dpi
M. avium 2447
M. avium 25291
E
Tnf gene expression (fold change)
210
180
150
120
90
60
30
0
###
30 dpi
60 dpi
80 dpi
30 dpi
60 dpi
80 dpi
M. avium 2447
M. avium 25291

FIGURE 23. *M. avium* 25291 but not 2447 infection induces thymic gene expression alterations of several molecules related to infection-induced premature thymic atrophy. Thymic gene expression levels of **(A)** *Ifng*; **(B)** *Inos*; **(C)** *Gr*; **(D)** *Il6* and **(E)** *Tnf* measured by qPCR. Relative expression was normalized to *18S* and *Hprt* housekeeping genes. Each dot represents individual fold change values (n=4-5 mice/group from one experiment). #p<0.05 compared between *M. avium* strains at a given infection timepoint, using two-way ANOVA and Sidak's post-hoc test. Dashed line on y=0, corresponding to no alterations compared to non-infected controls.

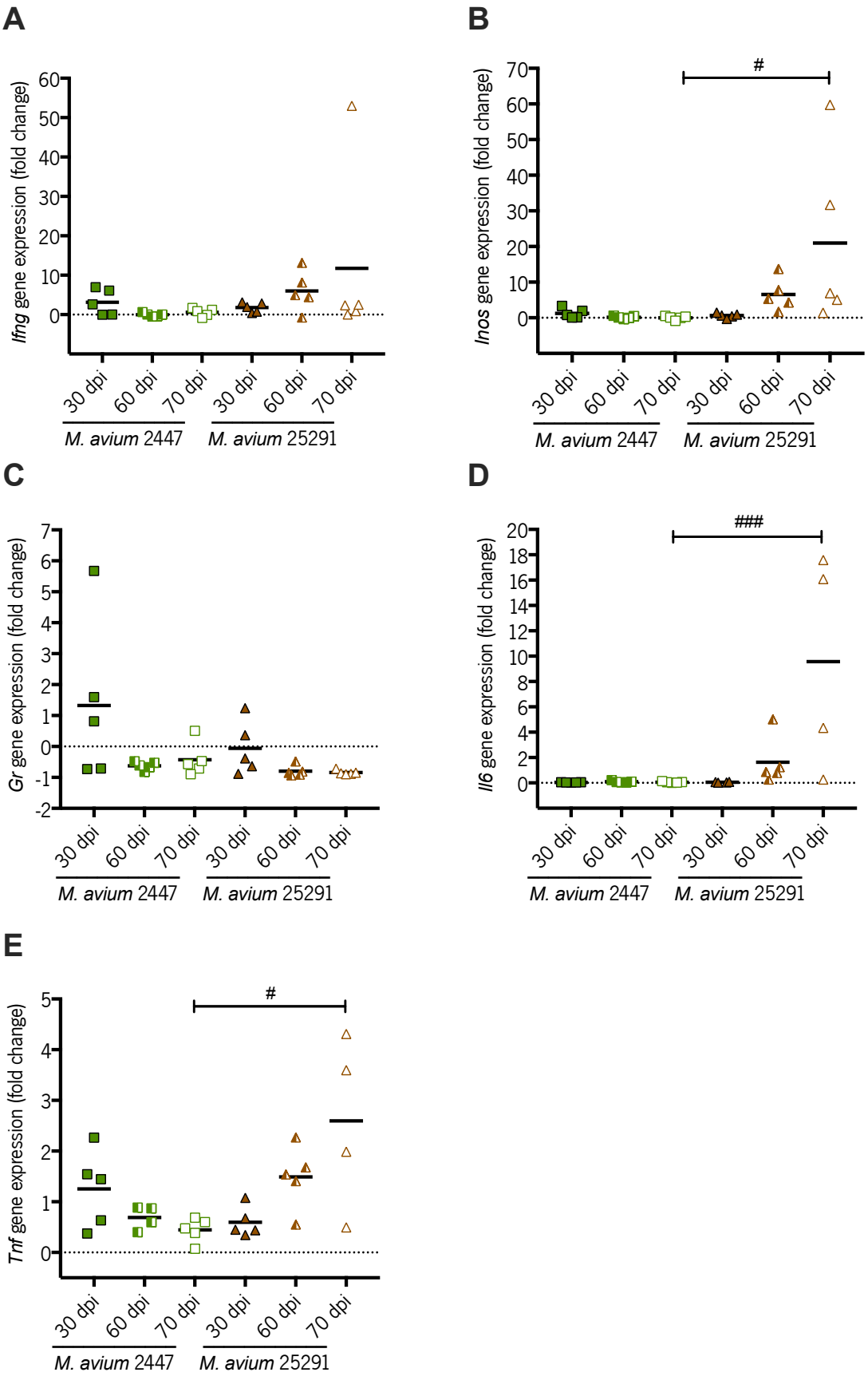
A
Ifng gene expression (fold change)
60
50
40
30
20
10
0
30 dpi
60 dpi
70 dpi
30 dpi
60 dpi
70 dpi
M. avium 2447
M. avium 25291
B
Inos gene expression (fold change)
70
60
50
40
30
20
10
0
#
30 dpi
60 dpi
70 dpi
30 dpi
60 dpi
70 dpi
M. avium 2447
M. avium 25291
C
Gr gene expression (fold change)
7
6
5
4
3
2
1
0
-1
-2
30 dpi
60 dpi
70 dpi
30 dpi
60 dpi
70 dpi
M. avium 2447
M. avium 25291
D
Il6 gene expression (fold change)
20
18
16
14
12
10
8
6
4
2
0
###
30 dpi
60 dpi
70 dpi
30 dpi
60 dpi
70 dpi
M. avium 2447
M. avium 25291
E
Tnf gene expression (fold change)
5
4
3
2
1
0
#
30 dpi
60 dpi
70 dpi
30 dpi
60 dpi
70 dpi
M. avium 2447
M. avium 25291

FIGURE 24. *M. avium* 25291 but not 2447 infection induces thymic gene expression alterations of several molecules related to infection-induced premature thymic atrophy. Thymic gene expression levels of **(A)** *Ifng*; **(B)** *Inos*; **(C)** *Gr*; **(D)** *Il6* and **(E)** *Tnf* measured by qPCR. Relative expression was normalized to *18S* and *Hprt* housekeeping genes. Each dot represents individual fold change values (*n*=5-8 mice/group from one experiment). #p<0.05, ###p<0.001 compared between *M. avium* strains at a given infection timepoint, using two-way ANOVA and Sidak's post-hoc test. Dashed line on y=0, corresponding to no alterations compared to non-infected controls.

4.3.2. NO is associated with changes in the gene expression of molecules related to infection-induced thymic atrophy

We questioned whether, in addition to being a mediator of infection-induced thymocyte apoptosis, NO could mediate alterations in thymic gene expression of other players like *Ifng*, *Gr*, *Il6* and *Tnf*.

In these two experiments, we found that *Ifng* was upregulated at 70 dpi both in WT and iNOS KO mice (Fig. 25A). If gene expression translates to protein levels in this context, these results strengthen the hypothesis that IFNγ *per se* may not be sufficient to induce the thymocyte apoptosis demonstrated in previous sections. Data on *Gr* expression revealed a tendency to upregulation but high variability in thymi from WT mice infected for 70 days, and no alteration in iNOS KO mice, which presented similar *Gr* levels in infected and non-infected mice (Fig. 25C). Similarly to previous results, we found that *Il6* is not upregulated in thymi from iNOS KO mice at 70 dpi, contrary to WT counterparts (Fig. 25D). On the other hand, *Tnf* levels were upregulated at 70 dpi in both WT and iNOS KO thymocytes (Fig. 25E). These data suggest that, contrary to *Il6*, *Tnf* overexpression may not have a role in the NO-dependent mechanisms of *M. avium* infection-induced thymic atrophy.

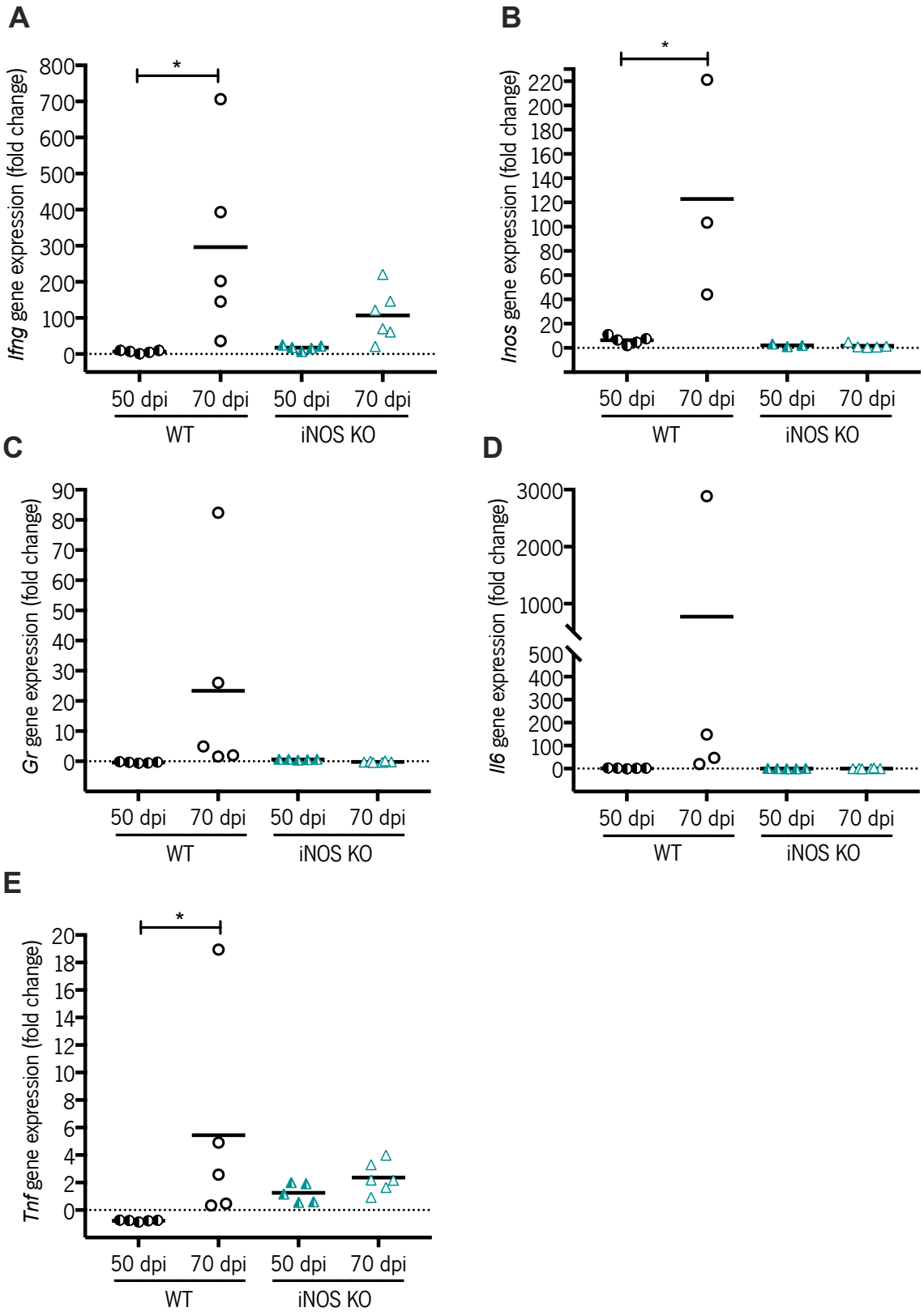
A
*
Ifng gene expression (fold change)
800
700
600
500
400
300
200
100
0
50 dpi
70 dpi
50 dpi
70 dpi
WT
iNOS KO
B
*
Inos gene expression (fold change)
220
200
180
160
140
120
100
80
60
40
20
0
50 dpi
70 dpi
50 dpi
70 dpi
WT
iNOS KO
C
Gr gene expression (fold change)
90
80
70
60
50
40
30
20
10
0
50 dpi
70 dpi
50 dpi
70 dpi
WT
iNOS KO
D
Il6 gene expression (fold change)
3000
2000
1000
500
400
300
200
100
0
50 dpi
70 dpi
50 dpi
70 dpi
WT
iNOS KO
E
*
Tnf gene expression (fold change)
20
18
16
14
12
10
8
6
4
2
0
50 dpi
70 dpi
50 dpi
70 dpi
WT
iNOS KO

FIGURE 25. There are gene expression alterations of molecules related to infection-induced premature thymic atrophy dependent on iNOS. Thymic gene expression levels of **(A)** *Ifng*; **(B)** *Inos*; **(C)** *Gr*; **(D)** *Il6* and **(E)** *Tnf* measured by qPCR. Relative expression was normalized to *18S* and *Hprt* housekeeping genes. Each dot represents individual fold change values (n=4-5 mice/group, representative from two independent experiments). *p<0.05 compared between infection timepoints within the same genotype using two-way ANOVA and Sidak's post-hoc test. Dashed line on y=0, corresponding to no alterations compared to non-infected counterparts.

In summary, our results show that thymocyte apoptosis may be a mechanism underlying *M. avium* 25291 infection-induced thymic atrophy. Thymocyte apoptosis seems dependent on the local production of IFNγ and iNOS, although requiring confirmation at the protein level. However, the apoptosis pathway remains unclear. Glucocorticoid signaling, IL-6 and TNF upregulation may also mediate apoptosis and/or atrophy.

5. DISCUSSION

Premature thymic atrophy has been described to occur after infection with several microorganisms, both in animal models and humans (36). Previous work with *M. avium* infection demonstrated that premature thymic atrophy occurs after infection of C57BL/6 mice with a highly virulent strain (25291), but not with a strain of intermediate virulence (2447) (108). Further research into the topic established that *M. avium* 25291 infection-induced thymic atrophy is mediated by glucocorticoids and NO production via iNOS by IFNγ-activated macrophages (14). Some of the mechanisms underlying infection-induced thymic atrophy may comprise: 1) Alterations in the BM precursors and/or seeding of the thymus; 2) Impairment on the ability of thymic stroma to differentiate new T cells; 3) Premature thymocyte egress; 4) Increased thymocyte death. In this work, we focused on the latter. Thus, we investigated if alterations in thymocyte apoptosis could have a role in *M. avium* infection-induced thymic atrophy, and if so, the role of IFNγ and NO in this mechanism.

Previous work suggests that IFNγ is implicated in thymocyte death upon infection by *M. avium* (pathway not determined) (109) and in apoptosis after infection by other microorganisms (80,85,110). In turn, NO has been reported to induce thymocyte death by oxidative damage (111) and to synergize with glucocorticoids to cause thymocyte death *in vitro, ex vivo* and *in vivo* (112,113). There are also reports implicating both IFNγ and NO in the death of splenocytes after *T. cruzi* infection (114) and of $CD4^+$ T cells after BCG infection (115).

Data generated in this thesis shows that *M. avium* 25291 infection progressively causes a decrease in the viability and an increase in apoptosis of thymocytes, this being particularly severe at late timepoints of infection (70 dpi). These results suggest that increased thymocyte apoptosis is a mechanism participating in premature thymic atrophy upon infection with *M. avium* 25291. This finding is in accordance with several other studies reporting increased thymocyte apoptosis in models of premature thymic atrophy induced by infection with other microorganisms (80,83–86,88,96,116). Moreover, here we show that the decrease in thymocyte viability and increase in apoptosis occurs in virtually all thymocyte populations (DN1, DN2, DN3, DP, CD4SP and CD8SP), the only exception being DN4. This does not necessarily mean that this subset is not affected, but could be explained by the fact that, from DN3 to DN4 stage during T cell differentiation, a burst of proliferation occurs (44), which could act as a compensatory mechanism for the increase in dying thymocytes.

In respect to caspase 3 activation, we observed that, in non-infected mice, particularly in total, DN and DP thymocytes, approximately 20% were positive for active caspase 3. It is not surprising that

caspase 3 is active in thymocytes in homeostatic conditions, as apoptosis is a crucial mechanism during T cell differentiation; however, this value is considerably higher than reported by others, that is around 2% or less (46,117,118). This could be related to differences between antibody clones used: the one we used binds to both subunits (12 and 17 kDa) constituting the heterodimer of active caspase 3, while other commonly used antibody, clone D3E9 from Cell Signaling, specifically detects only the 17 kDa subunit resulting from the cleavage at residue Asp175. To understand if the difference in antibodies is causing this discrepancy in active caspase 3 detection, we could compare them by staining thymocytes with both antibodies in parallel. Anyhow, as the infection progresses, the percentage of active caspase 3-positive thymocytes decreases or does not alter in WT, IFNγ KO and iNOS KO mice. This potentially means that thymocytes are not dying via caspase 3 but through another mechanism of apoptosis, such as caspase-independent apoptosis (119), and that IFNγ and NO production do not have specific effect on caspase 3 activation. Alternatively, apoptosis may be occurring through caspase 3 and these thymocytes are being rapidly cleared by the phagocytes in the infected thymus. Phagocytes, namely macrophages, are specialized in eliminating microorganisms by phagocytosis but also very efficient at clearing apoptotic cells and have been reported to bind to apoptotic thymocytes after only 60 min of contact *in vitro* (120). A third hypothesis is that, since caspase 3 activation occurs before phosphatidylserine externalization (103), activated caspase 3 may not be detected in later stages of apoptosis. Corroborating this hypothesis is the fact that in the positive control (dexamethasone administration), we were expecting similar percentages of annexin V-positive and caspase 3-positive thymocytes (as dexamethasone-induced apoptosis was described to be caspase 3-dependent (105)), but the percentage of annexin V-positive thymocytes is often higher than the caspase 3-positive ones. An approach to more clearly determine the role of caspase 3 in *M. avium* 25291 infection-induced thymocyte apoptosis would be to inhibit caspase 3 activation and evaluate apoptosis by Annexin V/PI stain. Reduction in apoptosis upon caspase 3 inhibition or depletion (by, for instance, infecting caspase 3-deficient mice) would suggest the participation of caspase 3 in this context.

Our data on *Bax/Bcl-2* ratio assessment showed no differences between infected and non-infected WT mice. Yet, absolute ratio values vary greatly between experiments. In iNOS KO mice, we observed a decrease at 70 dpi when compared to levels from non-infected counterparts; still, this difference may not be biologically relevant, as the control group presents high dispersion on the ratio values. In general, ratios are similar irrespective of time of infection and genotype, indicating that the intrinsic apoptosis pathway is not involved in *M. avium* 25291 infection-induced thymocyte apoptosis. Yet, this would benefit from confirmation at the protein level by, for example, western blotting.

We found that both IFNγ and NO via iNOS are involved in the decrease in thymocyte viability and increase in apoptosis upon infection with *M. avium* 25291. The role of these molecules seems to be thymocyte population-specific. Curiously, infection-induced apoptosis in the most immature thymocytes, the DN1, and in the most mature populations, CD4SP and CD8SP, is dependent on both IFNγ and NO. Data on DP thymocytes is variable thus far: IFNγ and NO seem to partially mediate an increase in apoptosis, although this result is not clear in both experiments and requires further experimental replication. Concerning DN2, only IFNγ shows a role, while in DN3 neither of them seems to impact on apoptosis upon infection. It is worth reinforcing that the alterations that are equally observed in mice lacking IFNγ or iNOS (as it is the case for DN1 and SPs) may be due to NO action alone, as IFNγ KO mice also lack the activation of iNOS. This means that, in these specific populations, increased thymocyte apoptosis can potentially be attributed to NO.

Regarding the increase in apoptosis of DN1 thymocytes, this could be influenced by the fact that BM T cell precursors are already altered and more prone to die. Results from our laboratory suggest that BM T cell precursor alterations are IFNγ-dependent and iNOS-independent (109), however more recent data may implicate NO as affecting in some way BM T cell precursors before they reach the thymus. Alternatively, three additional scenarios may be the underlying cause: 1) NO production in the thymus alone is affecting thymocyte viability; 2) NO effect in the thymus together with previous IFNγ-dependent alterations in the BM; 3) NO-induced alterations in the thymus together with IFNγ-dependent alterations both in the BM and in the thymus. Nevertheless, this result adds to the data on BM T cell precursors alterations, as it supports the concept that *M. avium* 25291 infection affects very early stages of T cell differentiation. In DN2 thymocytes, IFNγ but not iNOS plays a role in infection-induced thymocyte apoptosis, thus supporting the hypothesis that IFNγ-induced alterations in BM T cell precursors may be impairing thymocyte differentiation. Curiously, in the DN3 subset, an effect of these two molecules is not observed. It appears that, throughout T cell differentiation, especially from DN3 onwards, other players besides IFNγ and NO may have a role in infection-induced apoptosis. This may also be the case for DP thymocytes, as our data did not demonstrate a clear function for IFNγ or NO. This could be related to glucocorticoids action, since they also play an important role in *M. avium* 25291 infection-induced thymic atrophy and affect mainly DP thymocytes (14,121). In fact, the synergy between NO and glucocorticoids has been reported before to induce apoptosis of DP thymocytes (113). At the most mature stage of T cell differentiation (CD4SP and CD8SP), before T cells exit to the periphery, IFNγ and NO also mediate infection-induced apoptosis, hinting at a local action of these molecules. Thus, *M. avium* 25291 infection

induces thymocyte death in all stages of differentiation, challenging thymocytes throughout the entire process.

Considering our data in caspase 3 activation and *Bax/ Bcl-2* ratio, we were not able to unravel the underlying apoptosis mechanism induced by *M. avium* 25291 infection. There is a study showing that NO, together with glucocorticoids, induces caspase 3-dependent apoptosis (112). However, our results point to a caspase 3-independent apoptosis mechanism. Actually, NO has been reported to induce thymocyte apoptosis *in vitro* (122,123), in a caspase 3-independent and caspase 1-dependent mechanism (124), making it an interesting target for further exploration. However, these studies (122–124) only evaluated DNA fragmentation to identify apoptosis. In fact, caspase 1-induced cell death was shown to constitute a distinct type of programmed cell death: pyroptosis (125). Thus, it is possible that reports associating NO to caspase 1-dependent thymocyte apoptosis were actually observing pyroptosis. Yet, we found increased NO-dependent apoptosis and not pyroptosis, as thymocytes undergoing pyroptosis are positive for both Annexin V and PI and we observed an increase in Annexin V positive and PI negative cells after infection (126).

The fact that iNOS KO mice infected with *M. avium* 25291 do not have premature thymic atrophy even with an altered BM suggests that, in the absence of NO, BM precursors are able to recover when reaching the thymus. This strengthens the importance of the NO-mediated thymocyte apoptosis in premature thymic atrophy presented in this thesis. Yet, NO may also induce other mechanisms of thymic atrophy still to be uncovered. For instance, it is unknown if NO can lead to an impaired ability of the thymic stroma to differentiate new T cells. NO can also be inducing alterations on T cell BM precursors that we were not yet able to explore. Finally, NO may also be associated with the production of other molecules that can act as players of *M. avium* 25291 infection-induced thymic atrophy, a hypothesis we started to explore by evaluating *Il6* and *Tnf* gene expression in WT and iNOS KO mice (discussed below).

Following the observation that IFNγ and NO-dependent thymocyte apoptosis may be associated with infection-induced thymic atrophy, two main questions were raised: 1) is IFNγ and NO effect in thymocytes from local or systemic origin?; 2) since increased apoptosis in certain thymocyte populations occurs regardless of IFNγ or NO, do other pro-inflammatory molecules have a role?. Together, our data on thymic gene expression show that in WT mice, *Ifng* and *Inos* are upregulated at late timepoints of infection with *M. avium* 25291 but not with *M. avium* 2447, suggesting that its local overexpression is linked to infection-induced thymic atrophy. In iNOS KO mice, we found that *Ifng* is still upregulated at late infection timepoints. As these mice still present IFNγ-dependent and iNOS-independent apoptosis in some

thymocyte populations, this result supports that IFNγ might be causing thymocyte apoptosis by itself or by inducing the production of other molecules.

We observed an upregulation of *Gr* after infection of WT mice with *M. avium* 25291 (mainly at 80 dpi). This upregulation is in accordance with the fact that mice infected with *M. avium* 25291 present increased serum corticosterone and 2447-infected mice do not (14). In mice lacking iNOS expression, *Gr* upregulation is abrogated, hinting at an association between NO production and glucocorticoid sensitivity. It is now important to measure the levels of serum corticosterone in infected mice lacking iNOS.

Our work also revealed a coherent upregulation of *Il6* in the thymus at late timepoints of infection with *M. avium* 25291 but not 2447, suggesting that *Il6* gene overexpression might be associated with *M. avium* 25291 infection-induced thymic atrophy. Furthermore, *Il6* is not upregulated in iNOS KO mice, indicating that NO and IL-6 production may be associated. An increase in IL-6 mRNA levels was previously described during HIV-1 infection-induced thymic atrophy and associated with thymocyte apoptosis (82,96), but, to our knowledge, it is the first time being associated with NO production in a model of infection-induced thymic atrophy. Since IL-6 is usually produced at initial phases of inflammation, its upregulation so late in infection indicates dysregulated production that may be contributing to chronic inflammation and consequent tissue damage (127). Regarding *Tnf* expression, our results demonstrate its upregulation in the thymus of WT mice after infection with *M. avium* 25291 but not with 2447, suggesting a possible role in premature thymic atrophy. Yet, in this case, *Tnf* upregulation also occurs in iNOS KO mice, indicating that NO and TNF production are not linked. Thus, TNF production is probably not sufficient to cause *M. avium* 25291 infection-induced thymic atrophy. Nevertheless, mRNA transcript levels do not always directly translate into protein levels, as mRNA may undergo modifications (e.g. alternative splicing) and proteins may be subjected to post-translational regulation (128). Further studies are needed to better understand the role of IL-6 and TNF during *M. avium* infection-induced thymic atrophy.

In this thesis, we showed that *M. avium* 25291 infection-induced thymic atrophy is associated with an increase in thymocyte apoptosis, which is most likely mediated *in loco* by IFNγ and NO. This adds a new piece to the puzzle of the mechanisms underlying premature thymic atrophy induced by these mycobacteria. As human thymocyte apoptosis through NO participation has already been reported (111), this may become relevant, for instance, during treatment of persistent pulmonary hypertension in premature babies, that are subjected to NO inhalation therapy (129). At this age, thymus activity is at its peak and the peripheral pool of T cells is still under formation, thus premature thymic atrophy could lead

to a certain degree of immunodeficiency (74). Additionally, NO donor drugs are also used in adults in high concentrations for the treatment of cardiovascular diseases (130) and cancer (131). Cancer patients may already be immunocompromised as a consequence of certain therapies; in this case, a possible NO-induced thymic atrophy would aggravate immunodeficiency, as the remaining thymic function would be compromised. For these reasons, NO production in similar contexts of chronic infection should be further studied. We also uncovered the potential involvement of other cytokines that might be contributing to thymic atrophy in this model of infection. Taken together with previous data, these new results illustrate the complexity of the host-pathogen interaction and the need to dissect its mechanisms to improve scientific knowledge and potentially find new therapeutic approaches.

6. REFERENCES

1. Parte AC. LPSN - List of prokaryotic names with standing in nomenclature. Nucleic Acids Res. 2014;42(D1):613–6.
2. Gupta RS, Lo B, Son J. Phylogenomics and comparative genomic studies robustly support division of the genus Mycobacterium into an emended genus Mycobacterium and four novel genera. Front Microbiol. 2018;9:1–41.
3. Abrahams KA, Besra GS. Mycobacterial cell wall biosynthesis: A multifaceted antibiotic target. Parasitology. 2018;145(2):116–33.
4. World Health Organisation. Global Health TB Report [Internet]. Who. 2018. 277 p. Available from: https://www.who.int/tb/publications/global_report/en/
5. O. Falkinham J. Mycobacterium avium complex: Adherence as a way of life. AIMS Microbiol. 2018;4(3):428–38.
6. Kendall BA, Winthrop KL. Update on the epidemiology of pulmonary nontuberculous mycobacterial infections. Semin Respir Crit Care Med. 2013;34(1):87–94.
7. Bodle EE, Cunningham JA, Della-Latta P, Schluger NW, Saiman L. Epidemiology of nontuberculous mycobacteria in patients without HIV infection, New York City. Emerg Infect Dis. 2008;14(3):390–6.
8. Wentworth AB, Drage LA, Wengenack NL, Wilson JW, Lohse CM. Increased incidence of cutaneous nontuberculous mycobacterial infection, 1980 to 2009: A population-based study. Mayo Clin Proc. 2013;88(1):38–45.
9. Stout JE, Koh WJ, Yew WW. Update on pulmonary disease due to non-tuberculous mycobacteria. Int J Infect Dis. 2016;45:123–34.
10. Porvaznik I, Solovic I, Mokry J. Non-Tuberculous Mycobacteria: Classification, Diagnostics, and Therapy. Advs Exp Med Biol - Neurosci Respir. 2016;54(1):39–44.
11. Panel on Opportunistic Infections in Adults and Adolescents with HIV. Guidelines for the Prevention and Treatment of Opportunistic Infections in Adults and Adolescents with HIV: Recommendations from the Centers for Disease Control and Prevention. [Internet]. Vol. 58, AIDSinfo. 2019. p. 1–206. Available from: http://aidsinfo.nih.gov/contentfiles/lvguidelines/adult_oi.pdf
12. Nunes-Costa D, Alarico S, Dalcolmo MP, Correia-Neves M, Empadinhas N. The looming tide of nontuberculous mycobacterial infections in Portugal and Brazil. Tuberculosis. 2016;96:107–19.
13. Kim SY, Shin SH, Moon SM, Yang B, Kim H, Kwon OJ, et al. Distribution and clinical significance of Mycobacterium avium complex species isolated from respiratory specimens. Diagn Microbiol Infect Dis. 2017;88(2):125–37.
14. Borges M, Barreira-Silva P, Flórido M, Jordan MB, Correia-Neves M, Appelberg R. Molecular and Cellular Mechanisms of Mycobacterium avium-Induced Thymic Atrophy. J Immunol. 2012;189(7):3600–8.
15. Zhan L, Tang J, Sun M, Qin C. Animal models for tuberculosis in translational and precision medicine. Front Microbiol. 2017;8.
16. Lake MA, Ambrose LR, Lipman MCI, Lowe DM. “Why me, why now?” Using clinical immunology and epidemiology to explain who gets nontuberculous mycobacterial infection. BMC Med. 2016;14(1):1–13.
17. Honda JR, Alper S, Bai X, Chan ED. Acquired and genetic host susceptibility factors and microbial pathogenic factors that predispose to nontuberculous mycobacterial infections. Curr Opin Immunol. 2018;54:66–73.
18. Van Crevel R, Kleinnijenhuis J, Oosting M, Joosten LAB, Netea MG. Innate immune recognition of mycobacterium tuberculosis. Clin Dev Immunol. 2011;2011.

19. Pieters J. Mycobacterium tuberculosis and the Macrophage: Maintaining a Balance. Cell Host Microbe. 2008;3(6):399–407.
20. Frehel C, De Chastellier C, Lang T, Rastogi N. Evidence for inhibition of fusion of lysosomal and prelysosomal compartments with phagosomes in macrophages infected with pathogenic Mycobacterium avium. Infect Immun. 1986;52(1):252–62.
21. Barber-Mayer KD, Barber DL. Innate and adaptive cellular immune responses to Mycobacterium tuberculosis infection. Cold Spring Harb Perspect Med. 2015;5(12):1–19.
22. Herbst S, Schaible UE, Schneider BE. Interferon gamma activated macrophages kill mycobacteria by nitric oxide induced apoptosis. PLoS One. 2011;6(5).
23. Cooper AM, Dalton DK, Stewart TA, Griffin JP, Russell DG, Orme IM. Disseminated Tuberculosis in Interferon-gamma Gene-disrupted Mice. J Exp Med. 1993;178(December).
24. Flynn JL. An essential role for interferon gamma in resistance to Mycobacterium tuberculosis infection. J Exp Med. 2004;178(6):2249–54.
25. Jouanguy E, Doffinger R, Dupuis S, Pallier A, Altare F, Casanova J-L. IL-12 and IFN-g host defense against mycobacteria and salmonella in mice and men. Curr Opin Immunol. 1999;346–51.
26. Macmicking JD, North RJ, Mudgett RLJS, Shah SK, Nathan CF. Identification of nitric oxide synthase as a protective locus. Proc Natl Acad Sci. 1997;94:5243–8.
27. Jamaati H, Mortaz E, Pajouhi Z, Folkerts G, Movassaghi M, Moloudizargari M, et al. Nitric oxide in the pathogenesis and treatment of tuberculosis. Front Microbiol. 2017;8:1–11.
28. Idh J, Westman A, Elias D, Moges F, Getachew A, Gelaw A, et al. Nitric oxide production in the exhaled air of patients with pulmonary tuberculosis in relation to HIV co-infection. BMC Infect Dis. 2008;8:1–8.
29. Fowler CJ, Olivier KN, Leung JM, Smith CC, Huth AG, Root H, et al. Abnormal nasal nitric oxide production, ciliary beat frequency, and toll-like receptor response in pulmonary nontuberculous mycobacterial disease epithelium. Am J Respir Crit Care Med. 2013;187(12):1374–81.
30. Nozaki Y, Hasegawa Y, Ichiyama S, Nakashima I, Shimokata K. Mechanism of nitric oxide-dependent killing of Mycobacterium bovis BCG in human alveolar macrophages. Infect Immun. 1997;65(9):3644–7.
31. Cooper AM, Adams LB, Dalton DK, Appelberg R, Ehlers S, Cooper AM, et al. IFNγ and NO in mycobacterial disease - new jobs in old hands, 2002.pdf. 2002;10(5):221–6.
32. T-cell-independent granuloma formation in response to Mycobacterium avium: Role of tumour necrosis factor-α and interferon-γ. Immunology. 1997;92(4):413–21.
33. Flynn JAL, Goldstein MM, Chan J, Triebold KJ, Pfeffer K, Lowenstein CJ, et al. Tumor necrosis factor-α is required in the protective immune response against mycobacterium tuberculosis in mice. Immunity. 1995;2(6):561–72.
34. Stenger S. Immunological control of tuberculosis: Role of tumour necrosis factor and more. Ann Rheum Dis. 2005;64(SUPPL. 4):24–8.
35. Owen JA, Punt J, Stranford SA, Jones PP. T-cell development. In: Kuby Immunology. 7th ed. New York, NY 10010: Susan Winslow; 2013. p. 832.
36. Nunes-Alves C, Nobrega C, Behar SM, Correia-Neves M. Tolerance has its limits: How the thymus copes with infection. Trends Immunol. 2013;34(10):502–10.
37. Petrie HT, Zúñiga-Pflücker JC. Zoned Out: Functional Mapping of Stromal Signaling Microenvironments in the Thymus. Annu Rev Immunol. 2007;25(1):649–79.
38. Kurobe H, Liu C, Ueno T, Saito F, Ohigashi I, Seach N, et al. CCR7-dependent cortex-to-medulla migration of positively selected thymocytes is essential for establishing central tolerance. Immunity. 2006;24(2):165–77.
39. McCaughtry TM, Wilken MS, Hogquist KA. Thymic emigration revisited. J Exp Med. 2007;204(11):2513–20.

40. Owen JA, Punt J, Stranford SA, Jones PP. Receptors and Signaling: B and T-Cell Receptors. In: Kuby Immunology. 7th ed. New York, NY 10010: Susan Winslow; 2013. p. 832.
41. Oettinger MA, Schatz DG, Gorka C, Baltimore D, Oetringer MA, Schatz DG, et al. RAG-1 and RAG-2, Adjacent Genes That Synergistically Activate V(D)J Recombination. 1990;248(4962):1517–23.
42. Krangel MS. Mechanics of T cell receptor gene rearrangement. Curr Opin Immunol. 2009;21(2):133–9.
43. Yui MA, Rothenberg E V. Developmental gene networks: A triathlon on the course to T cell identity. Nat Rev Immunol. 2014;14(8):529–45.
44. Carpenter AC, Bosselut R. Decision checkpoints in the thymus. Nat Immunol. 2010;11(8):666–73.
45. Petrie HT. Multiple rearrangements in T cell receptor alpha chain genes maximize the production of useful thymocytes. J Exp Med. 1993;178(2):615–22.
46. Breed ER, Watanabe M, Hogquist KA. Measuring Thymic Clonal Deletion at the Population Level. J Immunol. 2019;202(11):3226–33.
47. Derbinski J, Schulte A, Kyewski B, Klein L. Promiscuous gene expression in medullary thymic epithelial cells mirrors the peripheral self. J Immunol. 2016;196(7):2915–22.
48. Daley SR, Hu DY, Goodnow CC. Helios marks strongly autoreactive CD4 + T cells in two major waves of thymic deletion distinguished by induction of PD-1 or NF-κB . J Exp Med. 2013;210(2):269–85.
49. Hu DY, Yap JY, Wirasinha RC, Howard DR, Goodnow CC, Daley SR. A timeline demarcating two waves of clonal deletion and Foxp3 upregulation during thymocyte development. Immunol Cell Biol. 2015;94(4):357–66.
50. Oda E, Ohki R, Murasawa H, Nemoto J, Shibue T, Tokino T, et al. Noxa, a BH3-Only Member of the Bcl-2 Family and Candidate Mediator of p53-Induced Apoptosis. Science (80-). 2000;288(5468):1053–8.
51. Slee EA, Adrain C, Martin SJ. Executioner Caspase-3, -6, and -7 Perform Distinct, Non-redundant Roles during the Demolition Phase of Apoptosis. J Biol Chem. 2001;276(10):7320–6.
52. Locksley RM, Killeen N, Lenardo MJ. The TNF and TNF receptor superfamilies: Integrating mammalian biology. Cell. 2001;104:487–501.
53. Germer M, Krammer PH, Hellbardt S, Kischkel FC, Pawlita M, Peter ME, et al. Cytotoxicity-dependent APO-1 (Fas/CD95)-associated proteins form a death-inducing signaling complex (DISC) with the receptor. EMBO J. 2018;14(22):5579–88.
54. Rathmell JC, Lindsten T, Zong WX, Cinalli RM, Thompson CB. Deficiency in Bak and Bax perturbs thymic selection and lymphoid homeostasis. Nat Immunol. 2002;3(10):932–9.
55. Strasser A, Harris AW, Corcoran LM, Cory S. Bcl-2 expression promotes B- but not T-lymphoid development in SCID mice. Nature. 1994;385(6619):810–3.
56. Newton K, Harris AW, Strasser A. FADD/MORT1 regulates the pre-TCR checkpoint and can function as a tumour suppressor. EMBO J. 2000;19(5):931–41.
57. Strasser A, Harris AW, von Boehmer H, Cory S. Positive and negative selection of T cells in T-cell receptor transgenic mice expressing a bcl-2 transgene. Proc Natl Acad Sci. 2006;91(4):1376–80.
58. Ma A, Pena JC, Chang B, Margosian E, Davidson L, Alt FW, et al. Bclx Regulates the Survival of Double-Positive Thymocytes. Proc Natl Acad Sci U S A. 1995;92(11):4763–7.
59. Bouillet P, Cory S, Zhang LC, Strasser A, Adams JM. Degenerative Disorders Caused by Bcl-2 Deficiency Prevented by Loss of Its BH3-Only Antagonist Bim. Dev Cell. 2001;1(5):645–53.
60. Dzhagalov I, Dunkle A, He Y-W. The Anti-Apoptotic Bcl-2 Family Member Mcl-1 Promotes T Lymphocyte Survival at Multiple Stages. J Immunol. 2008;181(1):521–8.
61. Newton K, Harris AW, Bath ML, Smith KGC, Strasser A. A dominant interfering mutant of FADD/MORT1 enhances deletion of autoreactive thymocytes and inhibits proliferation of mature

T lymphocytes. EMBO J. 1998;17(3):706–18.
62. Strasser A, Harris AW, Cory S. bcl-2 transgene inhibits T cell death and perturbs thymic self-censorship. Cell. 1991;67(5):889–99.
63. Gray DHD, Kupresanin F, Berzins SP, Herold MJ, O'Reilly LA, Bouillet P, et al. The BH3-Only Proteins Bim and Puma Cooperate to Impose Deletional Tolerance of Organ-Specific Antigens. Immunity. 2012;37(3):451–62.
64. Baldwin TA, Hogquist KA. Transcriptional Analysis of Clonal Deletion In Vivo. J Immunol. 2007;179(2):837–44.
65. Surh CD, Sprent J. T-cell apoptosis detected in situ during positive and negative selection in the thymus. Nature. 1994;372(6501):100–3.
66. Boehm T, Swann JB. Thymus involution and regeneration: Two sides of the same coin? Nat Rev Immunol. 2013;13(11):831–8.
67. Aw D, Silva AB, Maddick M, von Zglinicki T, Palmer DB. Architectural changes in the thymus of aging mice. Aging Cell. 2008;7(2):158–67.
68. Gruver AL, Sempowski GD. Cytokines, leptin, and stress-induced thymic atrophy. J Leukoc Biol. 2008;84(4):915–23.
69. Xiao S, Shterev ID, Zhang W, Young L, Shieh J-H, Moore M, et al. Sublethal Total Body Irradiation Causes Long-Term Deficits in Thymus Function by Reducing Lymphoid Progenitors. J Immunol. 2017;199(8):2701–12.
70. Yao G, Hou Y. Thymic atrophy via estrogen-induced apoptosis is related to Fas/FasL pathway. Int Immunopharmacol. 2004;4(2):213–21.
71. Besteman EG, Zimmerman KL, Holladay SD. Diethylstilbestrol (DES)-induced fetal thymic atrophy in C57BL/6 mice: Inhibited thymocyte differentiation and increased apoptotic cell death. Int J Toxicol. 2005;24(4):231–9.
72. Sun X-M, Carthew P, Dinsdale D, Snowden RT, Cohen GM. The Involvement of Apoptosis in Etoposide-Induced Thymic Atrophy. Toxicol Appl Pharmacol. 1994;128.
73. Keswani T, Mitra S, Bhattacharyya A. Copper-induced immunotoxicity involves cell cycle arrest and cell death in the liver. Environ Toxicol. 2015;30(4):411–21.
74. Sauce D, Appay V. Altered thymic activity in early life: How does it affect the immune system in young adults? Curr Opin Immunol. 2011;23(4):543–8.
75. Li T, Wu N, Dai Y, Qiu Z, Han Y, Xie J, et al. Reduced thymic output is a major mechanism of immune reconstitution failure in HIV-infected patients after long-term antiretroviral therapy. Clin Infect Dis. 2011;53(9):944–51.
76. Rb-Silva R, Nobrega C, Azevedo C, Athayde E, Canto-Gomes J, Ferreira I, et al. Thymic fuction as a predictor of immune recovery in chronically HIV-infected patients initiating antiretreoviral therapy. Front Immunol. 2019;10:1–13.
77. Morrot A, Terra-Granado E, Pérez AR, Silva-Barbosa SD, Milićević NM, Farias-de-Oliveira DA, et al. Chagasic thymic atrophy does not affect negative selection but results in the export of activated CD4+CD8+ T Cells in Severe Forms of Human Disease. PLoS Negl Trop Dis. 2011;5(8).
78. Papadopoulou AS, Dooley J, Linterman MA, Pierson W, Ucar O, Kyewski B, et al. The thymic epithelial microRNA network elevates the threshold for infection-associated thymic involution via miR-29a mediated suppression of the IFN-α receptor. Nat Immunol. 2012;13(2):181–7.
79. Kong Y, Li Y, Zhang W, Yuan S, Winkler R, Krohnert U, et al. Sepsis-Induced Thymic Atrophy Is Associated with Defects in Early Lymphopoiesis. Stem Cells. 2016;(34):2902–15.
80. Deobagkar-Lele M, Chacko SK, Victor ES, Kadthur JC, Nandi D. Interferon-γ- and glucocorticoid-mediated pathways synergize to enhance death of CD4+ CD8+ thymocytes during Salmonella enterica serovar Typhimurium infection. Immunology. 2013;138(4):307–21.
81. Roggero E, Perez A, Revelli S, Bottasso O. Differential susceptibility to acute Trypanosoma cruzi

infection in BALB/c and C57BL/6 mice is not associated with a distinct parasite load but cytokine abnormalities E. Clin Exp Immunol. 2002;128:421–8.
82. Su L, Kaneshima H, Bonyhadi M, Salimi S, Kraft D, Rabin L, et al. HIV-1-induced thymocyte depletion is associated with indirect cytopathicity and infection of progenitor cells in vivo. Immunity. 1995;2(1):25–36.
83. Auwaerter P G, Kaneshima H, McCune J M, Wiegand G, Griffin D E. Measles virus infection of thymic epithelium in the SCID-hu mouse leads to thymocyte apoptosis. J Virol. 1996;70(6):3734–40.
84. Yoshimura FK, Wang T, Yu F, Kim H-RC, Turner JR. Mink Cell Focus-Forming Murine Leukemia Virus Infection Induces Apoptosis of Thymic Lymphocytes. J Virol. 2002;74(17):8119–26.
85. Liu B, Zhang W, Deng W, Liu J, Li H, Wen M, et al. Severe influenza A(H1N1)pdm09 infection induces thymic atrophy through activating innate CD8+CD44hi T cells by upregulating IFN-g. Cell Death Dis. 2014;5(10):1–12.
86. Souto PCS, Brito VN, Gameiro J, Da Cruz-Höfling MA, Verinaud L. Programmed cell death in thymus during experimental paracoccidioidomycosis. Med Microbiol Immunol. 2003;192(4):225–9.
87. Chen W, Kuolee R, Austin JW, Shen H, Che Y, Conlan JW. Low dose aerosol infection of mice with virulent type A Francisella tularensis induces severe thymus atrophy and CD4+CD8+ thymocyte depletion. Microb Pathog. 2005;39(5–6):189–96.
88. Khanam S, Sharma S, Pathak S. Lethal and nonlethal murine malarial infections differentially affect apoptosis, proliferation, and CD8 expression on thymic T cells. Parasite Immunol. 2015;37(7):349–61.
89. Watson SR, Miller TB, Redington TJ, Bullock WE. Immunoregulation in experimental disseminated histoplasmosis: flow microfluorometry (FMF) studies of the Thy and Lyt phenotypes of T lymphocytes from infected mice. J Immunol. 1983;131(2):984–90.
90. Ayala A, Herdon CD, Lehman DL, DeMaso CM, Ayala CA, Chaudry IH. The induction of accelerated thymic programmed cell death during polymicrobial sepsis: Control by corticosteroids but not tumor necrosis factor. Vol. 3, Shock. 1995. p. 259–67.
91. Roggero E, Pérez AR, Tamae-Kakazu M, Piazzon I, Nepomnaschy I, Basedovsky HO, et al. Edogenous glucocorticoids cause thymus atrophy but are protective during acute Trypanosoma cruzi infection. J Endocrinol. 2006;190(2):495–503.
92. Watson SR, Redington TJ, Miller TB, Bullock WE. Flow microfluorometry analysis of alterations in T-lymphocyte subsets during murine listeriosis. Infect Immun. 1984;45(2):372–7.
93. Pérez AR, Roggero E, Nicora A, Palazzi J, Besedovsky HO, del Rey A, et al. Thymus atrophy during Trypanosoma cruzi infection is caused by an immuno-endocrine imbalance. Brain Behav Immun. 2007;21(7):890–900.
94. Zhang YH, Takahashi K, Jiang GZ, Kawai M, Fukada M, Yokochi T. In vivo induction of apoptosis (programmed cell death) in mouse thymus by administration of lipopolysaccharide. Infect Immun. 1993;61(12):5044–8.
95. Barke RA, Roy S, Chapin RB, Charboneau R. The role of Programmed Cell Death (Apoptosis) Thymic Involution Following Sepsis. Arch Surg. 1994;129.
96. Koka PS, Brooks DG, Razai A, Kitchen CM, Zack JA. HIV Type 1 Infection Alters Cytokine mRNA Expression in Thymus. AIDS Res Hum Retroviruses. 2003;19(1):1–12.
97. Schwartz JN, Daniels CA, Klintworth GK. Lymphoid cell necrosis, thymic atrophy, and growth retardation in newborn mice inoculated with murine cytomegalovirus. Am J Pathol. 1975;79(3):509–22.
98. Wood BA, Dutz W, Cross SS. Neonatal infection with mouse thymic virus: Spleen and lymph node necrosis. J Gen Virol. 1981;57(1):139–47.

99. Shibuta H, Adachi A, Kanda T, Matumoto M. Experimental Parainfluenzavirus Infection in Mice : Fatal Illness with Atrophy of Thymus and Spleen in Mice Caused by a Variant of Parainfluenza 3 Virus. Infect Immun. 1982;35(2):437–41.
100. Nobrega C, Cardona PJ, Roque S, Pinto do Ó P, Appelberg R, Correia-Neves M. The thymus as a target for mycobacterial infections. Microbes Infect. 2007;9(14–15):1521–9.
101. Haynes BF, Markert ML, Sempowski GD, Patel DD, Hale LP. The Role of the Thymus in Immune Reconstitution in Aging, Bone Marrow Transplantation, and HIV-1 Infection. Annu Rev Immunol. 2003;21(1):529–60.
102. Nobrega C, Roque S, Nunes-Alves C, Coelho A, Medeiros I, Castro AG, et al. Dissemination of Mycobacteria to the Thymus Renders Newly Generated T Cells Tolerant to the Invading Pathogen. J Immunol. 2010;184(1):351–8.
103. Mandal D, Mazumder A, Das P, Kundu M, Basu J. Fas-, caspase 8-, and caspase 3-dependent signaling regulates the activity of the aminophospholipid translocase and phosphatidylserine externalization in human erythrocytes. J Biol Chem. 2005;280(47):39460–7.
104. Wyllie AH. Glucocorticoid-induced thymocyte apoptosis is associated with endogenous endonuclease activation. Nature. 1980;284(5756):555–6.
105. Marchetti MC, Di Marco B, Cifone G, Migliorati G, Riccardi C. Dexamethasone-induced apoptosis of thymocytes: Role of glucocorticoid receptor-associated Src kinase and caspase-8 activation. Blood. 2003;101(2):585–93.
106. Flórido M, Borges M, Appelberg R, Pearl JE, Solache A, Haynes L, et al. Gamma interferon-induced T-cell loss in virulent Mycobacterium avium infection. Infect Immun. 2005;73(6):3577–86.
107. Appelberg R, Gomes MS, Flórido M, Pais TF. Improved clearance of Mycobacterium avium upon disruption of the inducible nitric oxide synthase gene. J Immunol. 1999;162(11):6734–9.
108. Flórido M, Gonçalvez AS, Silva RA, Ehlers S, Cooper AM, Appelberg R. Resistance of virulent Mycobacterium avium to gamma interferon-mediated antimicrobial activity suggests additional signals for induction of mycobacteriostasis. Infect Immun. 1999;67(7):3610–8.
109. Barreira da Silva P. T cells during mycobacterial infections: production and activation. PhD [dissertation]. Universidade do Minho; 2016.
110. Kato Y, Morikawa A, Sugiyama T, Koide N, Jiang GZ, Lwin T, et al. Augmentation of lipopolysaccharide-induced thymocyte apoptosis by interferon-γ. Cell Immunol. 1997;177(2):103–8.
111. Moulian N, Truffault F, Gaudry-Talarmain YM, Serrat A, Berrih-Aknin S. In vivo and in vitro apoptosis of human thymocytes are associated with nitrotyrosine formation. Blood. 2001;97(11):3521–30.
112. Cohen O, Kfir-Erenfeld S, Spokoini R, Zilberman Y, Yefenof E, Sionov RV. Nitric oxide cooperates with glucocorticoids in thymic epithelial cell-mediated apoptosis of double positive thymocytes. Int Immunol. 2009;21(10):1113–23.
113. Cohen O, Ish-Shalom E, Kfir-Erenfeld S, Herr I, Yefenof E. Nitric oxide and glucocorticoids synergize in inducing apoptosis of CD4+8+ thymocytes: Implications for “Death by Neglect” and T-cell function. Int Immunol. 2012;24(12):783–91.
114. Martins GA, Vieira LQ, Cunha FQ, Silva JS. Gamma interferon modulates CD95 (Fas) and CD95 ligand (Fas-L) expression and nitric oxide-induced apoptosis during the acute phase of Trypanosoma cruzi infection: A possible role in immune response control. Infect Immun. 1999;67(8):3864–71.
115. Dalton DK, Haynes L, Chu C-Q, Swain SL, Wittmer S. Interferon γ Eliminates Responding CD4 T Cells during Mycobacterial Infection by Inducing Apoptosis of Activated CD4 T Cells. J Exp Med. 2000;192(1):117–22.
116. Savino W, Leite-de-Moraes MC, Hontebeyrie-Joskowicz M, Dardenne M. Studies on the thymus in

Chagas' disease. I. Changes in the thymic microenvironment in mice acutely infected with Trypanosoma cruzi. Eur J Immunol. 1989;19:1727–33.
117. Dzhagalov IL, Chen KG, Herzmark P, Robey EA. Elimination of Self-Reactive T Cells in the Thymus: A Timeline for Negative Selection. PLoS Biol. 2013;11(5).
118. Hu Q, Sader A, Parkman JC, Baldwin TA. Bim-Mediated Apoptosis Is Not Necessary for Thymic Negative Selection to Ubiquitous Self-Antigens. J Immunol. 2009;183(12):7761–7.
119. Broker LE, Kruyt FAE, Giaccone G. Cell death independent of caspases: A Review. Clin Cancer Res. 2005;11(9):3155–63.
120. Scott RS, Matsushima GK, McMahon EJ, Pop SM, Reap EA, Caricchio R, et al. Phagocytosis and clearance of apoptotic cells is mediated by MER. Nature. 2001;411(6834):207–11.
121. Miyazaki T, Hirokami Y, Matsuhashi N, Takatsuka H, Naito M. Increased Susceptibility of Thymocytes to Apoptosis in Mice Lacking AIM, a Novel Murine Macrophage-derived Soluble Factor Belonging to the Scavenger Receptor Cysteine-rich Domain Superfamily. J Exp Med. 2002;189(2):413–22.
122. Fehsel K, Kröncke KD, Meyer KL, Huber H, Wahn V, Kolb-Bachofen V. Nitric oxide induces apoptosis in mouse thymocytes. J Immunol. 1995;155(6):2858–65.
123. Gordon SA, Abou-Jaoude W, Hoffman RA, McCarthy SA, Kim Y-M, Zhou X, et al. Nitric oxide induces murine thymocyte apoptosis by oxidative injury and a p53-dependent mechanism. J Leukoc Biol. 2001;70(1):87–95.
124. Zhou X, Gordon SA, Kim Y-M, Hoffman RA, Chen Y, Zhang X-R, et al. Nitric Oxide Induces Thymocyte Apoptosis Via a Caspase-1-Dependent Mechanism. J Immunol. 2000;165(3):1252–8.
125. Cookson BT, Brennan MA. Pro-inflammatory programmed cell death. Trends Microbiol. 2001;9(3):113–4.
126. Miao EA, Rajan J V., Aderem A. Caspase-1-induced pyroptotic cell death. Immunol Rev. 2011;243(1):206–14.
127. Tanaka T, Narazaki M, Kishimoto T. IL-6 in Inflammation, Immunity, and Disease. Cold Spring Harb Perspect Biol. 2014;6(Kishimoto 1989):1–16.
128. Edfors F, Danielsson F, Hallström BM, Käll L, Lundberg E, Pontén F, et al. Gene-specific correlation of RNA and protein levels in human cells and tissues. Mol Syst Biol. 2016;12(10):883.
129. Munson D, Padula M, Nawab U, Nilan K, Clifford P, Tyler L, et al. N/IICU Pathway for Inhaled Nitric Oxide Use in Newborns with Persistent Pulmonary Hypertension. 2018.
130. Münzel T, Daiber A. Inorganic nitrite and nitrate in cardiovascular therapy: A better alternative to organic nitrates as nitric oxide donors? Vascul Pharmacol. 2018;102:1–10.
131. Huang Z, Fu J, Zhang Y. Nitric Oxide Donor-Based Cancer Therapy: Advances and Prospects. J Med Chem. 2017;60(18):7617–35.

7. ANNEXES

Annex 1 – Gating strategies for flow cytometry analysis of thymocyte death

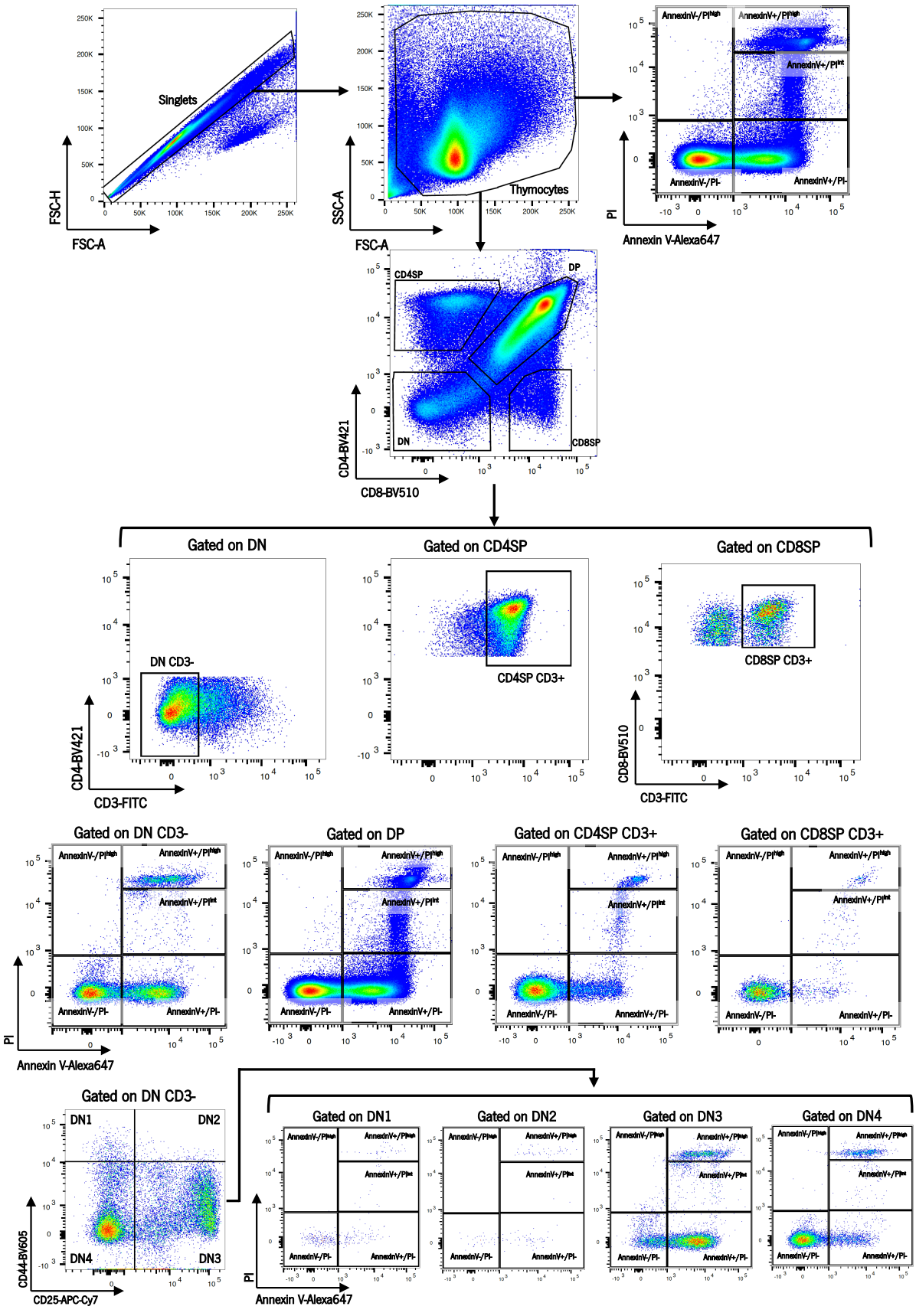

FIGURE 1. Schematic representation of the gating strategy used to analyze thymocyte death within thymocyte populations by Annexin V/PI flow cytometry staining. Single cells (singlets) were selected on total events, based on the fact that the size (FSC-A) and height (FSC-H) of a single cell are proportional. Total thymocytes were gated within singlets, and debris (very low size (FSC-A) and complexity (SSC-A)) was excluded. Thymocyte populations were defined according to CD4 and CD8 expression and further selected according to CD3 expression (DN: $CD3^{-}CD4^{-}CD8^{-}$; DP: $CD4^{+}CD8^{+}$; CD4SP: $CD3^{+}CD4^{+}CD8^{-}$; CD8SP: $CD3^{+}CD4^{-}CD8^{+}$). DN thymocytes were divided into four subpopulations based on CD25 and CD44 expression (DN1: $CD44^{+}CD25^{-}$; DN2: $CD44^{+}CD25^{+}$; DN3: $CD44^{-}CD25^{+}$; DN4: $CD44^{-}CD25^{-}$). Annexin V and PI fluorescence was evaluated within all populations (total thymocytes, DN, DP, CD4SP, CD8SP, DN1, DN2, DN3 and DN4). According to Annexin V and PI expression, five populations were considered: viable (Annexin V^{-}/PI^{-}), early apoptotic (Annexin V^{+}/PI^{-}), apoptotic (Annexin V^{+}/PI^{int}), late apoptotic/necrotic (Annexin V^{+}/PI^{high}) and necrotic (Annexin V^{-}/PI^{+}) thymocytes. Gate design for PI, Annexin V, CD44 and CD25 was defined taking into consideration the FMO control.

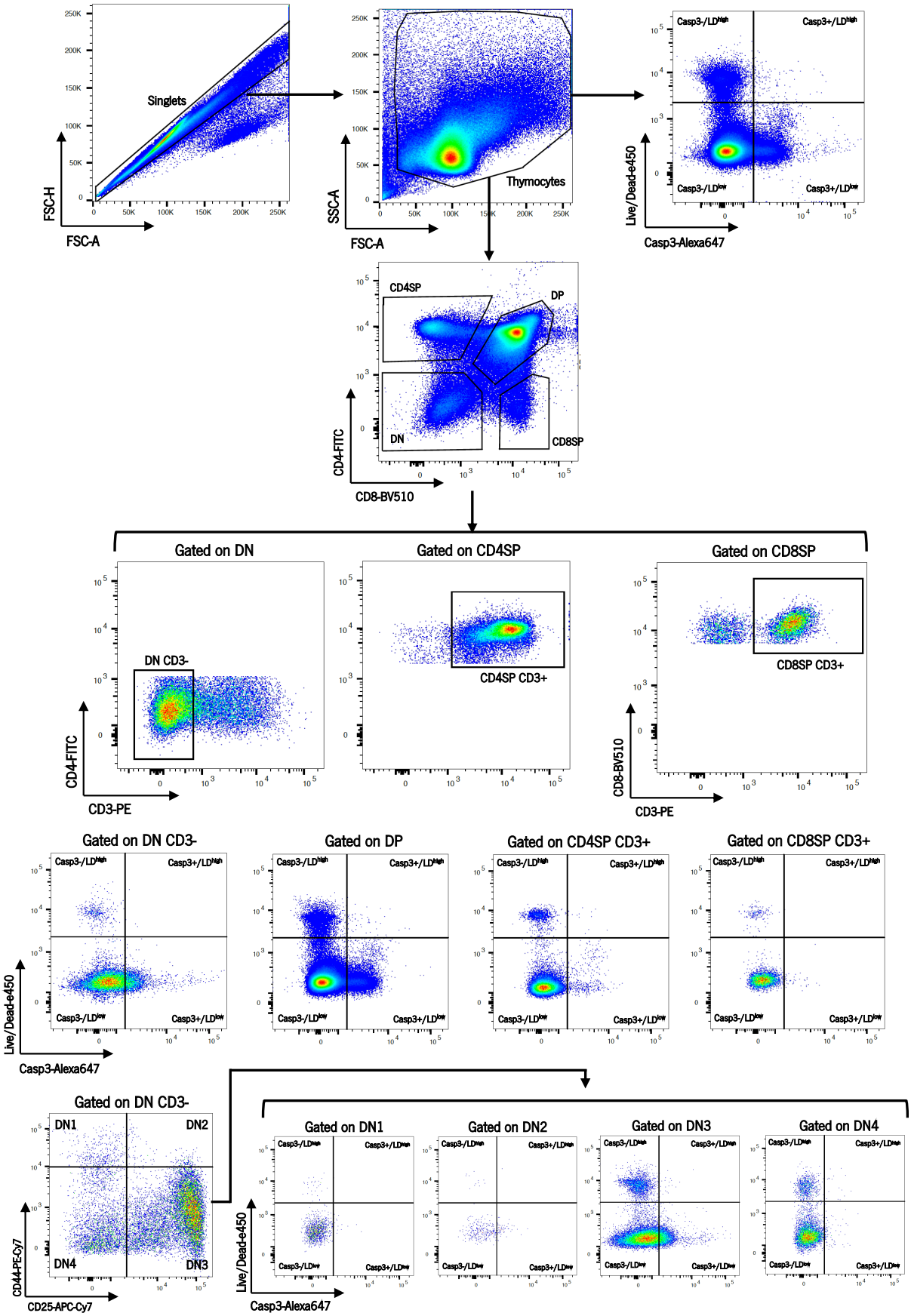
Singlets
FSC-H
FSC-A
Thymocytes
SSC-A
FSC-A
Casp3-/LDhigh
Casp3+/LDhigh
Casp3-/LDlow
Casp3+/LDlow
Live/Dead-e450
Casp3-Alexa647
CD4SP
DP
DN
CD8SP
CD4-FITC
CD8-BV510
Gated on DN
Gated on CD4SP
Gated on CD8SP
DN CD3-
CD4SP CD3+
CD8SP CD3+
CD4-FITC
CD3-PE
CD8-BV510
CD3-PE
Gated on DN CD3-
Gated on DP
Gated on CD4SP CD3+
Gated on CD8SP CD3+
Live/Dead-e450
Casp3-Alexa647
Gated on DN CD3-
DN1
DN2
DN4
DN3
CD44-PE-Cy7
CD25-APC-Cy7
Gated on DN1
Gated on DN2
Gated on DN3
Gated on DN4
Live/Dead-e450
Casp3-Alexa647

FIGURE 2. Schematic representation of the gating strategy used to analyze thymocyte death within thymocyte populations by Caspase 3/LiveDead flow cytometry staining. Single cells (singlets) were selected on total events, based on the fact that the size (FSC-A) and height (FSC-H) of a single cell are proportional. Total thymocytes were gated within singlets, and debris (very low size (FSC-A) and complexity (SSC-A)) was excluded. Thymocyte populations were defined according to CD4 and CD8 expression and further selected according to CD3 expression (DN: $CD3^{-}CD4^{-}CD8^{-}$; DP: $CD4^{+}CD8^{+}$; CD4SP: $CD3^{+}CD4^{+}CD8^{-}$; CD8SP: $CD3^{+}CD4^{-}CD8^{+}$). DN thymocytes were divided into four subpopulations based on CD25 and CD44 expression (DN1: $CD44^{+}CD25^{-}$; DN2: $CD44^{+}CD25^{+}$; DN3: $CD44^{-}CD25^{+}$; DN4: $CD44^{-}CD25^{-}$). Caspase 3 and Live/Dead expression were evaluated within all populations (total thymocytes, DN, DP, CD4SP, CD8SP, DN1, DN2, DN3 and DN4). According to Caspase 3 and Live/dead expression, four populations were considered: viable ($Casp3^{-}$/Live $Dead^{low}$), early apoptotic via caspase 3 ($Casp3^{+}$/Live $Dead^{low}$), late apoptotic via caspase 3 (Casp3+/Live $Dead^{high}$) and dead/dying cells not via caspase 3 ($Casp3^{-}$/$LiveDead^{high}$). Gate design for Caspase 3, CD44 and CD25 was defined taking into consideration the FMO control.

Annex 2 – Approval to perform animal experimentation from the local ethics committee

Universidade do Minho

Conselho de Ética

Conselho de Ética - Ciências da Vida e da Saúde

Identificação do documento: SECVS 017/2018

Título do Projeto: Avaliação dos mecanismos responsáveis pela atrofia tímica e alterações das células T após infeção de murganhos por micobactérias

Investigador Principal: Margarida Correia-Neves

Investigador responsável pela experimentação animal: Margarida Correia-Neves e equipa de investigadores com formação em Ciência de Animais de Laboratório

Subunidade orgânica: Instituto de Investigação em Ciências da Vida e da Saúde (ICVS)

PARECER

O Conselho de Ética analisou o processo relativo ao projeto de investigação acima identificado, que faz recurso a modelos animais, intitulado*: Avaliação dos mecanismos responsáveis pela atrofia tímica e alterações das células T após infeção de murganhos por micobactérias.*

Os documentos apresentados revelam que o projeto obedece aos requisitos exigidos para as boas práticas na experimentação com recurso à utilização de modelos animais, considerando a aplicação dos 3 Rs de Russel e Burch e a aplicação de limites críticos de sofrimento - *humane endpoints*.

Face ao exposto, o Conselho de Ética nada tem a opor à realização do projeto, emitindo o seu parecer favorável.

Salienta-se ainda que a autorização legal de projetos de investigação/ experimentação animal é feita pela DGAV a quem deverá submeter o respetivo formulário com o resumo não-técnico do projeto.

Braga, 11 de outubro de 2018.

A Presidente

Assinado por : **GRACIETTE TAVARES DIAS**
Num. de Identificação Civil: BI071230157
Data: 2018.10.12 10:36:01 GMT Daylight Time

CARTÃO DE CIDADÃO